Table of Contents

Abstract

Forecasting the genesis and rapid intensification (RI) of tropical cyclones (TCs) is performed utilizing a satellite-based overshooting top (OT) detection algorithm. Satellite-identified OTs can serve as a proxy in exploring a current TC genesis theory known as the "Vortical" Hot Tower theory, in which convective towers create vertical vorticity from already present horizontal vorticity and merge to form a cyclonic circulation. Furthermore, an increase in OTs associated with a TC can also be related to favorable environmental factors for the RI of TCs.

OTs are detected using a modified version an OT detection algorithm written by Bedka et al. (2010). In this modified algorithm, the tropopause temperature check is removed since the equilibrium level is below the tropical tropopause. In addition, the difference in the 11 μm brightness temperature between the OT and the surrounding anvil, which must consist of at least 9 of the 16 sampled pixels, is increased 9 K. This algorithm has been shown to capture OTs associated with tropical disturbances and weak TCs. Detection in strong TCs also occurs, however it can be hindered by some characteristics of these TCs. Detected OTs are categorized by distance and time to explore thresholds for forecasting the genesis and RI of TCs.

Genesis is observed to have a correlation with the average number of OTs. Given a 2-hour average of at least 4 OTs/scan within a 200 km radius of the storm center, a tropical disturbance tracked using the marsupial pouch paradigm, a closed storm-relative circulation within an easterly wave, has a 63.0% chance of genesis. Forecasting the time of genesis relies on a linear relationship involving the initial OT/scan value greater than 4.25 OTs/scan. For TCs exceeding tropical depression strength and forming west of 25º W, this forecast

results in a mean error of 1.25 days from actual genesis. This error can be reduced to 0.75 days, with 81.8% of correctly predicted TCs developing within ± 1 day of their forecasted time. This corresponds to 33.3% of all predicted genesis events.

In addition, OTs, as a single predictor, have proven skillful compared to climatology and the current operational Rapid Intensification Index (RII) in the forecasting of rapid intensification within 24 hours. In an independent test of 2006-2007 RI cases, the OT RI Index had a probability of detection ranging from 0.0% to 60.0% with a false alarm ratio of 70.4% to 100.0% when forecasting RI within the next 24 hours, ignoring all OTs within 24 hours of an exceeded OT/scan threshold. Furthermore, an increase in the Brier Skill Score upon the addition of the OTs to a logistic regression scheme, which provides improvements to the current RII, indicates additional improvements to the forecast skill of rapidly intensifying TCs.

I. Introduction

One of the essential ingredients to the formation and intensification of tropical cyclones (TCs) is intense convection and the associated latent heat release through condensation processes (Adler and Rodgers 1977, Kuo 1965). Theories have evolved as to the exact role of convection in TC genesis, beginning with Convective Instability of the Second Kind (CISK) (Charney and Eliassen 1964) and more recently with the "Vortical" Hot Tower theory (Montgomery et al. 2006; hereafter M06). Attempts have also been made to quantify the necessary convection associated with TC intensification. This thesis employs a satellite-based objective overshooting top detection algorithm in an effort to quantify tropical convection associated TCs; in particular, the genesis and rapid intensification (RI) stages.

Identifying and quantifying active convection in the tropics has been attempted in a variety of ways, mainly through the use of satellites. Steranka et al. (1986) used the infrared window channel (IRW) to capture clusters of convection as well as the temperature of the cloud tops. Other research has used precipitation features (PFs) deduced in microwave imagery from the Tropical Rainfall Measuring Mission (TRMM) to measure active convection (e.g. Alcala and Dessler 2002, Liu and Zipser 2005, Romps and Kuang 2009). Attempts at quantify regions of strong convection have also turned to identifying potentially overshooting convection, or overshooting tops (OTs).

The American Meteorological Society (AMS) *Glossary of Meteorology* (Glickman 2000) defines an OT as "A domelike protrusion above a cumulonimbus anvil, representing the intrusion of an updraft through its equilibrium level." However, the very nature of what is categorized as overshooting convection in the tropics varies. Recent research has defined overshooting convection exceeding the level of zero net radiative heating (Alcala and Dessler

2002) at 14 km or the tropical tropopause at ~16 km (Montgomery and Farrell 1993, Simpson et al. 1998). Yet, Liu and Zipser (2005) suggest the equilibrium level in the tropics is below the tropical tropopause. Applying this concept to TCs, Olander and Velden (2009) employed bispectral satellite imagery that involves the differencing of the IRW and water vapor (WV) channel brightness temperature values to isolate more active, potentially overshooting, convection in the core of TCs to infer intensity changes.

The study identifies the frequency and trends in OTs during selected tropical disturbance cases, and examines these for correlations with TC genesis and RI. Finally, the correlations are investigated as a tool for probabilistic forecasting of these events. The OT algorithm, developed by research scientists at the Cooperative Institute for Meteorological Satellite Studies (CIMSS), utilizes the 11 μm IRW brightness temperature (BT) (Bedka et al. 2010). Its original form, and subsequent modifications for detections of OTs associated with TCs, is described in sections III.a.1 and III.a.2, respectfully. While this algorithm is described as an overshooting top detection algorithm, it is important to note that no measure for evaluating the ambient height of the tropical tropopause has been included in the final modifications based on the analysis from Liu and Zipser (2005).

II. Background

a. Tropical Cyclogenesis

Tropical cyclogenesis continues to be a leading area of research in the tropical field, with experiments such as the PRE-Depression Investigation of Cloud systems in the Tropics (PREDICT) and the Genesis and Rapid Intensification Project (GRIP) taking place in the fall of 2010. TCs usually form in association with mesoscale convective systems (MCSs), with pre-tropical cyclone disturbances occurring on the poleward side of the doldrum Equatorial

Trough (Gray 1968). These MCSs are usually collocated with synoptic scale disturbances, such as easterly waves. Dominant in the Atlantic Ocean are African easterly waves (AEWs). A positive correlation between the 850 hPa AEW and the Atlantic TC activity, especially from 1985-1998, is observed in Thorncroft and Hodges (2001). These waves, which usually originate between 10° and 15° N in the much drier Saharan region, are in sharp contrast to the rainy zone 600 hPa AEW which originate equatorward of 15° N. About 87% of tropical cyclones form equatorward of 20° N, in regions of weak tropospheric vertical shear of the horizontal wind and sea surface temperatures (SSTs) greater than 26.5° C (Gray 1968). However, only a small fraction of tropical disturbances, ~20%, develop into TCs (Frank 1970).

1. Historical Review of Tropical Cyclogenesis theory

Charney and Eliassen (1964) presents one of the first theories of tropical cyclogenesis, called convective instability of the second kind (CISK). A conceptual model of CISK can bee seen in Figure 1. In this theory, cooperation between cumulus convection a

Figure 1: A conceptual model of CISK. An anticyclone is located aloft with a cyclone collocated in the lower troposphere. Moisture is provided to cumulus convection and warming occurs due to latent heat release. The accompanying thickness change yields a stronger anti-cyclone aloft and stronger cyclone below, providing more convergence and moisture to the cumulus convection in a self-amplifying process. Image courtesy of Schubert and Hack (1982).

and the large-scale circulation acts to develop a TC. Cumulus convection supplies latent heat to the developing TC, while the large-scale convergence supplies moisture to the convection in a self-amplifying process. In the pre-TC, under the CISK theory, the latent heat released by the cumulus convection is two orders of magnitude greater than that needed to maintain kinetic energy from frictional dissipation. This additional heating contributes to a local warming of the mid-level in the vortex center (Schubert and Hack 1982).

As mentioned above, CISK is driven by latent heat release. However, in the theory of quasi-balanced vortex flow, presented by Schubert and Hack (1982), when the convective horizontal scale is much smaller than the Rossby radius of deformation (as it is in pre-TCs), adiabatic cooling is "nearly as large as the heating due to cumulus convection" (Schubert and Hack 1982). For a typical latitude of TC genesis and value of the Brunt-Vaisala frequency (N^2), the given Rossby radius of deformation is about 1000 km. Thus Schubert and Hack (1982) indicate linear CISK can be viewed as an inefficient process due to adiabatic cooling with nonlinear feedbacks more efficiently warming the vortex center.

In the theory of linear CISK, an air parcel moving toward the center of the circulation is met with little air resistance. The inertial stability is approximated by the squared Coriolis parameter (f^2). However, in the theory of quasi-balanced vortex flow, during the most rapid deepening, the inertial stability is not dominated by the f^2 and is instead much larger than when approximated by f^2 (Schubert and Hack 1982). This provides added resistance to air parcel movement. Using a frictionless, axisymmetric, balanced flow in a thermally forced vortex on an f-plane, Schubert and Hack (1982) derive a diagnostic equation for forced secondary circulation. Solutions to this equation include a reduced secondary circulation as the relative vorticity exceeds the Coriolis parameter and an increase in heating efficiency

occurring as a consequence of increased inertial stability. Thus, inertial stability enables latent heat release to produce a local temperature and tangential wind change. This type of nonlinear interaction is not addressed by the linear CISK hypothesis (Shubert and Hack 1982).

Another challenge to the CISK theory is presented by Emanuel (1989). Suggesting the energy used for CISK is absent; Emanuel (1989) proposes that TCs develop from "a finite amplitude instability involving the feedback between the cyclone and wind-induced evaporation" (Emanuel 1989). A simple axisymmetric model, with the cumulus updraft mass flux depending simply and directly on buoyancy without being explicitly constrained by moisture convergence, is utilized. Upward motion and adiabatic cooling are first induced by Ekman pumping, resulting in clouds with very low precipitation efficiency. These clouds are ineffective in opposing adiabatic cooling and act to dry out the subcloud layer outside of the system core. This preserves convective neutrality while maintaining the present vortex; however the TC will eventually decay unless high equivalent potential temperature (θ_e) air is imported into it. Surface fluxes can counteract the drying effect of convective downdrafts once the lower-to-middle troposphere is saturated, allowing θ_e to increase. One mechanism for this saturation is air above the subcloud layer descending to the surface in convective downdrafts. It is then moistened by surface evaporation before ascending to the tropopause in deep, heavy precipitating convection, confined to the core due to the subcloud layer. The resulting increase in θ_e increases the temperature aloft and amplifies the TC.

External factors have also been tied to tropical cyclogenesis. Instead of looking at internal processes, which assume the transformation to a finite-amplitude rotary systems has already taken place, Montgomery and Farrell (1993) investigates upper level potential

vorticity (PV) in TC genesis. Montgomery and Farrell (1993) uses two and three dimensional moist geostrophic momentum models to conclude that deep, saturated ascent is essential to produce strong vertical coupling between upper and lower level PV disturbances, making a convective connection to the upper levels. Deep ascent is implied by the thermal wind balance and acts to enhance the upper vortex. In addition, latent heat release with the deep ascent produces a narrow region of PV extending from the upper levels to the surface.

Building on work from 1993, Montgomery and Enagonio (1998) present a different genesis theory through vorticity enhancement. Commonly called "bottom-up" genesis, the convergence of small-scale vorticity are observed to strengthen the overall vorticity of the pre-TC, as (potential) vorticity anomalies are produced by moist penetrative convection and relax into axisymmetry in the presence of a preexisting vortex. Through the dynamic feedback involving the location of the already-occurred heating and the produced PV anomalies (Jascourt 1997), like-sign PV anomalies are ingested into the parent vortex, while opposite-sign anomalies are expelled

In a three-dimensional nonlinear quasigeostrophic balance model, the realistic nature of small-scale convective disturbance interaction with the larger-scale vortex circulation can be observed (Montgomery and Enagonio 1998). Convective heating profiles have a positive (negative) heating rate at low (high) levels, resulting in positive (negative) PV anomaly at low (high) levels. When this convection is modeled in the presence of a mid-level vortex, low-level PV anomalies are drawn into the center of the vortex, with negative PV anomalies expelled outward (Figure 2). This gives the impression of the vortex appearing to "build downward" (Montgomery and Enagonio 1998) in the presence of peripheral convection. In addition, a warm core develops, with a temperature anomaly of 5 K after 7.3 days. Full spin-

up of the model tropical cyclone occurred at 3.6 days, and thus the warm core timing is reasonable for tropical cyclogenesis. Both eddy-heat and eddy-momentum fluxes are found to contribute to this warm core, with subsidence warming initially being too small but playing a factor later in development.

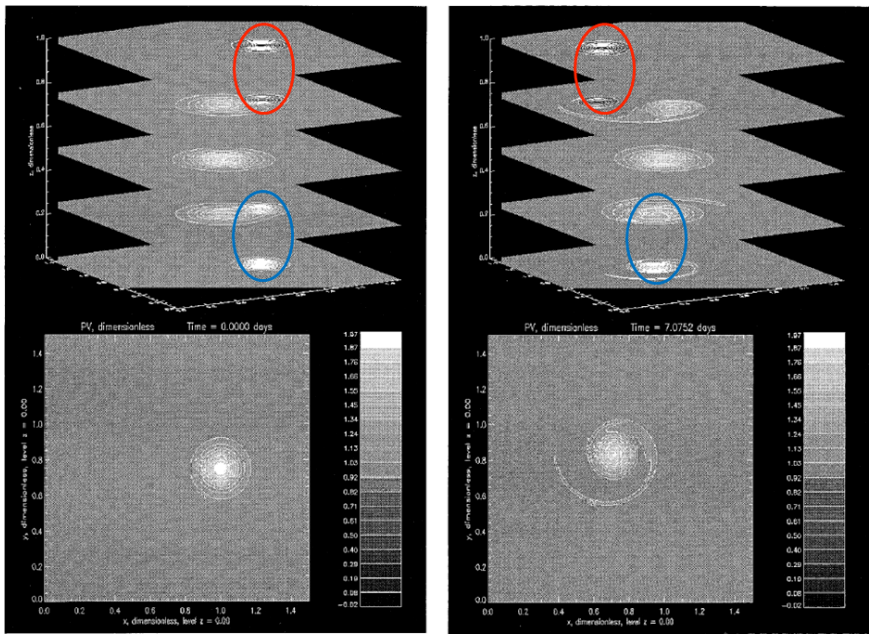

Figure 2: Contours of potential vorticity at t=0 (left) and t=7 (right) days. Positive PV anomaly (blue circle) resulting from low level convergence is drawn to the center by day 7, creating a vertically stacked vortex, while the negative PV anomaly (red circle) aloft is expelled from the vortex center. Image courtesy of Montgomery and Enagonio (1998).

The "bottom-up" theory is not the only theory to tropical cyclogenesis presented around this time. Basing its hypothesis from Emanuel (1989), the Tropical Experiment in Mexico (TEXMEX) in 1991 seeks to answer the question: is "the elevation of θ_e in the middle troposphere just above the near-surface vorticity maximum a necessary and perhaps sufficient condition for tropical cyclogenesis?" (Bister and Emanuel 1997) Resulting from a case and model study of Hurricane Guillermo in the Eastern Pacific, a new theory for tropical cyclogenesis, the "top-down showerhead," is produced The "showerhead" theory suggests a midlevel mesocyclone develops in a region of stratiform precipitation. Evaporation cools

and moistens the mesocyclone, while a low-level anticyclone experiences warming and drying. However, this warm and dry low level air cannot support convection. Eventually, evaporation cools and humidifies the lower troposphere, allowing the low-level θ_e to recover and convection to be supported. This cooling of the low level is balanced by intensification of the mid-level vortex, corresponding to a downward extension of cyclonic circulation. New convection develops in the now cool, humid unstable air, with a warm core vortex developing near the surface. For this warm core to develop, stratiform precipitation must be long enough to drive the midlevel vortex to the boundary layer.

Analysis of Hurricane Guillermo indicates the increase in middle-troposphere θ_e is not sufficient enough to start intensification, as suggested in Emanuel (1989). Instead, according to Bister and Emanuel (1997), three things are important in the downward vortex extension under the "showerhead" theory. First, precipitation has to last longer than the time frame needed for air to descend through the evaporation layer. Numerical simulations with an axisymmetric model showed rain rate has an influence on TC genesis and decreasing the rain rate or the duration of the precipitation resulted in a slower TC development. Second, if the precipitation is weak, a moistened upper troposphere can increase evaporation close to the surface. Finally, relative flow through the system should be small.

Only two years after the completion of the TEXMEX experiment, the Tropical Ocean Global Atmosphere Coupled Ocean Atmosphere Response Experiment (TOGA COARE) took place in the Western Pacific Ocean. Capitalizing on what had been previously rare tropical cyclogenesis data before this experiment and TEXMEX; Simpson et al. (1997) develops a new tropical cyclogenesis theory based on the development of Tropical Cyclone Oliver (1993). This theory is commonly known as "top-down merger." Vortices form near

the stratiform cloud base of the MCS. With the help of latent heating in the stratiform cloud and evaporation cooling below, a potential temperature gradient is experienced near the cloud base. Combining this potential temperature gradient with stretching and tilting from mesoscale convergence produces a PV anomaly with a relative scale of the stratiform cloud region. This then extends to the surface to initiate cyclogenesis.

During Oliver's development, several short-lived vortices were observed prior to cyclogenesis. However, the necessary convection was not attained due to vertical wind shear. Once the monsoon trough within which pre-Oliver was located strengthened, these vortices were observed to merge. While these mergers are stochastic in nature, they are enhanced by the presence of a monsoon trough with its low-level cyclonic flow. Associated with the increasing vorticity from the mergers in the mid-levels and low-level cyclonic flow is a reduction in the Rossby radius of deformation. This reduction suppresses gravity waves, enabling convective heating to be transferred to vortex spin-up instead of propagating away. Also, as observed in Oliver, this convective heating provided an environment for the extension of midlevel vortices to the surface to initiate cyclogenesis. This is similar to "bottom-up" genesis, with Montgomery and Enagonio (1998) indicate top-down merger and bottom-up "are not mutually exclusive." The difference between the two theories, however, lies in the importance places on convective ("bottom-up") or stratiform ("top-down merger") heating.

With modifications made to Montgomery and Egagonio's "bottom-up" theory, a new theory is presented by in M06. Now called the "Vortical Hot Tower" (VHT) theory, M06 uses a nonhydrostatic cloud model to demonstrate that the preferred coherent structures in a mesoscale convective vortex (MCV), a by-product of a MCS, are small-scale cumulonimbus

towers which possess intense cyclonic vorticity. This vorticity is obtained from tilting and stretching the horizontal MCV vorticity. The initial absolute vertical, as well as Rossby-Ertel's potential vorticity, associated with the MCV can be seen in Figure 3. Vorticity is centered around 4 km, extending from the surface to about 8 km. Multiple vortex mergers will then serve to vortically prime the environment for tropical cyclogenesis.

Figure 3: Initial absolute vertical vorticity (left) and Rossby-Ertel's potential vorticity (right) of the initial MCV from the nonhydrostatic cloud model used by M06.

2. "Vortical" Hot Tower Theory

Earlier hypotheses, presented in M06, proposed hot towers contribute to TC genesis through subsidence warming and the accompanying hydrostatic pressure falls. However, Hendricks et al. (2004) provides a two phase hypothesis to VHT tropical cyclogenesis. The first phase involves preconditioning the lower troposphere through the generation of multiple VHTs, which tilts and stretches the already present horizontal vorticity. A dynamic feedback then expels the acting to expel negative PV (Jascourt 1997, Montgomery and Enagonio 1998). The second phase, known as diabatic vortex merger, consists of vortex merging and axisymmetrization of the VHTs, a decay of the axisymmetries in favor of creating a master vortex. This diabatic concentration of PV produces an intensification of the $z < 2$ km PV. In addition, the strong vorticity associated the VHTs and diabatic vortex merging act to trap the released latent heat, creating the warm core associated with TCs.

a. Preconditioning the lower troposphere

Using the Regional Atmospheric Modeling System (RAMS), M06 is able to simulate the absolute vertical vorticity associated with the first VHT at 20 minutes and again at 40 minutes after model initialization (Figure 4). By 40 minutes, a strong vorticity dipole can be observed, with regions of positive and negative vorticity alternating above and below 4 km.

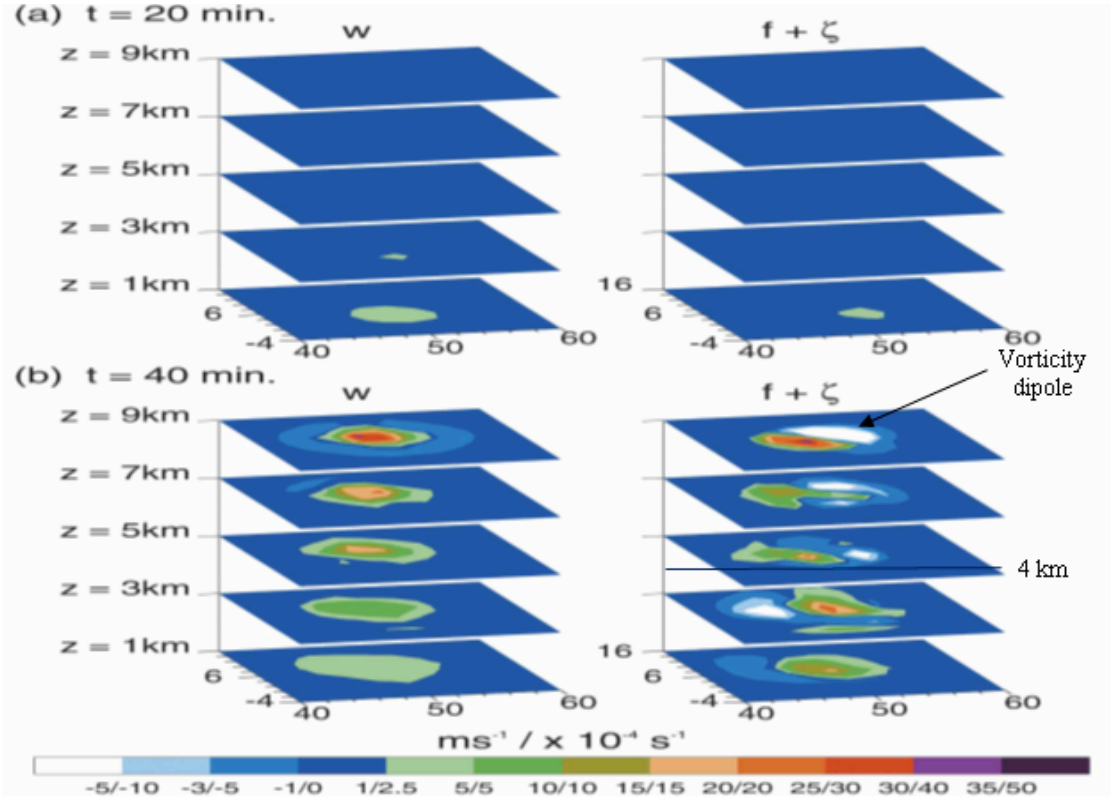

Figure 4: Examples of vertical velocity and vertical vorticity signatures associated with the first VHT from RAMS at 20 minutes (a) and 40 minutes (b) after initialization. Figure courtesy of M06.

This absolute vorticity dipole suggests the MCV horizontal vorticity is being tilted vertically, which continues as the updraft strengthens. A schematic of this dipole creation through the updraft can be observed in Figure 5, with the purple line representing vortex filaments induced rotation from the given vertical shear profile which are then tilted by the updraft. Given the MCV wind shear profile, two areas of positive (negative) vorticity below (above) 4

km are observed (Figure 5a). The VHT updraft acts to tilt this horizontal vorticity vertically (Figure 5b), resulting in the observed dipole. Also, as the VHT updraft intensifies, the vertical vorticity is further increased through stretching (not shown). Note the rotation of the axis in between Figure 5a and 5b. The creation of a circulation is then accomplished by diabatic vortex mergers.

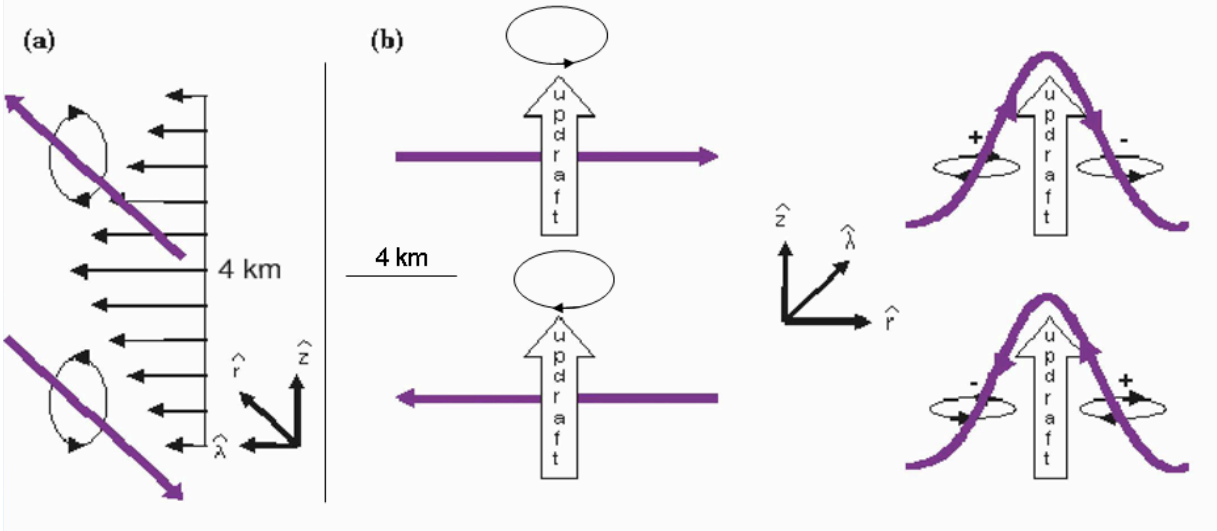

Figure 5: Schematic of tilting (b) the horizontal vorticity associated with the MCV (a). The purple line represents vortex filaments created from the given shear profile which is then tilted by the updraft. Figure courtesy of M06.

b. Diabatic vortex merger

When simulated by the Mesoscale Model (MM5) in Hendricks et al. (2004), TC Diana (1984) undergoes many occurrences of vortex merging. One such case can be observed in Figure 6, where the two vortices circled in white (left) merged, occurring 33 hours after model initialization. As a result of this merger, a broad area of spin-up occurs (right). In the momentum budget, as seen in Equation 1 from M06:

$$\frac{\partial \overline{v}}{\partial t} = -\overline{u}\overline{\eta} - \overline{u'\zeta'} - \overline{w}\frac{\partial \overline{v}}{\partial z} - \overline{w'\frac{\partial v'}{\partial z}} + \overline{F}_{sg}, \qquad \text{(Eq. 1)}$$

Figure 6: Vortex merger 33 hours after initialization in TC Diana from Hendricks et al. (2004), circled in white. Before image on left and after image, approximately 0.5 hours later, on the right.

where υ is the tangential velocity, ζ is the relative vorticity, η is the absolute vorticity, and $\overline{F}_{sg}$ is mean subgrid-scale tendency of tangential momentum, the summation of the horizontal terms agree with the observed spin-up, this event appears barotropic. Thus, Hendricks et al. (2004) utilizes a shallow water primitive equation model (SWPE), which simulates the vortex mergers, indicating their strong analogs to barotropic dynamics. However, the fact that the SWPE merger took twice as long indicates net convergence can accelerate mergers in the real atmosphere. In addition, these vortex mergers occur more strongly at lower levels. This can be observed in the cross-section from RAMS (M06), seen in Figure 7, of a vortex merger from 6 hours 40 minutes to 7 hours 20 minutes. The dry Rossby-Ertel PV increased from 18.13 PVU to 32.43 PVU, with the maximum lowering from 5 km to within the lower 2 km. After this merger, other small- scale PV maxima continue to merge, overall resulting in an increase at z= 500 m to 40 PVU from 12 PVU over 1 hour and 40 minutes.

Assuming the circulation produced by the vorticity stretching and vortex merging maintains hydrostatic and gradient wind balance, the behavior of the balanced vortex in the presence of location heating and momentum sources, by using the Boussinesq approximation and insisting the vortex remains in thermal wind balance, results in the Sawyer-Eliassen

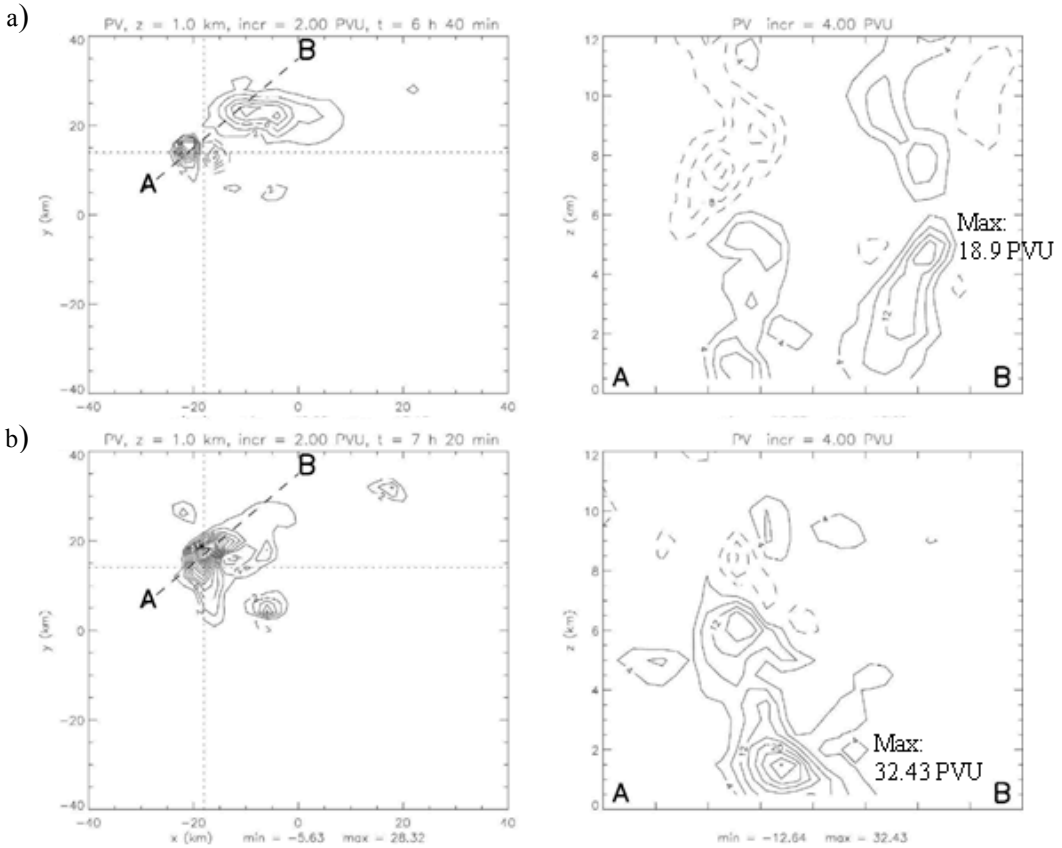

Figure 7: Rossby-Ertel PV at z=1 km at (a) 6 hours 40 minutes and (b) 7 hours 20 minutes (left) with corresponding cross sections (right) from M06. The dashed lines in the left images represent the locations on the cross section.

equation for a toroidal streamfunction. This equation is dominated by the diabatic heating rate (to one order of magnitude), instead of subsidence heating, the result of latent heat release trapped inside convective cores. The characteristic structure of deep convection can be seen in Figure 8. Associated with the area of upward vertical motion is positive diabatic heating, which increases with ensuing vortex mergers. These vortex cores, as well as the overall MCV, create a locally protected environment to support a more efficient conversion of latent heat energy. This thermodynamically direct toroidal circulation generates inflow at $z < 2$ km (near surface) and at 6 km $< z <$ 9 km (mid-to-upper troposphere), and outflow above 9 km. This circulation converges cyclonic vorticity from the MCV and the VHTs at the near-surface and mid-to-upper troposphere, accelerating the vortex mergers (M06).

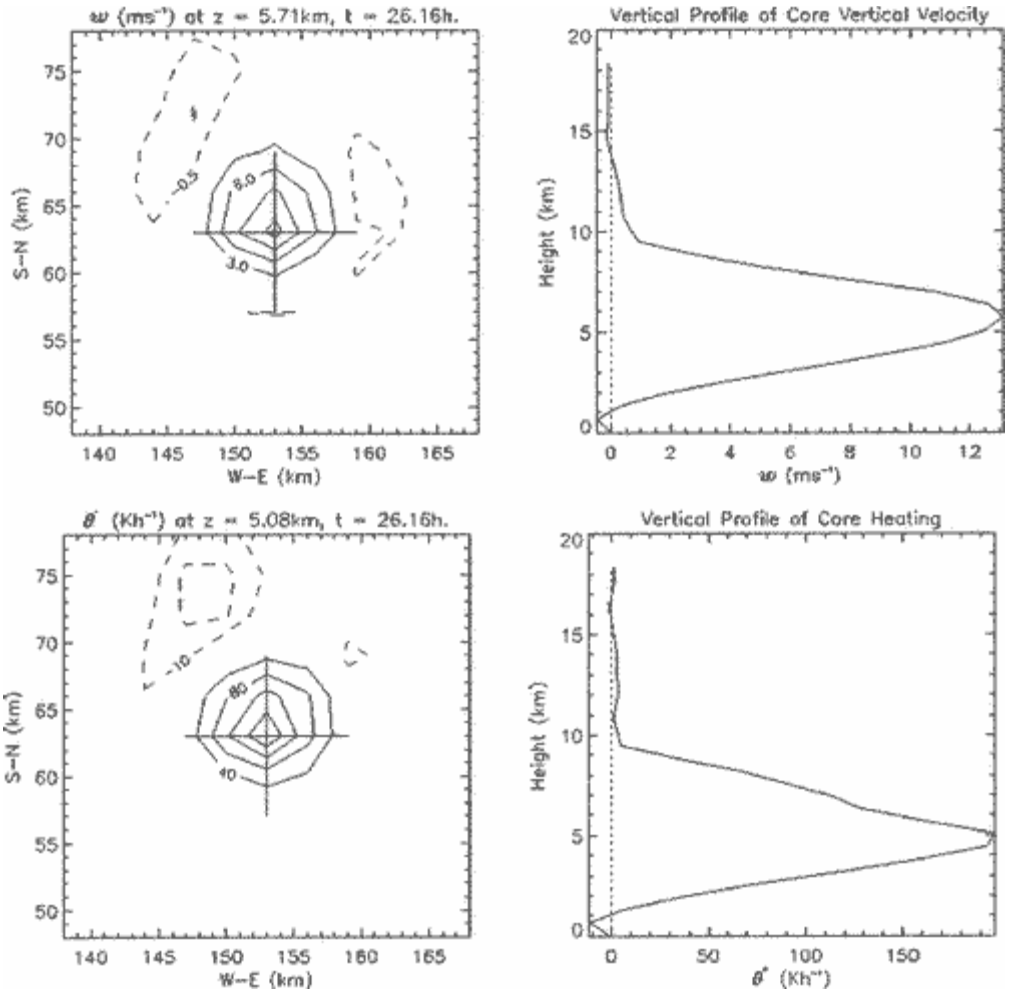

Figure 8: Characteristic vertical velocity and heating profile of a "Vortical" Hot Tower, plane view (left) and vertical profile (right) at the point marked with the cross of vertical velocity (top) and diabatic heating (bottom) from Hendricks et al. (2004).

One problem arises from the generation of convective VHTs, convective downdrafts. Air transported by convective downdrafts has a lower θ_e value, which can inhibit convection due to entrainment of drier air. Using RAMS, M06 indicates an area of convective inhibition 15 hours after initializing the control experiment. This stable environment associated with a downdraft in subsaturated air is seen in Figure 9a. However, 24 hours after initialization, conditionally unstable soundings are observed both on the periphery of the downdrafts (location C in Figure 9b) and in the area of the downdraft itself (location B in Figure 9b).

This indicates deep convection is still supported despite detrimental downdrafts associated with VHTs.

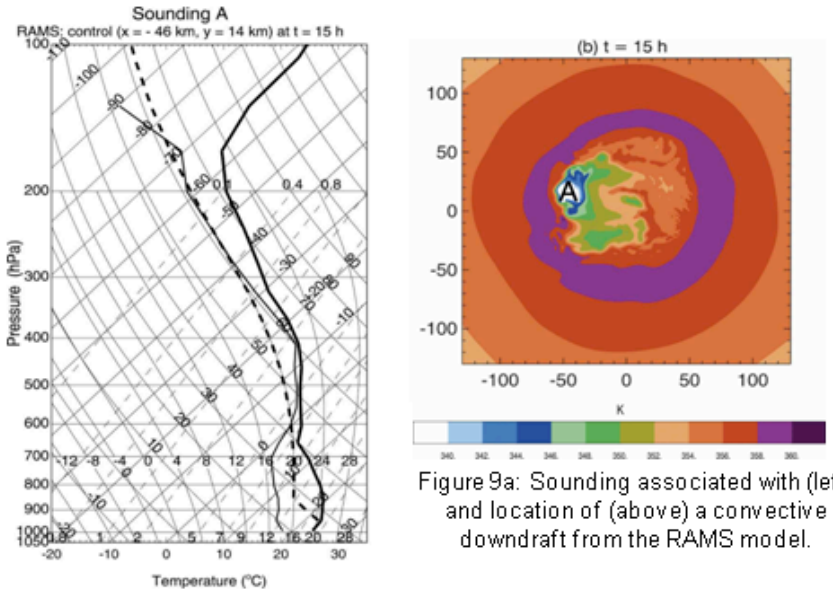

Figure 9a: Sounding associated with (left) and location of (above) a convective downdraft from the RAMS model.

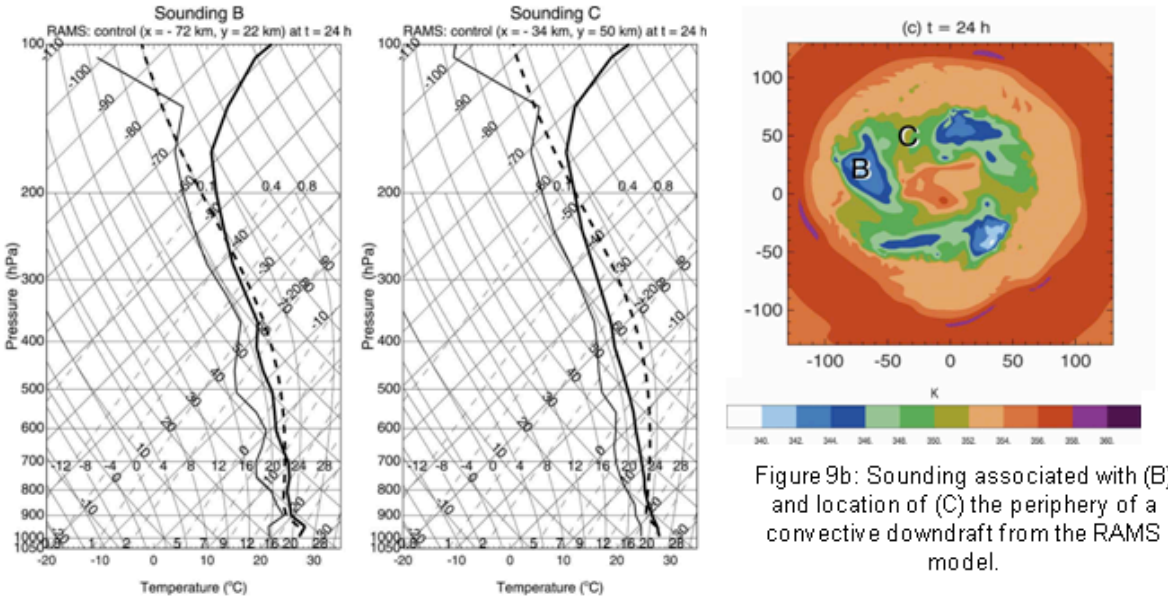

Figure 9b: Sounding associated with (B) and location of (C) the periphery of a convective downdraft from the RAMS model.

These VHTs can be observed within already developed TCs. Figure 10 contains a cross-section of a VHT from Western Pacific Supertyphoon Jangmi (2008), while at TS strength. This cross-section is from the airborne ELectra DOppler RAdar (ELDORA)

between 2310 and 2320 UTC on 24 Sept 2008 and is courtesy of Lieutenant Colonel Neil Sanger, United States Air Force. As seen in Figure 10, an updraft on the order of 9 m/s vertical motion (Figure 10a) is co-located with relative vertical vorticity values around 4 x 10^{-3} s^{-1} (Figure 10c) and z < 2 km convergence (Figure 10d). This convergence is a result of the inflow associated with the thermodynamically direct toroidal circulation from Equation 2. This updraft has a cloud top temperature colder than -80º C, colder than any tropical tropopause analysis (Jordan 1958). At 2330 UTC, the Multifunctional Transport SATellites 1R (MTSAT-1R) Full Disk scan, the only type of MTSAT-1R scan available for OT detection in GeoCAT (K. Bedka 2011, personal communication), detects 55 OTs using the modified OT detection algorithm. However, this VHT is not detected, as the coldest cloud pixel the closest OT is located too far away, at approximately 86.6 km with a BT of -87º C.

Yet, it is possible the VHT is beginning to decay by the time of satellite detection. Image acquisition time from MTSAT-1R is 27 minutes for a whole Earth scan like the one at 2330 UTC (Barton et al. 2004). Therefore, approximately 20 to 30 minutes, instead of 10, has elapsed between the ELDORA examination and MTSAT-1R detection. OTs can have a life span as short as 10 minutes (Gettelman et al. 2002), allowing for this VHT to decay prior to satellite detection. When reducing the required difference between the OT and the anvil temperature to 6.5 K, the original Bedka et al. (2010) threshold, the closest algorithm-detected OT is now only 20.4 km from the VHT location with an OT-anvil temperature difference of 7.3 K. Due to the elapsed time and the proximity of the OT to the VHT, this OT is likely the signature of the decaying VHT. Increased temporal resolution from the 1 hour MTSAT-1R used in this analysis, which will be available in the Atlantic Basin, could detect this VHT at the original OT/anvil temperature difference.

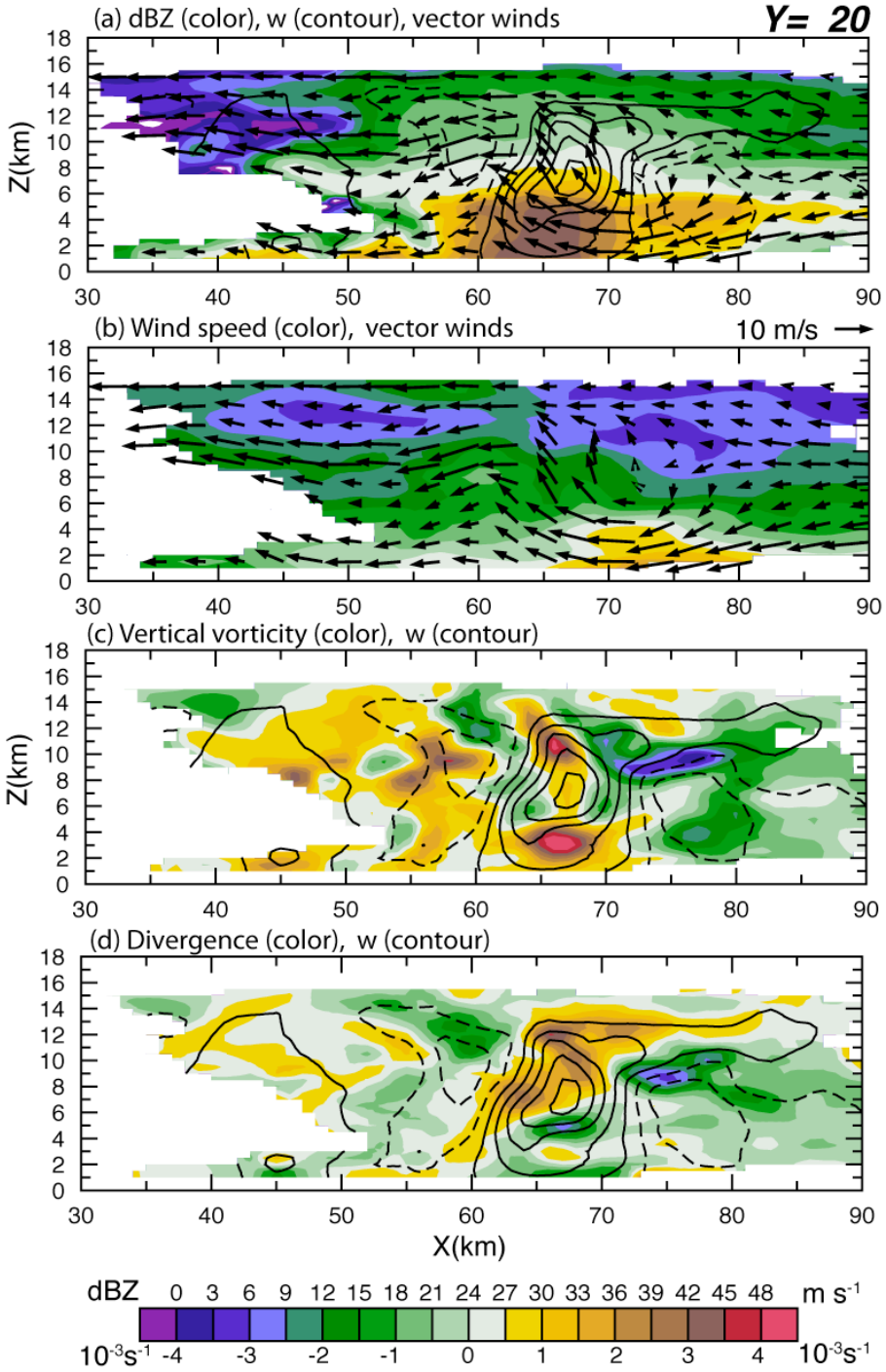

Figure 10: ELDORA vertical cross-section analysis from 2310-2320 UTC 24 September 2008. (a) Reflectivity (color), wind vectors and vertical velocity (contours, 2 m s^{-1} increments; solid contours are positive) (b) Earth-relative wind velocity in m s^{-1} (color), and wind vectors (c) Vertical relative vorticity (color) and vertical velocity in m s^{-1} (contours, 2 m s^{-1} increments; solid contours are positive. (d) Divergence (color, 10^{-3} s^{-1}) and vertical velocity (contour, 2 m s^{-1} increments; solid contours are positive) All figures are in the X-Z plane. Figure courtesy of Lieutenant Colonel Neil Sanger, United States Air Force.

3. Synopsis

In addition to the VHT theory, many additional studies have pointed to the role of convection in tropical cyclogenesis. For example, Simpson et al. (1998) indicates that, in the formation of Hurricane Daisy (1958), hot towers we necessary for tropical cyclone development. Particularly, the 500 hPa synoptic chart at 0000 UTC on August 24 indicated a small circulation with north winds of about 10 m/s and with a core temperature that was 1º C warmer than the surroundings. Since no explanation could be garnished from synoptic features, convective towers were necessary to produce this warm core. When reviewing the cyclogenesis of Tropical Storm (TS) Allison in 2001, Sippel et al. (2006) notes the generation of potential vorticity (PV) within organized updrafts and/or the merger of PV anomalies as a requirement for cyclogenesis. In addition, low level PV was being produced by the convection.

As vigorous hot towers can be defined as extending to (or through) the tropopause (Simpson et al. 1998, M06), the overshooting top (OT) detection algorithm will be applied in this research to detect these hot towers in an attempt to associate them with the genesis of a tropical disturbances. In later sections, correlations between detected OTs and the averaged vertical vorticity of selected tropical disturbances will be shown and whether these correlations might be used to forecast if and when TC genesis will occur.

a. Rapid Intensification

Predicting the rapid intensification (RI) of TCs continues to prove a challenge for operational forecasters. Error trends in the difference between forecasted intensity and actual intensity have seen little reduction since 1990 (Figure 11). Improving the prediction of RI continues to be a top priority for the National Hurricane Center (NHC) (Rozoff and Kossin 2011,

hereafter RK11). Forecasting RI, which has been defined as 24-h increases in the 1 minute maximum sustained surface wind speed of at least 25, 30, or 35 knots (Kaplan et al. 2010, hereafter KDK10), has proven to be difficult due to incomplete understanding of underlying physical processes (RK11). Most researchers link the ocean, inner-core processes, and/or environmental interactions to TC RI. However, few studies were solely devoted to the topic until Kaplan and DeMaria (2003, hereafter KD03).

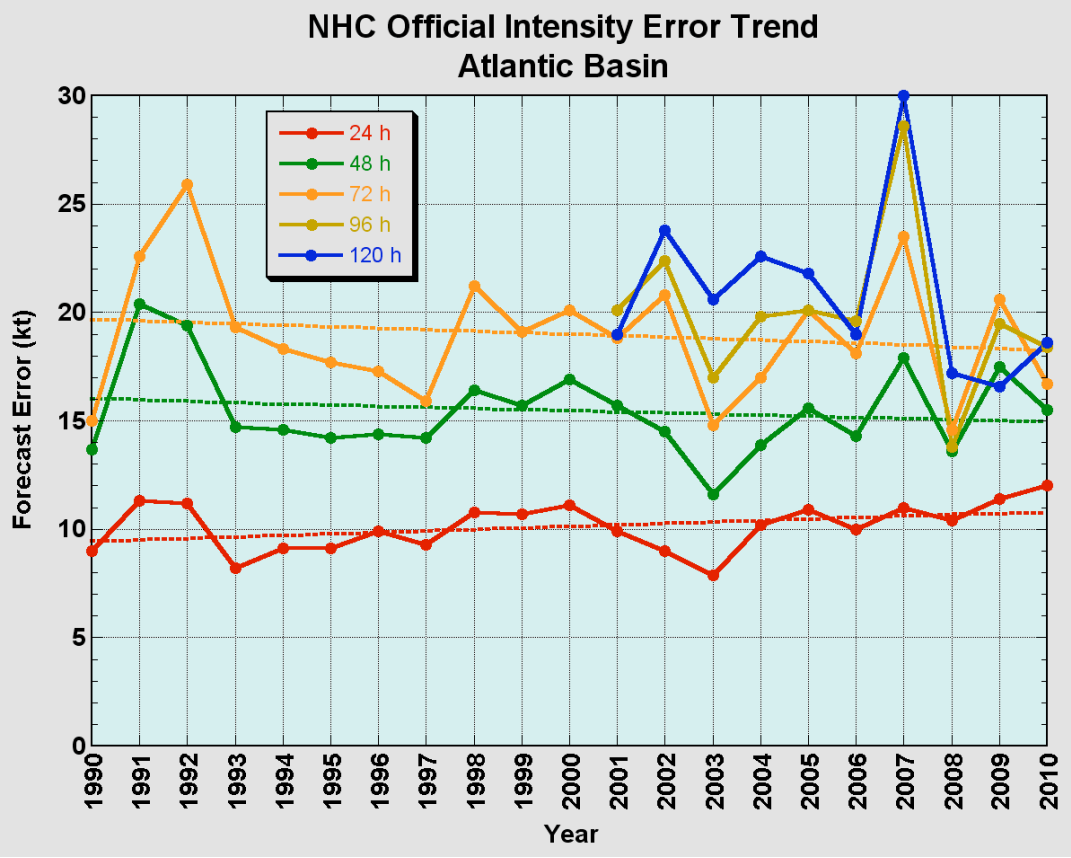

Figure 11: Official NHC intensity error trend from 1990 to 2010. Dots represent the average error in knots between the forecast and the actual intensity for each respective year, with dashed lines representing the trends. Image courtesy of Franklin and Cangialosi (2011).

1. Historical Review of Rapid Intensification Prediction

Operational TC intensification prediction began with the Statistical Hurricane Intensity FORecast (SHIFOR) model. Presented by Jarvinen and Neumann (1979), it

combines the 7 predictors selected from the CLImatology and PERsistence (CLIPER) model for the statistical prediction of TC motion and was developed using TCs from 1900-1972 that were at least 30 nautical miles from land. The employed stepwise regression procedure developed 3rd order prediction equations with up to 10 terms plus the intercept constant. Any insignificant predictors are assigned low regression coefficients and the most important predictor is a function of the forecast time. SHIFOR and CLIPER were the only intensification models run in near real-time until 1993 (DeMaria and Kaplan 1999).

The Statistical Hurricane Intensity Prediction Scheme (SHIPS) looked to improve the SHIFOR intensity forecasts. The original SHIPS used 10 climatological, persistence, and synoptic predictors for intensity prediction out to 72 hours. Using a multiple regression scheme, a predictor is considered significant if the probability a regression coefficient is different from 0 exceeds 95%. SHIPS was developed from named storms during 1989-1992, including the depression stage, but only for cases over open water during the entire forecast period -- landfalling TCs are not used. Results indicated the average intensity errors associated with SHIPS are 10-15% smaller than SHIFOR; however only 50% of the variance observed with TC intensity changes was explained by SHIPS (DeMaria and Kaplan 1994a).

SHIPS continued to receive upgrades from its 1994 form. Removal of the TC circulation from synoptic models was done using a Laplacian filter, allowing for a more accurate representation of the surrounding synoptic environment (DeMaria and Kaplan 1999). Additional predictors were also added, including satellite data, namely Geostationary Observing Environmental Satellite (GOES) IRW information and oceanic heat content estimates from satellite altimetry observations. These changes lead to addition forecast improvements of 3.5% in the Atlantic Basin. Beginning in 1996, SHIPS was run on the

synoptic times (0000, 0600, 1200, and 1800 UTC) using a 6 hour old National Center for Environmental Prediction (NCEP) forecast from the previous synoptic time to increase timeliness. Operational implementation of the SHIPS during the 1997 Atlantic hurricane season revealed the forecast had statically significant skill relative to climatology and persistence. Forecasts were extended to 5 days, and a method for storm decay over land was also added (DeMaria et al 2005).

SHIPS now allowed for skillful official NHC prediction of TC intensity out to 72 hours. However, forecasting RI still proved challenging, with the unanticipated RI of Hurricanes Opal (1995) and Bret (1999) within 72 hours of landfall in the US illustrating the need for a better understanding of RI. KD03 investigated the large-scale characteristics of RI, then defined as a 30 knot increase in the one-minute maximum sustained surface winds, in TCs from 1989 to 2000. Five predictors from SHIPS were recognized that could identify the probability of RI. These predictors included intensity change during the previous 12 hours (PER), 850-200 hPa vertical shear averaged within a 200 and 800 km radius (SHRD), SST, maximum potential energy minus current intensity (POT), and 850-700 hPa relative humidity averaged within a 200 and 800 km radius (RHLO). The probability of RI increased to 41% when all 5 of the respective thresholds are reached. However, even with the additional knowledge, the NHC did not correctly predict the 12 instances of RI in the Atlantic Ocean from 2003-2004 (Elsberry et al. 2007).

A revised rapid intensification index (RII) for the Atlantic Ocean was proposed by KDK10, using TCs from 1995 to 2006. The RII included 4 of the original RI predictors from the KD03 RI prediction, PER, SHRD, POT, and RHLO. In addition, 4 new predictors were added. They include 200 hPa divergence within 1000 km of the TC center (D200), and 3

satellite predictors: the percent area within 50 to 200 km covered by IR cloud top brightness temperature (CTBT) ≤ 30º C (PX30), the standard deviation of the IR CTBT within 50 to 200 km (SDBT) and the ocean heat content (OHC). Unlike KD03, scaled magnitudes of the predictors were used to determine the likelihood of RI within the next 24 hours. KDK10 also introduced addition RI thresholds: 25 kt and 35 kt. The now three thresholds of RI: 25 knots, 30 knots, and 35 knot, represent the 90th, 94th, and 97th percentile, respectfully, of all Atlantic basin tropical and subtropical over water intensity changes for the period 1989-2006. Independent analysis of the 2006 and 2007 indicated the RII correctly predicted 15% (35 kt) to 59% (25 kt) of the RIs occurring within the succeeding 24 hours. However, 71% (25 kt) to 85% (35 kt) of the predicted RI events did not occur, demonstrating the difficulty in predicting RI.

Additional modifications to the SHIPS RII have been proposed by RK11, providing further probabilistic prediction of RI using both a logistic regression and an empirical Bayesian probability models. These models included optimal SHIPS predictors; however the optimal predictors varied slightly for the logistic and Bayesian schemes. In a dependent test of TCs from 1995-2009, the logistic scheme showed reliability at lower RI forecast probabilities while the Bayesian model was more likely to successfully produce high RI probabilities. While both of these models were competitive compared to the operational RII, an ensemble mean of the SHIPS-RII, logistic, and Bayesian improved the Briar skill scores by 33% compared to the current operational SHIPS-RII.

2. Theory of Rapid Intensification

Initial investigation into the causes of RI focuses on three main areas: the role of the ocean, inner-core processes, and environmental interactions. Early studies of ocean indicated

its beneficial impacts on TC intensity. However, as indicated by Hennon (2002), the ocean can play both a beneficial and a detrimental role to a RI. While the ocean can provide heat to fuel a convective burst, a highly asymmetric convective burst can disrupt the circulation. Nolan et al. (2007) further confirms that purely asymmetric heating sources, used to represent the rapid latent heat release in cumulus updrafts, causes vortex weakening due to the extraction of energy as the asymmetries undergo transient growth. In addition, oceanic upwelling and vertical mixing by the TC vortex may act cool the underlying ocean. Modeling studies undertaken by Bender et al. (1993) indicates the sea surface cooling produced by the TC can reduce the ultimate TC intensity. The effects of oceanic cooling on Hurricane Opal (1995) can be seen in Figure 12a, courtesy of Emanuel et al (1999). When modeling Opal using a fixed oceanic temperature, the maximum intensity achieved is greater than either the actual intensity or the intensity derived when not accounting for oceanic interactions.

However, warm ocean eddies may reduce the magnitude of the oceanic cooling. Hurricane Opal (1995) experienced one such warm eddy, with about 60% of Opal's intensification is due to the warm ocean eddy according to Hong et al. (2000). Modeling results (Figure 12b) from Emanuel (1999) indicates a more accurate intensity prediction when accounting for the ocean eddy. Overall, despite its potential harmful effects on TCs through asymmetric convection, results from RK11 indicates that RI TCs experience a warmer SSTs and greater ocean heat OHC than non-RI cases. Therefore, a greater OT response could be observed in RI cases, as convection in regions with strong ascending large-scale motion increases monotonically with SST in the range of 26º - 29º C. However, other research has shown SSTs to be similar in intensifying and rapidly intensifying TCs,

indicating the rate of intensification is not significantly dependent on SST (Hendricks et al. 2010).

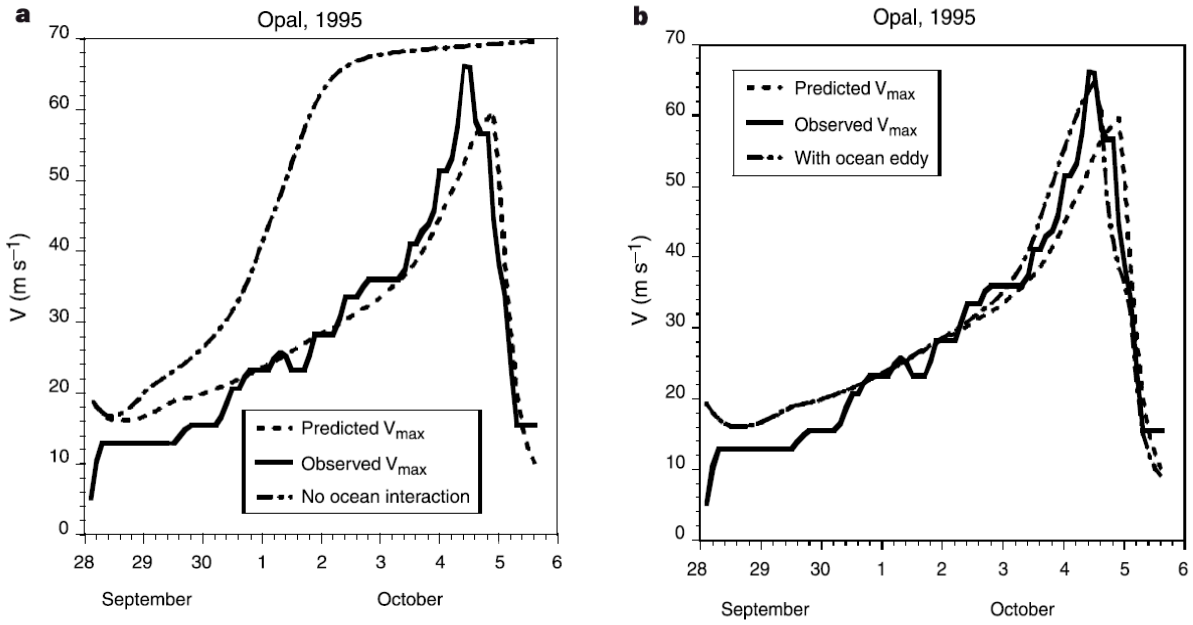

Figure 12: (a) Hurricane Opal (1995) predicted wind speeds with no model ocean interaction (dotted dashed) compared to the observed (solid) and predicted (dashed) wind speeds. (b) Hurricane Opal (1995) predicted wind speeds with ocean eddy (dotted dashed) and predicted (solid) wind speeds without the ocean eddy. Images courtesy of Emanuel (1999).

Another oceanic influence on TC intensification is the wind induced surface heat exchange. Commonly known as WISHE, Emanuel (1986) notes evaporation from the sea surface was essential to intense storms. WISHE is a positive feedback process, in which the wind speed further increases the evaporation. This increases the boundary layer specific humidity, with further leads to an increase in the wind speed. Should the boundary layer saturate, however, this process would cease (Montgomery and Smith 2010). To avoid the problem of saturation, Montgomery et al. 2009 suggests the vortex is intensified by buoyant VHTs, OT proxies, as a simulated vortex intensifies even when the wind speed is capped at a trade-wind value. This intensification is achieved either through the conservation of angular momentum wither in the boundary layer or above it.

In addition to the oceanic influence, many sources have indicated that an increase in convection within the inner core as a precursor to RI. However, the role of inner-core dynamics and RI is complicated by the unresolved issues of internal TC dynamics (RK11), with different mechanisms attributed to RI. Heymsfield et al. (2001) indicates the intensification of Hurricane Bonnie (1998) results from an increase in subsidence. On the other hand, using 1.67 km mesoscale mode, Rodgers (2010) notes the onset of RI in Hurricane Dennis (2005) is tied to an increase in the convective precipitation in the inner core, with the immediate cause of the RI being a significant increase in upward mass flux. This mass flux is accomplished primarily by updrafts on the order of 1-2 m/s. During genesis, the defined VHTs from M06, which will be approximated by OTs, experienced the same updraft speeds. Other research have also linked latent heat release from convection and enhanced inertial instability to TC intensification changes (Schubert and Hack 1982, Nolan et al. 2007).

Another inner-core process linked to TC intensity changes has been concentric eyewall cycles. Willoughby et al. (1982) describes concentric eyewalls as a secondary ring of active convection outside in pre-existing eyewall. This outer eyewall can often contract and intensify while the inner eyewall weakens. Intensity and inner-core changes result from these events, known as eyewall replacement cycles (Kossin and Sitkowski 2009). This can reduce the maximum wind speed, as reconnaissance aircraft observed in Typhoon Sarah (1956) (Willoughby et al. 1982). However, the TC vortex can ultimately intensify through this cycle. Research has suggested this possibly is a result of convectively induced regions of PV, caused by VHTs and potentially indicated by OTs, undergoing axisymmetrization. As Montgomery and Kallenbach (1997) indicates, an increase in the eyewall tangential winds

occurs if the PV is introduced near the radius of maximum winds (RMW). However, even if the PV in located a sufficient distance outside the RMW, the tangential winds beyond the eyewall increase, with the outer wind maximum contracting (Moller and Montgomery 2000).

Many environmental factors can also play a role in modulating TC intensity. When developing SHIPS, DeMaria and Kaplan (1994a) noted that vertical shear is the second most important predictor of intensification changes, behind oceanic influences such as SST. Typically, RI cases have lower 850-200 hPa vertical shear than non-RI cases (RK11). There are competing factors explaining why vertical shear inhibits TC intensification. One theory suggests vertical shear increases the ventilation of heat and moisture, advecting it away from the low-level circulation (Gray 1968) or through fluxes of low-entropy air into the eyewall (Tang and Emanuel 2010). In addition, vertical wind shear may also act to tilt the vortex, inducing a mid-level warming which suppresses convection and inhibits further development (DeMaria 1996). OTs can potentially be used as indicators of sheared TCs, as vertical wind shear confines convection to the downshear side of the TC (Corbosiero and Molinari 2002). Vertical wind shear may also be associated with the Saharan Air Layer (SAL), with an easterly wind maximum located on the southern or southwestern edge of the SAL. The intensity of TCs not located on this edge can also be suppressed by the SAL, as seen with Hurricane Joyce (2000) (Dunion and Velden 2004). Those that emerge, however, like Hurricane Erin (2001), rapidly becoming strong TCs. In addition, other research has linked TC intensification, such as the RI of Hurricane Opal (1995), to an upper level trough and jet increasing upper level divergence (Bosart et al 2000). Divergence at 200 hPa is greater for RI cases than non-RI cases (RK11).

3. Synopsis

In addition to SHIPS-RII, other endeavors of identifying intensification changes through the use of satellite-analyzed convection in the tropics have also been undertaken. Steranka et al. (1986) indicates that 71% of TCs producing surges of convection lasting at least 9 hours and have cloud tops within 222 km of the center colder than 238 K experience an increase in the maximum sustained winds by at least 5 m/s (9.7 kt) within 24 hours. Olander and Velden (2009) identifies proxy overshooting convection through the differencing of the IR and WV channels which has strong correlations to the TC intensity changes.

Even though OTs cannot be tied to all variables considered by operation RI models, such as divergence and ocean heat content, the above research has suggested the potential role of convection in TC RI. Thus, an attempt will still be made to forecast RI solely based on the OTs. In later sections, RI forecasts will be made based on exceeding an average OT/scan threshold for each respective RI threshold defined by KDK10. OTs will then be added as a predictor to the logistic regression model presented by RK11 to investigate if they can further improve multi-predictor RI models.

III. Data

a. Satellite Data

1. Overshooting Top Detection Algorithm

The original objective satellite-based overshooting cloud top detection algorithm used in this analysis was developed by Bedka et al. (2010). The method is formulated around the premise that OTs appear as small clusters of IRW pixels (≤ 15 km diameter) that are significantly colder than the surrounding anvil cloud. Identification begins by first looking

for relative BT minima that are lower than 215 K and the numerical weather prediction (NWP) tropopause temperature (Figure 13a). A BT of 215 K was chosen as the maximum temperature of OTs because it captures 96% of 450 1 km Moderate Resolution Imaging Spectroradiometer (MODIS) and Advanced Very High Resolution Radiometer (AVHRR) thunderstorms analyzed by Brunner et al. (2007). These minima are then sorted by increasing BT and subsequently looped through to ensure that no temperature minima are located within 15 km of each other, as the analysis of the Brunner et al. (2007) dataset revealed the largest OT diameter was 12 km. This ensures portions of the same OT are not classified as two independent tops (Bedka et al. 2010).

Next, the IRW BT of the anvil cloud surrounding the potential OT is then sampled at a 3 pixel radius (~12 km radius) in 16 directions (22.5° equally spaced angle intervals) (Figure 13b). These surrounding anvil pixels must have an IRW temperature at least as cold as 225 K to be included in the computation of the mean anvil BT. At least 5 valid anvil pixels must satisfy this criteria for the BT minima to be considered a "candidate overshooting pixel." Pixels warmer than 225 K (circled in Figure 13c) are not included in the anvil mean BT. The 5-of-16 pixel criterion is imposed to ensure that the anvil is of relatively large horizontal extent while still allowing the anvil to occupy as small as a 90° quadrant, which might occur if horizontal winds are shearing the cloud anvil (Bedka et al. 2010).

A "candidate overshooting pixel" is classified as an overshooting top if it is at least 6.5 K colder than the mean BT of the surrounding anvil cloud. This would imply that the pixel is slightly lower than 1 km above the anvil, assuming a 7-9 K/km lapse rate (Adler et al. 1983). As this process identifies only one pixel at the location of an OT minimum BT, a filling procedure can performed when necessary to capture the remaining neighboring pixels

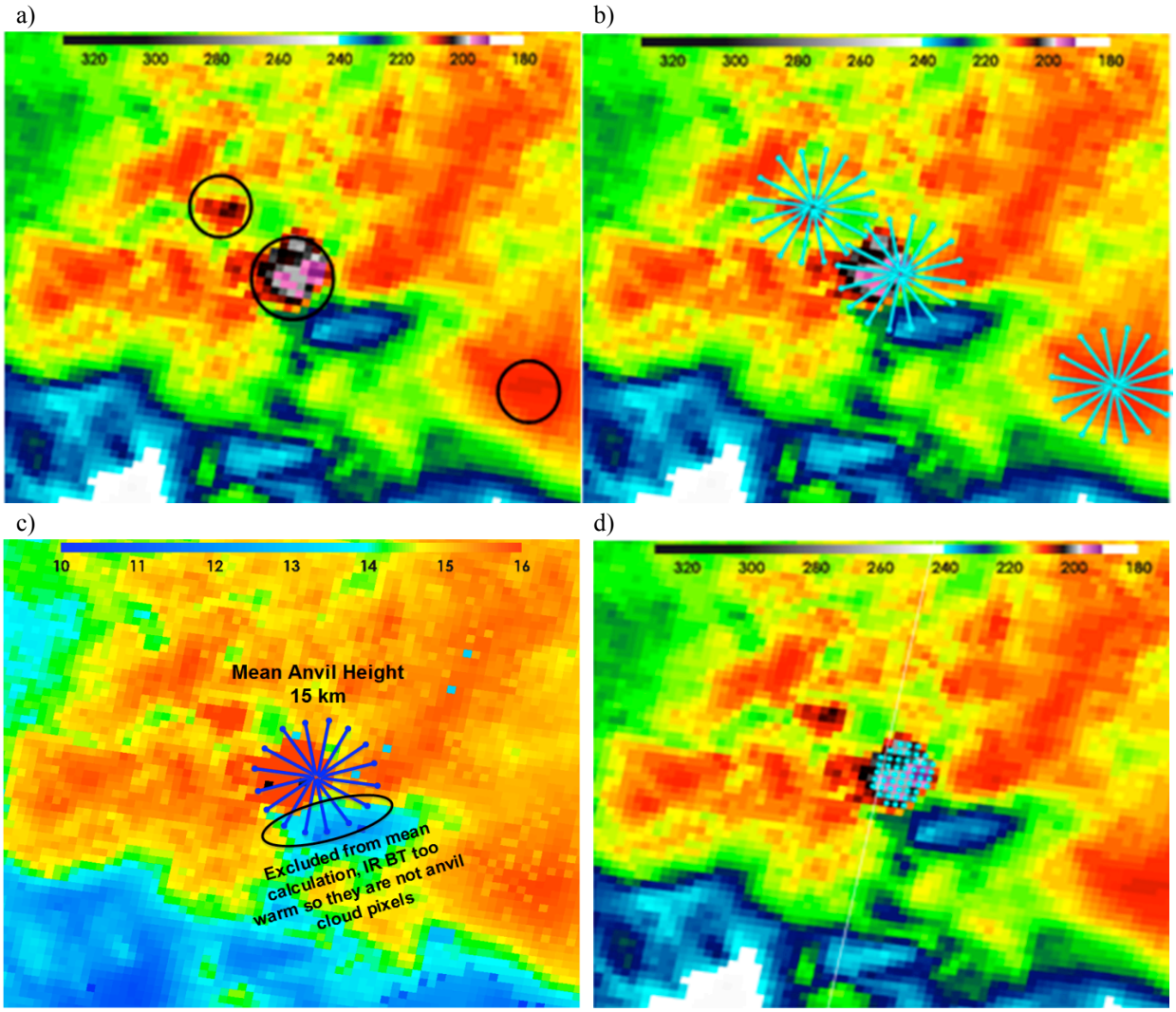

Figure 13: The process of identifying an overshooting top from the 11 μm brightness temperature window. (a) Minima colder than 215 K identified. (b) The surrounding anvil is sampled. The mean surrounding anvil must have a temperature colder than 225 K. (c) Pixels which do not satisfy the BT ≤ 225 K are not included in the mean anvil temperature (note temperature scale change). At least 9 of the 16 anvil pixels must be included for the minima to be classified as a "candidate" OT. (d) The final OT pixels are filled in. These pixels must be within a 6 km radius of the identified OT pixel and colder than the OT temperature plus 50% of the difference between the mean anvil BT and the OT temperature. Images courtesy of Kristopher Bedka, Science Systems and Applications, Inc.

that comprise the entire OT. These pixels must be within a 6 km radius of the identified OT pixel and at least colder than the OT BT plus 50% of the difference between the mean surrounding anvil BT and the OT temperature (Bedka et al. 2010). The final filled OT from the image sequence in Figure 13 can be observed in Figure 13d. For this research, only the coldest OT pixel will be used.

Using a combination of synthetic satellite imagery and cloud top height derived from a cloud-resolving NWP simulation, Bedka et al. (2010) shows that both a greater Anvil - OT BT difference (magnitude of the overshooting top) and a greater number of pixels included in the mean can be used to reduce the false alarm ratio (FAR) of OT detections, percentage of identified OTs which are not OTs. Results show a FAR ranging from 4.2 to 38.8% depending on the values of these two parameters. Comparison between the GOES-12 OT detections with CloudSat observed OT events indicates an algorithm false alarm rate of ~18% when 5 of 16 pixels are included in the mean anvil BT computation with an Anvil and OT BT difference of at least 6.5 K.

OTs are detected from the IRW BT data through the use of Geostationary Cloud Algorithm Testbed (GeoCAT), a cloud retrieval algorithm development tool. GeoCAT implements arbitrary algorithms via entries through an xml file. Since the algorithms implemented by the Center for Satellite Applications and Research (STAR) algorithm working group require a significant amount of ancillary data, GeoCAT has developed efficient routines to make this available to all pixels. Current ancillary data-sets include Global Forecasting System (GFS) model, Global Data Assimilation System (GDAS), Interactive Multisensor Snow and Ice Mapping System (IMS) snow, SEEBOR surface emissivity, digital elevation, surface typing, a land mask, a coast mask, and a volcano mask. GeoCAT has been demonstrated on multiple satellites including GOES-10, GOES-11, GOES-12 and METEOrological SATellite (METEOSAT)-1, with GeoCAT also being able to handle temporal demands and scan-line overlap (Heidinger 2008).

2. Applications to TC Genesis

In this analysis, both the GOES-E Northern Hemisphere and the METEOSAT-9

Second Generation Full Disk scans were employed at a temporal resolution of 30 minutes, as advocated by Hendricks et al. (2004), to sample OTs. METEOSAT-9 does provide a temporal resolution of 15 minutes; however this cannot be matched by the GOES-E NH satellite scan. However, assuming these OTs are proxy-VHTs, their lifetime should be on the order of an hour (M06), allowing for adequate sampling with the 30 minute temporal resolution. A boundary of 40° W is placed between the two satellites. The GOES-E satellite is located at a longitude of 72° W, while the METEOSAT-9 satellite is positioned a 0° W. While the scan angle on the METEOSAT-9 satellite at 40° W is greater than the GOES-12 scan angle at 40° W, the METEOSAT-9 satellite boasts a higher spatial resolution in the IRW than the GOES-12, 3 km instead of 4 km, respectively, allowing for approximately equal scan footprints at 40° W.

3. Applications to Rapid Intensification

For this analysis, three different satellite scans will be employed. The GOES-E Contiguous United States (CONUS) scan is utilized, which has a temporal resolution of 15 minutes and a scan range from 110º W to 62º W. Also available for analysis in 2004 (L. Cronce 2010, personal communication), METEOSAT data is used. The use of the METEOSAT scan would provide almost complete coverage of the Atlantic Ocean every 15 minutes, as the METEOSAT scan extends to the eastern most edge of the CONUS scan. This greater temporal resolution is desired, as the duration of an OT can be as short as 10 minutes (Gettelman et al. 2002). However, the analysis of developed TCs, the end of the METEOSAT scan will be defined as 55º W. This is because OTs at the westernmost edge of the METOESAT scan area may not be identified due to the large scan angle due to the location of METEOSAT at 0º W. As seen in Figure 14, with gray background representing

the area scanned by METEOSAT, the OTs surrounding Hurricane Dean (2007) are not observed by METEOSAT even though they fall within the scan area. Thus, TCs occurring after 2004 located between 55º W and 62º W are analyzed with the GOES-E NH scan at 30 minute temporal resolution. Prior to 2004, TCs east of 62º W are analyzed by the GOES-E NH scan up to 40º W, with no analysis east of 40º W. In addition, TCs located west of 62º W but south of 15º N are also only analyzed every 30 minutes due to the extent of the CONUS scan range. The satellite scans used for this analysis can be seen in Figures 15a for 1995-2004 and 15b beginning in 2004.

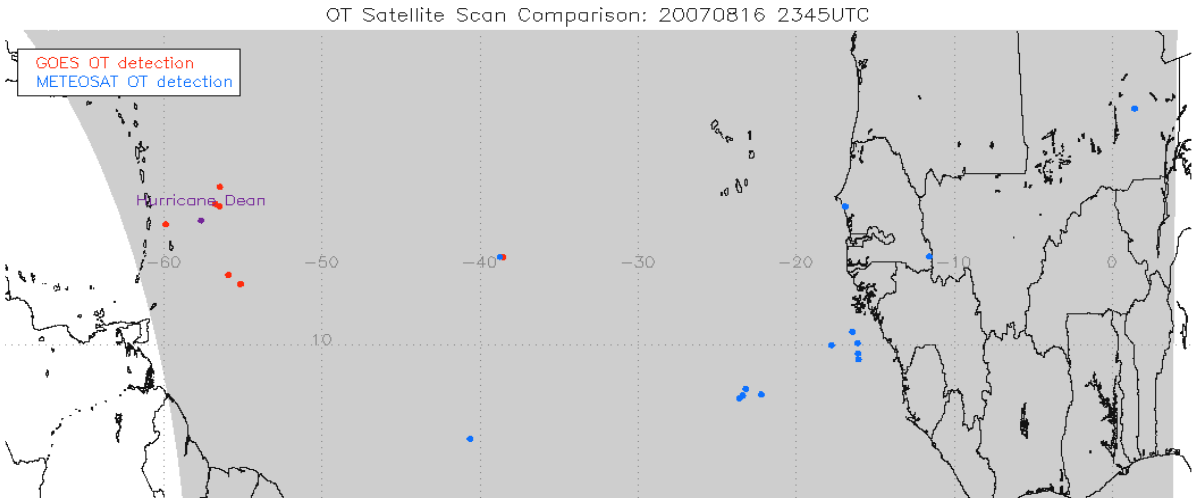

Figure 14: OT detections from METEOSAT (blue) and GOES-NH (red) satellite scans. The gray background represents the METEOSAT area scanned. Note the OTs not detected by METOSAT around Hurricane Dean. The METEOSAT analyzed OTs are restricted to 55º W because of the missed OTs around Hurricane Dean.

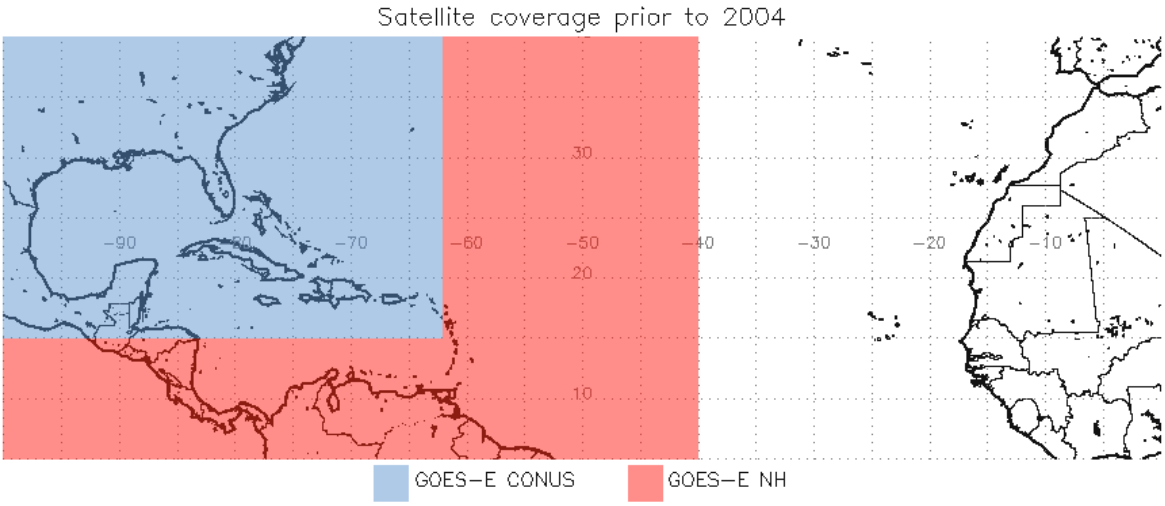

Figure 15a: Satellite scan coverage for 1995-2004. Areas in blue have a 15 minute temporal resolution with GOES-E CONUS while areas in red experience 30 minute temporal resolution with GOES-E NH.

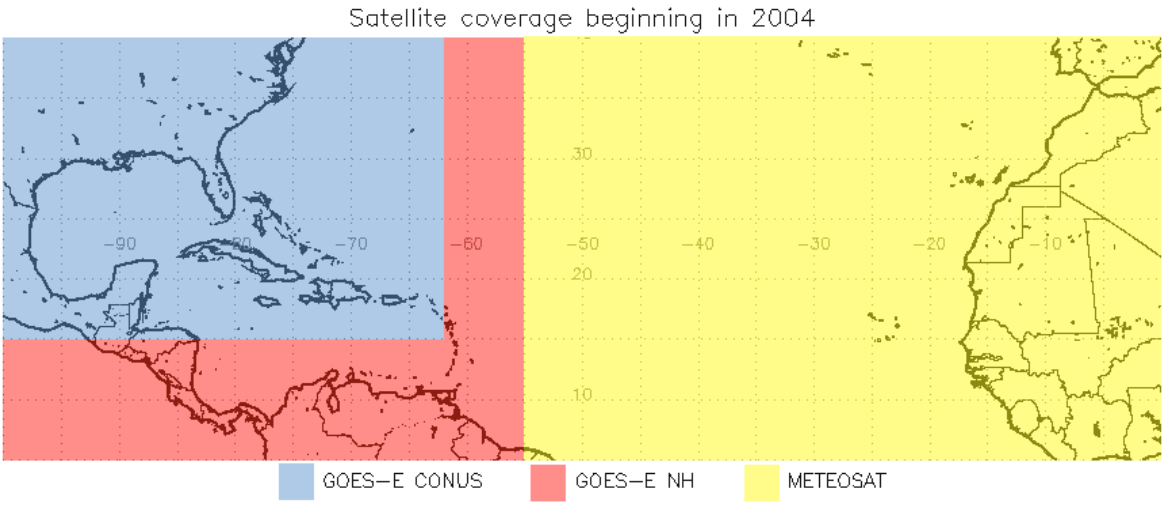

Figure 15b: Satellite coverage beginning in 2004. Areas in blue and yellow have a 15 minute temporal resolution with GOES-E CONUS and METEOSAT. Areas in red have 30 minute temporal resolution with GOES-E NH.

b. Numerical Weather Prediction Data

Bedka et al. (2010) developed an OT algorithm for the mid-latitudes. In this algorithm, candidate overshooting top pixels are compared to the NWP tropopause temperature to verify that these pixels are indeed cloud tops "overshooting" their equilibrium levels in the tropopause region. However, there are some questions as to whether the NWP

tropopause temperature (TT) is accurate in the tropics for OT analysis. In the Tropical Western Pacific, the NWP tropical tropopause systematically has a cool bias, which is intensified during convection (Culverwell and Milton 2000); however it is unclear whether this bias extends to the Tropical Atlantic. TCs may also lift and cool the tropopause more than other mesoscale systems which, if true, implies that the higher frequency of cold cloud tops might not imply higher overshooting in TCs (Romps and Kuang 2009). Ed Zipser (2010, personal communication) also indicates that trying to extend this analysis to the tropopause should not be considered, as "One could get an order of magnitude difference in number of towers by varying the definition, and the worst problem came with trying to define the tropopause Z (height) or T (temperature)." Using PFs from the TRMM radar, Liu and Zipser (2005) calculates the total number of PFs with a radar reflectivity of 20 dBZ with a brightness temperature colder than the tropopause is approximately 7 times greater than PFs reaching 14 km, the level of zero net radiative heating. Liu and Zipser (2005) also indicates the mean reference height for the tropical equilibrium level, which must be exceeded based on the AMS definition of an OT, is almost 2 km lower than the NCEP tropopause height in the tropics.

After removal of the NWP TT check, other factors are considered when setting the maximum temperature of the candidate OTs pixels. According to Jordan (1958), the temperature of the mean reference height for the equilibrium level (14.55 km) from Liu and Zipser (2005) is approximately 205 K during the "hurricane season" of July-October. This is colder than the cloud top temperature used by Bedka et al. (2010) when analyzing 1 km data. However, the 4 km spatial resolution GOES-East (GOES-E) satellite has a cloud top height approximately 1 km lower than the visible cloud top heights which have a spatial resolution

of 1 km (Sherwood et al. 2004), experiencing a warm bias in the IRW of around 5-7 K. Thus, the analyzed MODIS and AVHRR IR cloud tops are lower and warmer than the cloud tops analyzed as the same temperature by GOES-E. It is also important to note that the location of the 20 dBZ PFs top used in the global convection distribution by Liu and Zipser (2005) is typically lower in the atmosphere than the IRW detected cloud top. Therefore, a warmer 215 K maximum OT BT is maintained for this initial analysis while removing the NWP TT from the algorithm criteria. Further analysis will include limiting the OT BT colder than 205 K and 200 K, a tropopause height of 16 km (Jordan 1958, Montgomery and Farrell 1993, Simpson et al. 1998). Since most clouds can be approximated as a blackbody in the IRW, the BT is a good measure of physical temperature (Petty 2006). In addition, this research attempts to produce a climatology of TC pre-genesis and intensification OTs, and therefore does not want to rely on the accessibility of NWP tropopause data, first available for the 2001 Atlantic hurricane season.

However, removal of the NWP TT can introduce many false alarms. Table 1a compares the accuracy of the 6.5 K Anvil – OT BT difference (BTD) when using 5 out of 16 candidate anvil pixel threshold when both the NWP TT is used and is not used for the 1 km MODIS to CloudSat OT events, where a > 0.5 K OT magnitude is required. The probability of detection (POD) and FAR for the satellites used in the research, using the original Bedka et al. (2010) algorithm, can be seen in Table 1b. Table 1a indicates that, while the OT POD increases when not using NWP TT, the OT pixel FAR also increases by 44%. Therefore, an additional 44/100 detected OTs without the NWP TT would not be detected when using the NWP TT. This is 3.75 times the FAR associated with the NWP TT. Applying this increase to Table 1b, the FAR would equate to 37.5% for the GOES-E and 85.5% for the

METEOSAT Second Generation satellite. However, it is important to note the OT detection algorithm may be capturing smaller magnitude OTs not found in CloudSat, thus not all false alarms are false alarms when the TT check is removed.

a)

OT detection Method	OT pixel FAR	POD for Top Regions	Number of OT Detected Pixels Along CloudSAT Track
IRW-texture (with GDAS Tropopause Temperature Check)	16.0%	75.4%	943
IRW-texture (without GDAS Tropopause Temperature Check)	60.0%	92.1%	2612

b)

Satellite	OT pixel FAR	POD for Top Regions
GOES-E	10.0%	46.2%
METEOSAT-9	22.8%	64.7%

Table 1: (a) Comparison of Anvil – OT BT ≥ 6.5 K and 5 out of 16 Anvil pixels for both when the Global Data Assimilation System (GDAS) NWP tropopause temperature (TT) check is included and removed from the original Bedka et al. (2010) OT detection algorithm criteria at 1 km resolution. (b) FAR and POD for the satellites used in this analysis. Table courtesy Bedka et al. (2011a).

Two modifications are made to the no NWP TT OT detection algorithm to reduce the number of false OT detections from the GOES-E and METEOSAT-9 satellites. The BTD is increased to 9 K, now a 1.2 km height difference (Adler et al. 1983) instead of just below a kilometer. This is done to increase the likelihood that the algorithm is not simply detecting the "bumpiness" of a growing cumulus cloud potentially below the equilibrium level, since a BT of 215 K is approximately 13 km above the surface (Jordan 1958). However, analysis from 2002 indicates the Jordan mean sounding is colder at any given level (Dunion and Marron 2008), increasing the height of the 215 K temperature level above the surface however still below 14 km. When increasing the BTD to 9 K in analysis including the NWP TT, a reduction of the FAR by half is observed (Bedka et al. 2010). In addition, the number of candidate anvil pixels is increased to 9, still allowing for strongly sheared storms to be

analyzed but reducing the likelihood of falsely detecting a single growing cloud.

1. Validation: Comparison between the modified and the original OT detection algorithm

Validation of the tropical OT detection algorithm can be achieved through comparisons with the original algorithm as presented by Bedka et al. (2010) and the visible image. One such case can be observed in Figure 16, which contains the northern most edge of an area of potential tropical cyclogenesis from the end of the 2010 Atlantic hurricane season. When using the original Bedka et al. (2010) satellite detection algorithm (Figure 16a) the number of detected OTs is greatly reduced compared to the 8 detected by the tropical OT detection algorithm in Figure 16b. This occurs even though the original algorithm requires less BTD between the OT and the anvil, thus missed OTs by the tropical algorithm could be the result of a BTD below 9 K but greater than 6.5 K used in the original algorithm. Thus, the observed increase in the number of OTs is a result of the lack of use of the NWP TT in the tropical algorithm.

However, comparison with the IR image (Figure 16c) does not appear to indicate that the areas detected by the tropical OT algorithm are not overshooting. With the exception of the westernmost OT, each detected OT appears as an isolated cold region surrounded by a region of uniform temperature. Furthermore, these OTs also have the lumpy or "cauliflower" textured appearance indicative of an OT (Bedka et al. 2011b) in the visible image (Figure 16d). Note the latitude and longitude lines have been removed in Figure 16d to observe the texture of the OT located at 48º W. OTs detected in Figure 16a were post-processed, using the NWP TT from both the 12 Z (prior to time of Figure 16) and 18 Z (subsequent to time of Figure 16). Both of these NWP TTs would not be available for the real-time analysis in

Figure 16b; however a 6 hour TT forecast may be used for running in real time.

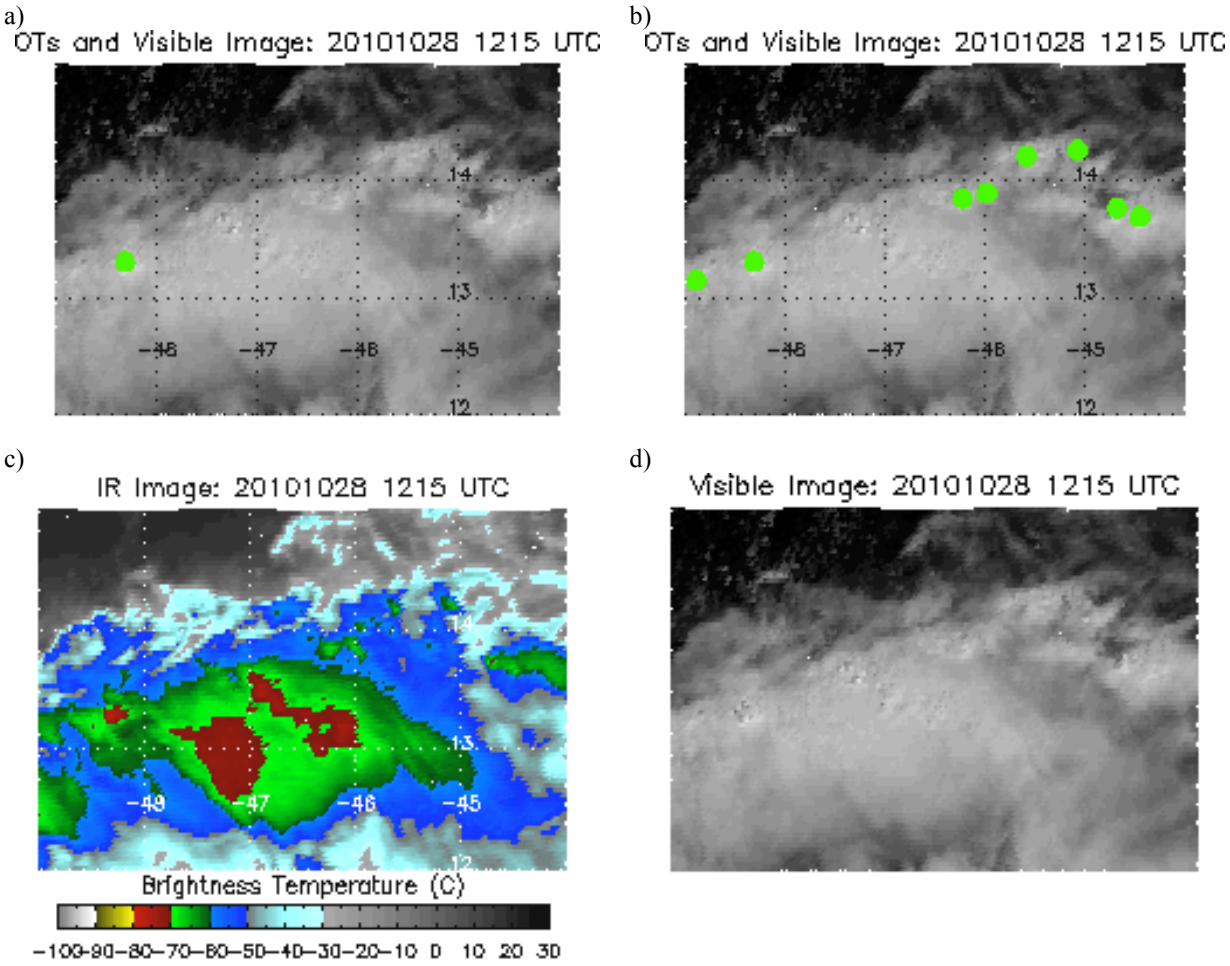

Figure 16: Comparison between the original OT detection algorithm presented by Bedka et al. (2010) and the modified version presented in the paper for 1215 UTC on 28 October 2010. (a) OTs detected by the original Bedka et al. (2010) detection algorithm. (b) OTs detected by the modified detection algorithm. (c) Infrared and (d) visible image for the same time as Figure 14a to identify OT characteristics such as isolated cold region surrounded by a region of uniform temperature in the infrared image or a lumpy/"cauliflower" texture in the visible image.

2. Example: OTs in a weak (Tropical Storm strength) Tropical Cyclone

Tropical storms are categorized as having a 1-minute maximum wind speed between 34 and 63 knots (Hurricane Research Division 2011). Seen in Figure 17a is a visible image of TS Fiona from the GOES-13 satellite. The seven detected OTs corresponding to this image are shown in Figure 17b. However, there is a possible OT, circled in red on the visible image and white on the IR image, not detected. This possible OT is also not detected during

re-analysis using the original Bedka et al. (2010) OT detection algorithm (not shown), even though it has a BT of at least -70 º C, or 203 K as seen in Figure 17b. As mentioned previously, the original OT detection algorithm, when removing the NWP TT, still experiences a POD equal to 90% (Table 1). Therefore, approximately 1 out of every 10 OTs can still be missed by this algorithm, with more missed when increasing the BTD to 9 K.

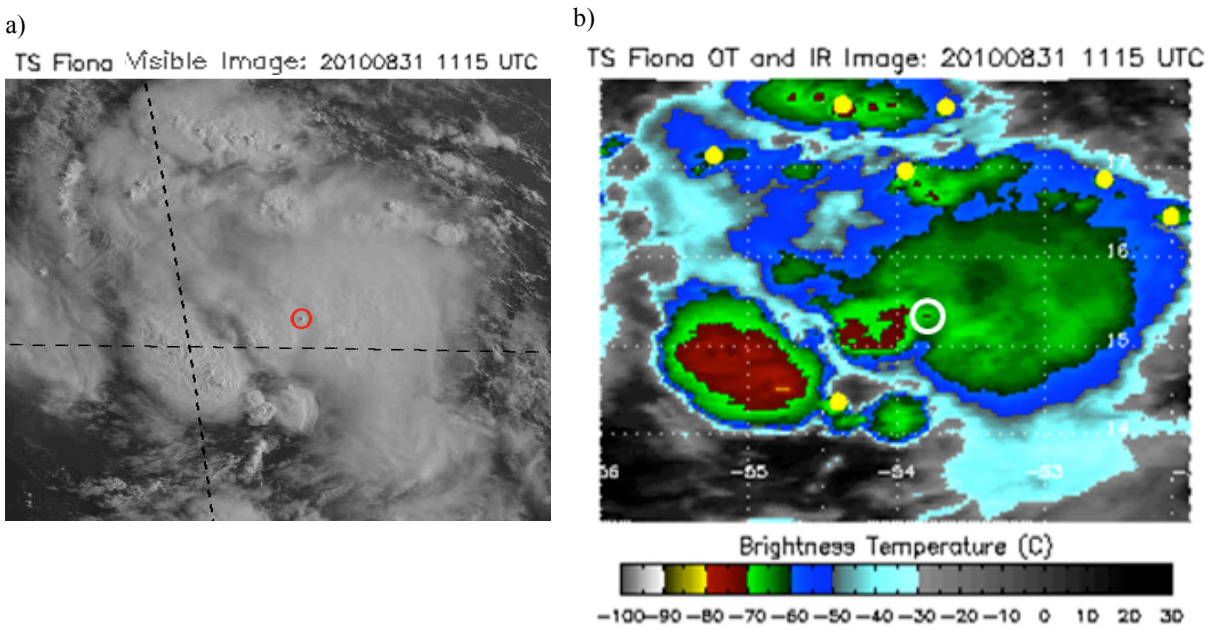

Figure 17: Visible image and detected OTs from TS Fiona. (a) Visible image courtesy of the Naval Research Laboratory. (b) OTs detected by the modified OT detection algorithm. A potential OT is circles in red (left) and white (right), however it is not detected by the OT detection algorithm.

3. Example: OTs in a strong (Hurricane Strength) Tropical Cyclone

Hurricanes have a 1-minute maximum sustained wind speed of at least 64 knots. While these systems continue to produce OTs, some of their aspects can hinder OT identification. Guimond et al (2010) investigates the effects of hot towers (HTs) on the RI of Hurricane Dennis (2005), indicating a convective burst preceded the RI event. Around 1453 UTC on 9 July 2005, a HT is identified near the eye of Dennis, using an ER-2 Doppler Radar (EDOP). The location of this HT can be seen in Figure 18a, with the corresponding IRW and

detected OTs, indicated by the yellow points, and the path of EDOP in white at 1445 UTC in Figure 18b. While the EDOP detects a HT very near the eye of the storm, there is no detection in this region by the OT algorithm. As indicated in Figure 16b, the area along the EDOP flight is approximately -70º C (203 K). However, the Special Sensor Microwave/Imager (SSM/I), which measures precipitation cores (Naval Research Laboratory 2002), indicates the top of the HT around 210 K and thus warmer than the IRW cloud tops and obscured. This is an example of the Central Dense Overcast (CDO), a cirrus cloud shield that results from the thunderstorms in the eyewall of a TC, hindering the OT algorithm's ability to detect OTs in that region.

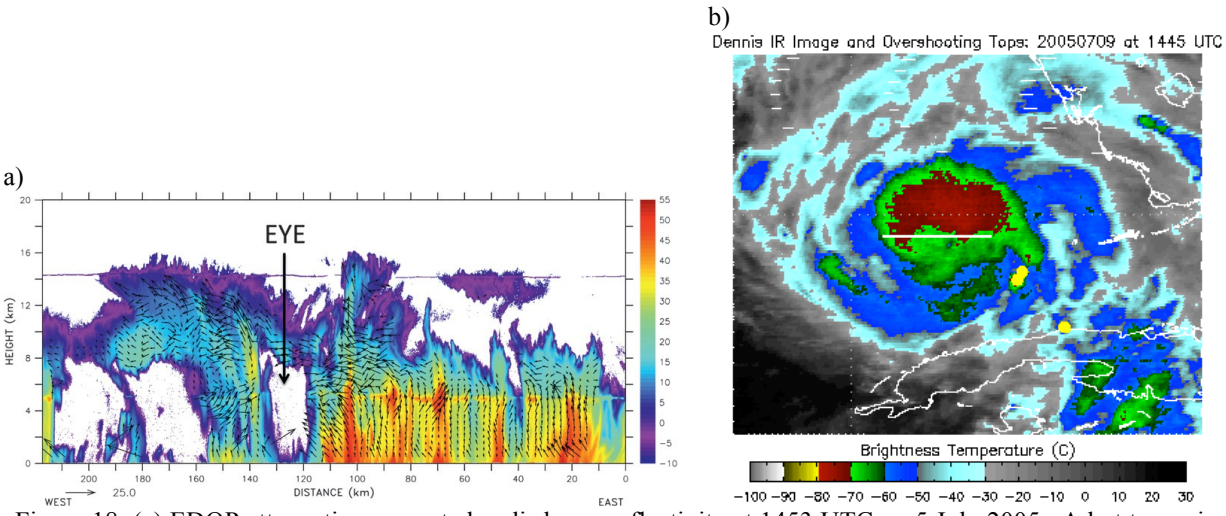

Figure 18: (a) EDOP attenuation-corrected nadir-beam reflectivity at 1453 UTC on 5 July 2005. A hot tower is located east of Dennis's eye. Image courtesy of Guimond et al. (2010). (b) IR image, EDOP track (white) and detected OTs (yellow dots) at 1445 UTC on 5 July 2005. No OT is detected along the EDOP track due to the CDO.

c. Best Track data

1. Applications to TC Genesis

Potential areas of TC genesis are tracked based on a framework for TC formation presented by Dunkerton et al. (2009). In an examination of named Atlantic TCs from 1998-2001, it was found that 88% developed from "monochromatic easterly waves." The

preferred genesis location is the intersection between the critical layer, defined as the region surrounding an easterly wave's level in shear flow, and trough axis at the center of a developed Kelvin cat's eye. The cat's eye is a region where mean flow (in the direction of wave propagation) and wave phase speed are similar. Thus, cutoff vorticies are able to travel with the easterly wave, with the Lagrangian mean flow discontinuous at the layer edges, pseudo-protecting the vortex within the cat's eye from the surrounding environment. This cat's eye organizes lower-tropospheric vorticity, contains moisture entrained by the developing gyre and/or lofted by deep convection (VHTs), confines mesoscale vortex aggregation, and has a convective-type heating profile. Maintenance or enhancement by the parent wave can also occur until the vortex self-sustaining. This genesis theory has been coined the "marsupial pouch" theory, as the parent easterly wave carries the growing vortex much like a marsupial developing within the mother's pouch. The vortex is known as the "wave's pouch" or simply "pouch". An algorithm developed by Wang et al. (2009), which tracks the propagation of a moisture front, is used to predict the wave pouch tracks.

Data utilized to investigate the usefulness of OTs as proxy VHTs, as well as predicting TC genesis, is from the 2009-2010 Atlantic hurricane seasons. Pouches are manually tracked using the marsupial pouch theory previously described with 4 difference numerical models. These models include the United Kingdom Meteorology Office (UKMET), the GFS, the Navy Operational Global Atmospheric Prediction System *(*NOGAPS), and the European Centre for Medium-Range Weather Forecasting (ECMWF). Courtesy of Mark Boothe (Department of Meteorology: Naval Postgraduate School) almost daily pouch forecasts locations were made available. During 2009, these forecasted locations featured 12 hour latitude and longitude position forecasts, and during the PREDICT

experiment from 15 August – 30 September 2010, hourly pouch positions were provided for each individual model. A combined consensus model track was also provided for PREDICT. Both of these datasets are then linearly interpolated to give the approximate pouch location at every 15 minutes and 45 minutes after the hour, the time of the available satellite scans. Twelve hour vertical vorticity component NWP forecasts were also issued daily. These are again linearly interpolated to give the approximate vertical vorticity component for the pouch at any given time. While this dataset is small, it is the first attempt at continuously tracking pre-depression TCs presently known to the author.

2. Applications to Rapid Intensification

The data used in the development of an OT RI index includes 114 landfalling Atlantic TCs from 1995-2008 of at least TS strength. These dates were chosen as they represent the first year satellite data is formatted for use in GeoCAT (Space Science and Engineering Center 2011) and the end of the online HURricane DATabase (HURDAT) (available at http://www.nhc.noaa.gov/tracks1851to2009_atl_reanal.txt). Landfalling is categorized as eye of the storm crossing over land anywhere in the Caribbean, Mexico, and the United States, with TCs landfalling in Canada not used in this study. The NHC Tropical Cyclone Reports (TCRs) are used to identify which TCs made landfall during this time frame. In addition, 11 TCs from 2004-2008 whose entire track is within the METEOSAT scan are also analyzed, bringing the dependent TC dataset to 125. METEOSAT data is not available for use in GeoCAT prior to 2004 (L. Cronce 2010, personal communication). In addition to these 125 TCs, a smaller subset of data, consisting of every TC from 2006 and 2007 will be analyzed, regardless of track location. This will be done to provide a direct comparison between the developed OT RI index and the current RII presented by KDK10.

IV. Approach and Methodology

a. Applications to TC Genesis

Tropical convection has been found to have a diurnal maximum (Hendon and Woodberry 1993). Using 11 μm BT data, Yang and Slingo (2001) found an early morning maximum in all oceanic deep convection. This diurnal convection has the potential to hinder genesis forecasts, should a greater percentage of pouches than develop (19 out of 56, or 32.8%) experience it. To accommodate this diurnal signal, OTs are averaged into two hour time frame to reduce any single satellite scan OT peaks. A radius of 200 km is chosen, as a downward looking LIDAR over TC Oliver (1993) measured VHTs at a distance no greater than 200 km from the estimated center during the genesis (Simpson et al. 1998). Furthermore, Montgomery and Enagonio (1998) initiated a vortex with a 200 km radius of maximum winds when simulating the convection interaction in the "bottom-up" genesis theory.

Before analysis of the diurnal cycle can begin, the time of the OTs must be converted to local standard time (LST). OTs along the UKMET track are analyzed, as that model provides the greatest number of pouches for analysis. The time of each OT average is converted to LST from universal time (UT) by assuming the LST equals UT minus one hour for each 15º the center of the pouch is west of 7.5º W. If two local times are the same, due to a westward moving pouch entering a new time zone, the 2-hour average OTs/scan are averaged again to create one average for this time. If there is a 2 hour difference in local time, for example in an eastward moving pouch entering a new time zone, the missing LST time is added with 0 OTs/scan. This was done to allow each 24 hour period to have 24 OT/scan averages from genesis until dissipation or final landfall.

Finally, a power spectral analysis is conducted to reveal if averaging the OTs negates the diurnal signal found in tropical convection. An AR(1) process is used, which uses a single auto-regressive parameter, in this case the correlation coefficient between 2 successive OT averages, to smooth over short-term variations while emphasizing the slower variations (Wilks 2006). A Hamming window, which adds one period of a cosine function to a rectangular window (Smith III 2010), at one quarter of the average OT time series length, rounded to the lowest integer, is also utilized. The power spectrum density, in cycles per day, is estimated using the Welch method.

A diurnal signal was found if the OT power spectrum exceeded the 95% confidence interval of the AR(1) process around a frequency of 1 cycles per day. An example of this can be seen in Figure 19 from pouch PGI44L (2010). However, of the 59 pouches, only 3 (5.1%) indicate the presence of a diurnal signal, an OT power spectrum exceeding the 95%

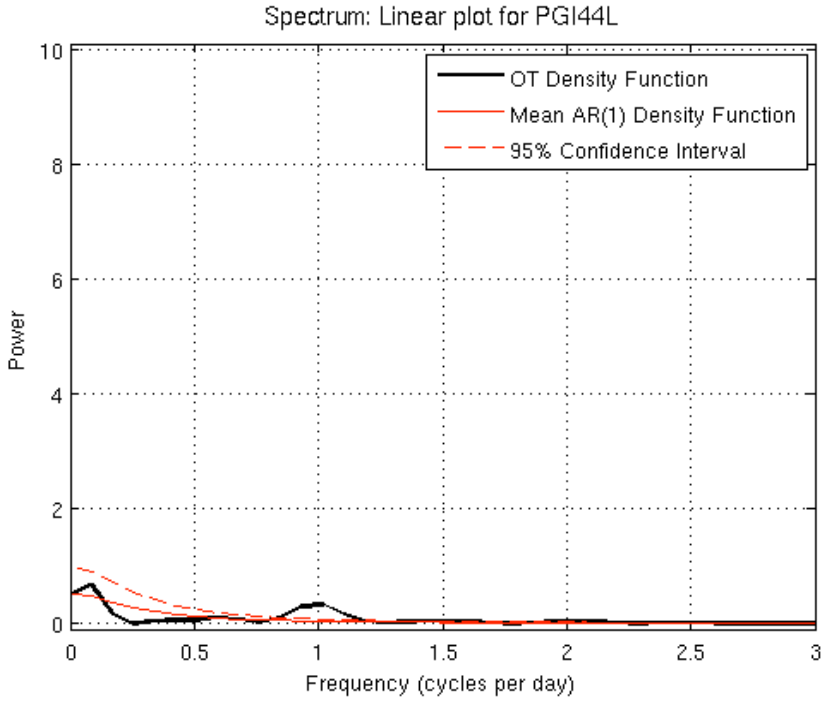

Figure 19: Power Spectrum from PGI44L (2010). The OT density function above the 95% confidence interval at 1 cycle per day signifies a diurnal cycle.

confidence interval between 0.75 and 1.25 cycles per day, between identification and genesis/dissipation. Thus, no additional modifications are made to account for the diurnal cycle.

Two different methods of OT analysis will be conducted for genesis. First, OTs will be compared to the vertical vorticity component to further prove they can act as proxy-VHTs in addition to Figure 10. This comparison begins by correlating the number of OTs produced per day within 200 km of the pouch center and the vertical component of vorticity associated with the pouch at a given longitude. When correlating the OTs to the vertical component of vorticity, each satellite scan, beginning at pouch identification, is used, as the component of vertical vorticity associated with these pouches has grown/diminished since the identification of the pouch, with no preference made to land interaction. Pouches located over the African continent may have more OTs associated with them, as Liu et al (2007) indicates the percent of PFs between 20° N to 20° S reaching the tropopause over land is greater than that over the ocean. However, these additional OTs, or proxy-VHTs, are included in this analysis as they could act to increase the pouches' component of vertical vorticity, according to the VHT theory and analysis in Figure 10.

For this correlation, OTs along the UKMET model track are averaged, as it has the most 2009 and 2010 location and vertical vorticity component forecasts of the 4 NWP models. Before analysis began, some limiting requirements were put on the pouches which could be considered in the correlation between OTs/day and the vertical component of vorticity. Requirements for consideration included:

1) having a vertical vorticity component observed at 700 hPa when crossing the chosen longitude of analysis, or a forecast from the day prior to crossing the given longitude

2) not undergoing genesis east of the given longitude. Systems developing east of the chosen longitude of analysis are not included in this analysis, as there is the "possibility" TCs lift and cool the tropopause (Romps and Kuang 2009), therefore reducing the number of OTs observed at the set temperature. OT detection would also be hindered by the CDO in developed TCs.

When forecasting if and when a pouch will develop, average OT/scan will also be compared. For this analysis, OTs within 200 km of the pouch center are divided into 2 hour time segments, beginning at the time from either initial pouch identification or departure from the African coast, defined as 17º W, until either tropical development or pouch dissipation. Therefore, African OTs are ignored in this analysis. Even though the vertical vorticity component could be enhanced by land OTs, these OTs would still lack other necessary conditions for development, including factors such as evaporation from the sea surface (Emanuel 1986, Wang et al. 2001). Since this research looks to employ an average OTs/scan threshold for tropical cyclogenesis, an additional threshold could be created for those over land. However, seeing as such a sample set would be small and the environmental conditions over Africa are not frequently related to cyclogenesis, such an endeavor is not undertaken.

Where analyzing the accuracy of yes-no decisions based on the number of OTs/scan, forecasts are compared using their Peirce Skill Score (PSS). A PSS of 1 represents a perfect forecast and a PSS of 0 characterizing a random forecast (Wilks 2006). The PSS is equal to the POD minus the probability of false detection (POFD). The POD is the ratio of the correct yes forecasted events to the number of times the events occurred. Thus, if 10 events occurred but only 8 were forecasted to occur, the POD would equal 80% (8/10). The Probability of

False Detection (POFD), or false alarm rate, is the number of false alarms divided by the total number of non-occurrences of the event. Thus, if 20 non-events occurred, but 2 of those events were forecasted to occur, the POFD would equal 10%, (2/20). The POFD experiences a negative orientation; therefore smaller values of POFD are preferred. In addition, the FAR will also be computed. It is the fraction of yes forecasts which turn out to be incorrect, calculated by dividing the number of incorrect yes forecasts by the total number of yes forecasts. Like the POFD, the FAR also has a negative orientation and thus smaller values are favored (Wilks 2006). Three different types of OT characteristics are analyzed: OT BT less than or equal to 215 K, OT BT less than or equal to 205 K and OT BT less than or equal to 200 K.

b. Applications to Rapid Intensification

To conform to KD03, KDK10, and RK11, OT data when the TC center is over land between t = -12 h to t = 24 h is not used in this analysis. Therefore, RI occurring in a land-weakened TC is not detected in this method. Removing this data disallows identification of the RI in Hurricane Dennis (2005) presented in section III.a.1.c. Landfalling times for each TC were gathered from the NHC TCR for each TC, with departure from land estimated from the NHC TCR best track or CIMSS storm track archive (available at http://tropic.ssec.wisc.edu/storm_archive/atlantic.php). Unlike KDK10, no exclusions were made to cases where the TC's potential intensity (PI) and current intensity (CI) difference is less than the RI threshold; however OTs were not analyzed when a TC is at a category 4 or greater strength. Excluding other instances where the difference between the PI and CI occurs may improve the performance of the OTs. In addition, no exclusions were made when environmental conditions are outside the range of climatology.

Additional modifications were made to this dataset outside of the restrictions placed by KDK10 and RK11. As noted by KDK10, it is very uncommon for a TC with category 3 intensity or higher to undergo RI. Of the 57 cases of 25 knot RI within this dataset, no RI was observed when the TC was at category 4 or 5 intensity. However, TCs at this intensity can still produce multiple OTs. Therefore, to reduce the number of false indications of RI, OTs are not analyzed when the TC is at a category 4 strength or greater. This is potentially analogous to KDK10 not forecasting RI when the difference between the CI and PI is lower than 25 kt. Furthermore, times when the TC was categorized as an open wave are also removed from this analysis, as the OTs during this timeframe would be indicating re-formation of the TC and not rapid intensification of the TC, as well as sub/extratropical TCs. Again, this removal was done using the TC tracks from the online CIMSS archive. After data exclusions, the RI dataset used in this analysis consists of 57 instances of 25 knot RI by 47 TCs, 42 instances of 30 knot RI by 36 TCs, and 33 instances of 35 knot RI by 30 TCs.

As mentioned in Section III.b.1, many sources have indicated the presence of a diurnal cycle in oceanic convection. Kossin (2001) confirms this in developed TCs, indicating the coldest 11 μm BT cloud tops near a TC center are found around 0400 LST. In addition, a second maximum around 1600 LST is also found, indicating TCs have a semidiurnal signal. In an attempt to counteract this diurnal and semidiurnal signal in this analysis, OTs are again averaged during an established time frame no shorter than 3 hours in length due to the preciseness of the cycle. Thus, when averaging OTs every hour during the TC lifecycle, 2/3 of the OTs will also be a portion of the preceding and subsequent hour averages. OT averages were taken for the number of OTs within a 200 km disk of the TC center, as Steranka et al. (1986) examines the relationship between TC intensification and

satellite-measured convective bursts within this radius. These OT times are converted to LST and a power spectrum analysis via the method described in Section III.b.1.

A semidiurnal signal was found if the OT power spectrum exceeded the 95% confidence interval of the AR(1) process around a frequency of 2 cycles per day. An example of a semidiurnal signal in Hurricane Ike (2008) can be seen in Figure 20. However, of the 121 TCs whose lifecycle between genesis and landfall was long enough for a power spectrum analysis, only 19.8% (24 out of 121) have an OT density function which is greater than the 95% confidence interval between 1.75 cycles per day and 2.25 cycles per day. An even smaller 3.3% (4 out of 121 TCs) have an OT density function greater than the 95% confidence interval between 0.75 and 1.25 cycles per day, representing a less prominent diurnal cycle. Therefore, no additional modifications will be made to the calculated average OTs to account for the diurnal and semidiurnal cycles, as the percentage of storms

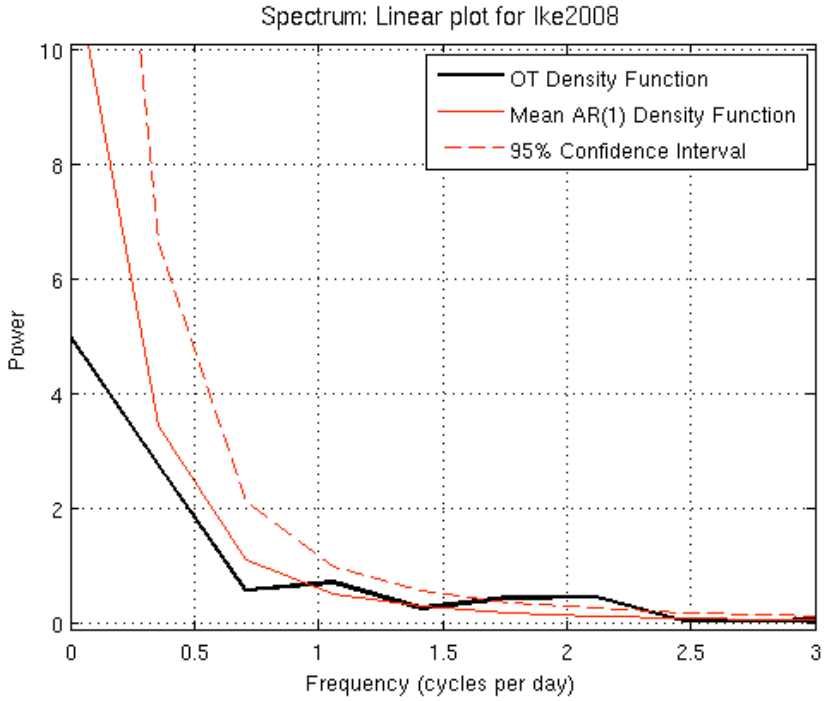

Figure 20: Power Spectrum from Hurricane Ike (2008). The OT density function above the 95% confidence interval at 2 cycles per day represents the semidiurnal pattern in TCs explained by Kossin (2001).

experiencing this signal is less than the 37.6% of storms undergoing 25 knot RI. This fits research by Kossin (2001) that suggests the diurnal signal is radiatively, and not convectively, driven.

Identification of OTs began at identification of the TC in HURDAT. TC tracks are archived during post-season analysis at 4 daily times (Jarvinen et al. 1984). The 6 hour HURDAT location, to the nearest tenth of a degree, and maximum wind speed, rounded to 5 knot intervals, are made available at an interpolated temporal resolution of 15 minutes by Dr. James Kossin (National Oceanic and Atmospheric Administration (NOAA) National Climatic Data Center and CIMSS). Unlike genesis, a running average of OTs along the TC track is calculated from a specified number of prior hours. This change from genesis is made as slight differences in the variables subjectively evaluated, such as the departure of the TC from land, could offset the analyzed time frames and therefore provide an inaccurate forecast.

Unlike KDK10 and RK11, OT RI Index forecasts do not have to be made only on the synoptic hours. Instead, once an average OT/scan threshold reached, RI is forecasted to occur within the subsequent 24 hours. This timeframe was chosen as KDK10 predicts RI within the following 24 hours. Initially, any other thresholds within the subsequent 24 hours after the first exceeded threshold are ignored for RI indication. If RI occurred within the subsequent 24 hours, this was considered a correct yes forecast, and analysis of OTs begins again after the RI event is completed. If RI does not occur within 24 hours, an incorrect yes forecast was made, and analysis of OTs begins 24 hours after the reached threshold occurred. Correct no forecasts occur when 24 hours passes with no RI and no exceeded thresholds. If the lifespan of the TC was not greater than 24 hours and RI did not occur, this TC is still

counted as a correct no forecast. An incorrect no forecast occurred when RI happened even though it was not forecasted to occur, either because no threshold was reached in the previous 24 hours or a reached threshold occurred within the subsequent 24 hours of an incorrect yes forecast and was therefore ignored.

Missed forecasts could arise from ignoring the OT thresholds with the subsequent 24 hours. For example, a forecast of RI at t=0 hours with an ignored exceeded OT/scan threshold at t=15 hours would incorrectly forecast an RI event at t=26 hours twice, as this would fall outside the 24 hour forecast period for RI based on the initial OT/scan threshold at t=0 hours (false alarm) and no addition RI forecast was made (miss). This could be remedied, however, by accounting for each OT/scan threshold reached. In the above example, a forecast period for RI would then extend from t=0 hours to t=39 hours. While the initial forecast at t=0 would still be a false alarm, the OT/scan at t=15 would accurately predict RI. Once again, correct no forecasts occur when 24 hours passes with no RI and no reached thresholds. Since each individual satellite scan produces an independent forecast, each running average instigated by a new satellite scan that does not exceed the OT/scan threshold is either a correct no (missed) forecast if RI does not (does) occur in the subsequent 24 hours.

Yet, producing an RI forecast every 15 minutes has the potential to be excessive. Instead of every 15 minutes, forecasts could be made at the beginning of each hour, thus eliminating 75% of the forecasts made when using each individual satellite scan as a new forecast. These forecasts would still be considered independent, with an OT/scan threshold exceeded at t=0 hour and t=15 hours resulting in RI forecasted from t=0 hours to t= 39 hours. Again, each hour forecast that does not exceed the OT/scan threshold is a correct no forecast.

As KDK10 states, "the POD (Wilks 2006) is the percentage of RI cases that are correctly identified," or the number of storms predicted to undergo RI divided by the number of storms that do, the POD for this analysis, and the forecast accounting for each new satellite scan, is calculated by dividing the number of correctly forecasted RI TCs by the total number of TCs undergoing RI. FAR, however, is calculated by taking the ratio of the number of OT/scan thresholds with no RI in the subsequent 24 hours and the total number of OT/scan thresholds exceeded.

Introduced for the every satellite scan forecast and the hourly forecast are two new method of analysis. The Percent Correct (PC) is the number of correct yes forecasts and correct no forecasts divided by the total number of forecasts issued (Wilks 2006). A modified POD, called Running Probability of Detection, or RPOD, will also be calculated. The hourly forecast has the potential to indicate (miss) RI 24 times before it occurs, with the individual satellite scan having even more occasions. Thus, the RPOD is the total number of times RI is correctly forecasted to occur divided by the total number of opportunities to correctly forecast RI. For example, if in the 24 hours prior to an RI event, an hourly OT/scan threshold is exceeded 6 times, the RPOD is 6/24 or 25%.

Forecasts for each threshold of RI will be verified by their PSS. Initially, each radius is analyzed with the forecast that ignored the OTs within the subsequent 24 hours after an OT/scan threshold is exceeded, assuming this forecast would have the lowest POD due its skipped OTs/scan averages after a forecast of RI is made. Five different types of OT characteristics are analyzed: OT BT less than or equal to 215 K, OT BT less than or equal to 205 K, OT BT less than or equal to 200 K, OT – Anvil BT less than or equal to 12 K, and OT – Anvil BT less than or equal to 15 K. OT/scan values began at 0.5 and are incremented

every 0.5 OTs/scan to a maximum of 6.5. Running averages were calculated for 3, 6, 12, and 24 hours at radii of 150, 200, 300, and 500 km. Once the optimal forecast radius and threshold is found, the statistics for forecast at each satellite scan at forecast at hour are also calculated.

As mentioned in section II.b.2, one of the inhibiting factors to intensity increases in a TC is vertical wind shear. A study of the effect of wind shear on convection was conducted Corbosiero and Molinari (2002), which uses National Lightning Detection Network (NLDL) cloud-to-ground (CG) lightning flashes as a proxy for convection. Results showed that, in the outer bands of a TC, defined as 100-300 km from the center, 84% of the CG flashes occurred in the 2 quadrants downshear of the vertical wind shear vector. CG lightning strikes have been correlated to OTs locations, with Bedka et al (2010) indicating there was 47% frequency of a CG lightning strike within 5 km of an OT, during May-September, 2008. However, no calculated frequency of an OT within 5 km of a CG lightning strike, such as those observed by Corbosiero and Molinari (2002), has been found. Furthermore, asymmetric temperature perturbations, which can be associated with the diluted updrafts of the OTs (Zipser 2003), have been found to have a negative effect on intensity (Nolan and Grasso 2003).

Therefore, analysis also considers the area of the TC circle encompassed by the OTs. The area of the TC can be split into 4 quadrants, like the graph paper seen in Figure 21. OT angle from zonal are calculated by the "due north and south" method, an extension of a zonal line from the center of the TC to the latitude of the OT. Assume the center of the TC is located at the point (0, 0) as in Figure 21, with an OT located at the point (4, 5) indicated by the red circle. A right triangle can thus be formed between the OT, the center of the TC, and

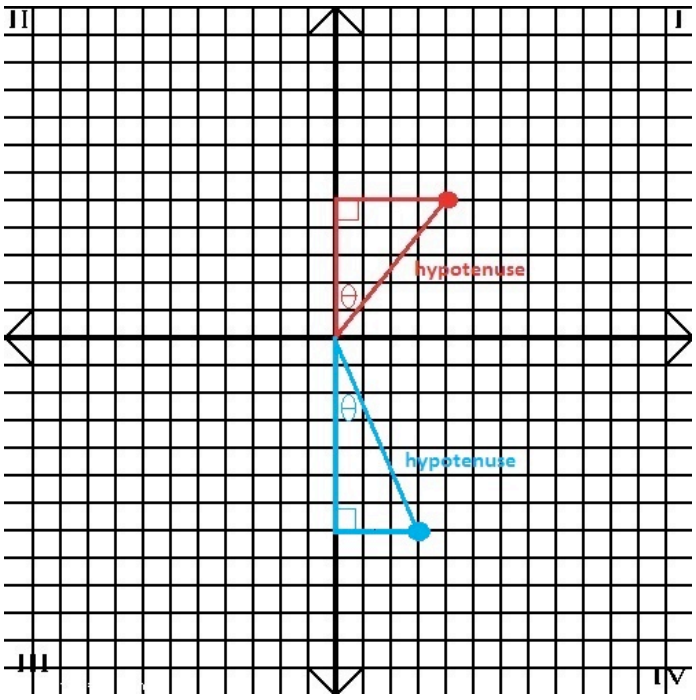

Figure 21: Example calculation of the OT angle from the longitudinal center of the TC using the "due north and south method," which calculates θ using the inverse cosine. Modifications are then made to θ for the clockwise OT angle from due-north of the TC.

the point (0, 5) representing the OT latitude due north of the TC. The line extending from the center of the TC to the OT represents the hypotenuse of the triangle, with the adjacent leg extending from the TC center to the OT latitude due north of the TC. Since the length of both the hypotenuse and adjacent leg can be calculated, the meridional angle deviation (MAD) of the OT is:

$$\cos\theta = \text{adjacent/hypotenuse} \quad \theta = \cos^{-1}(\text{adjacent/hypotenuse}) \qquad \text{(Eq. 2)}$$

where θ is the MAD. All MADS north of the TC are calculated in the manner. MADs of the OTs located south of then TC center can be calculated in a similar manner, as seen with the blue OT located at the point (3, -7). Final modifications have to be made to the calculated OT MAD θ from Equation 2 to calculate the final OT angles as measured clockwise from due-north. The due-north clockwise OT angles for the individual quadrants are:

Quadrant 1: θ_N equals θ_1

Quadrant 2: θ_N equals 360º minus θ_2

Quadrant 3: θ_N equals 180º plus θ_3

Quadrant 4: θ_N equals 180º minus θ_4

In an attempt to reduce the FAR associated with the OT forecasts, the azimuthal standard deviation (ASD) of the OTs is considered to calculate of the area of the TC circle encompassed by the OTs. The ASD of OT angles from 0º to 360º was calculated. Then, to account for the discontinuous boundary between 0º and 360º due north of the TC, 360º is added to the angles of the OTs in quadrant 1 with the ASD recalculated. If either of these two ASDs are less than or equal to 36º, the average OTs/scan are set to zero, therefore not indicating a reached OT threshold and not forecasting RI. This degree value is chosen as it represents, assuming a normal distribution, 64.2% of the OTs are within 20% of the TC circle. While this could act to account for vertical wind shear, many other RI predictors remain unaccounted for.

Current methods of forecasting RI rely on many predictors. The logistic scheme presented in RK11 can account for these factors. OTs are added to a logistic regression scheme, as RK11 indicates predictors from individual geostationary satellite channels may further improve forecast skill. The logistic regression scheme is a discriminative model where fitted coefficients for the predictors are obtained through an iterative least squares approach. Eighteen OT combinations, seen in Table 6a, are compared to find the optimal predictor radius and hour combination. Optimal predictors for the logistic regression are chosen to minimize the deviance of the logistic fit. Predictors are added as long as the decrease in deviance is statistically significant at the 95% level according to a χ^2-test. Since

the optimal logistic regression model predictors in RK11 are selected for 35 kt RI, this threshold is also analyzed for optimal OT predictors.

V. Results

a. Applications to TC Genesis

1. Correlation to the Vertical Vorticity Component

Initial analysis conducted on the 2009 pouch data revealed the best correlation between the vertical component of vorticity and the average number of OTs per day occurred at 40º W, with a Pearson correlation coefficient equal to 0.78. The number of days a pouch existed is calculated as the time of pouch identification until the longitudinal degree was crossed, subtracting 0.02083 (1/48) days for each the 30 minute period without satellite scans. However, this dataset only included 11 of the 31 pouches (35.5%) satisfying both of the above criteria. Even including the remnants from Hurricane Fred and TD 8 in the correlation, as both developed and decayed before 40º W, only 41.9 % of the 31 pouches satisfy the above criteria in section IV.a, with a correlation coefficient equal to 0.79. While this indicates a strong correlation between the pouches' vertical vorticity component and the average OTs/day with a BT less than or equal to 215 K, additional analysis could not be continued at this longitude for 2010, as an even smaller percentage of pouches during this year satisfied the necessary criteria.

Unlike 2009, of the 27 pouches containing daily location forecasts for 2010, only 5 pouches, or 18.5% of the entire dataset, satisfy both of the above criteria at 40º W. Thus, the longitude of interest is moved eastward by 10º to 30º W to allow for sampling of the TCs which developed between 30º W and 40º W. Still, at 30º W, only 8 out of the 27 (29.6%) of the pouches from 2010 can be analyzed based on the above criteria, however this number is

comparable to the number of analyzed storms available at 25º W, 50º W, and 60º W and thus analysis will be conducted at this longitude. Fortunately, 19 of the 31 pouches, or 61.3%, from 2009, satisfy the criteria for analysis, for almost half (46.6%) of the 58 pouches from 2009-2010 pouches.

Figure 22 shows a correlation coefficient of 0.576 between the average number of OTs per day and the linearly interpolated component of vertical vorticity. This correlation is obtained by dividing the covariance of the two variables by the product of their standard deviation (σ), as seen in Equation 3:

$$\operatorname{corr}(X,Y) = \frac{\operatorname{cov}(X,Y)}{\sigma_X \sigma_Y} = \frac{E[(X-\mu_X)(Y-\mu_Y)]}{\sigma_X \sigma_Y}. \quad \text{(Eq. 3)}$$

where the covariance is the average difference between each value from its the mean value multiplied together. Therefore, a moderately skillful relationship exists between the average number of OTs/day generated within 200 km of a pouch center and the pouch's vertical vorticity component, allowing for further comparison of OTs to tropical cyclogenesis based on the theory the OTs increase the pouches vertical component of vorticity. This correlation is consistent with VHT theory (M06) indicating that convection enhances the vertical vorticity of a pouch, as well as additional recent research (Enagonio and Montgomery 2001, Montgomery and Enagonio 1998).

Included in this correlation in Figure 22 are 10 pouches which developed west of 30º W, indicated by red, as well as 17 pouches which did not undergo genesis in the Atlantic Ocean Basin. A threshold can be observed between the number of OTs/day generated by developing pouches and non-developing pouches. For pouches producing greater than or equal to 35 OTs per day from identification until 30º W, 76.9% (10 out of 13) underwent genesis at some point along the UKMET model track lifetime. One of the pouches that did

not develop, due to mid-level dry air intrusion, is PG26L (2009) (Wang et al. 2010). Convection in PG26L diminished on 19 September, after PG26L had already crossed 30º W.

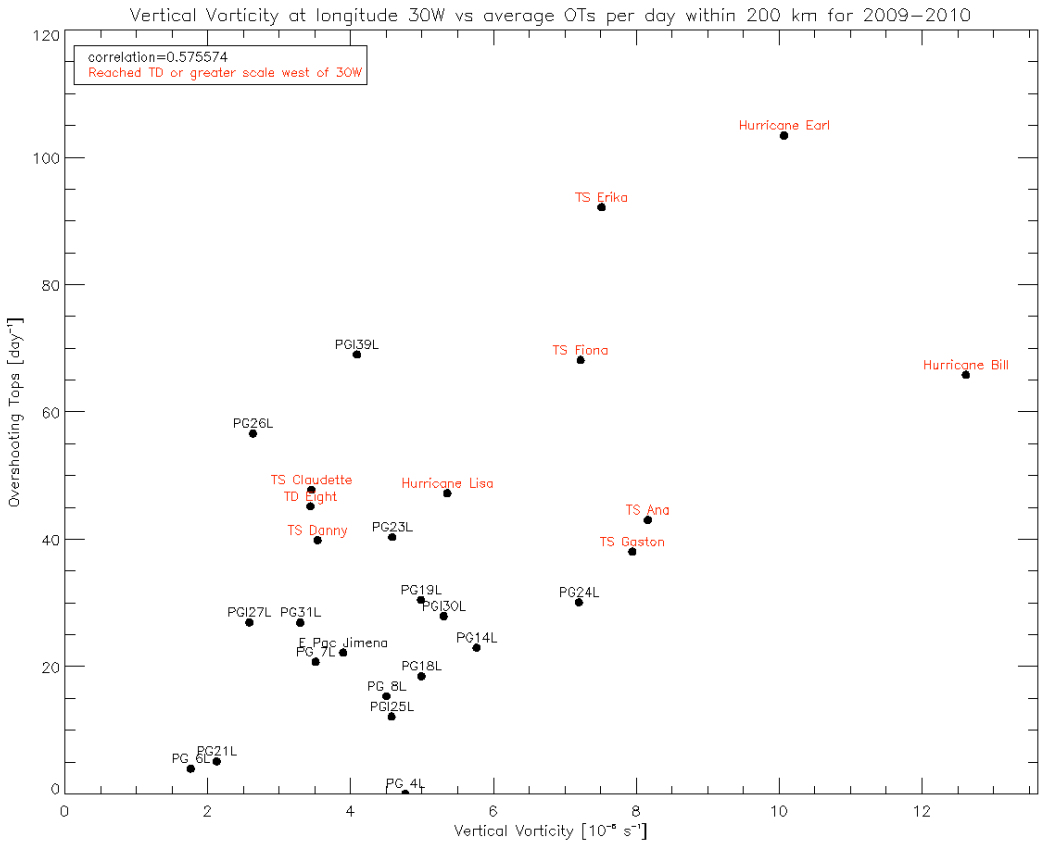

Figure 22: Correlation between number of OTs per day between identification and 30º W (y-axis) and linearly interpolated component of vertical vorticity at 30º W (x-axis). The correlation coefficient of 0.576 represents a moderately skillful relationship, allowing for further comparison of OTs to tropical cyclogenesis based on the "Vortical" Hot Tower theory.

Of those that did not produce at least an average of 35 OTs per day between identification and 30º W, 0% developed in the Atlantic Ocean Basin, However one pouch, PG15L, did tracked across Nicaragua and undergo genesis as Eastern Pacific Hurricane Jimena (2009). Pre-Jimena was categorized as "shallow pouch" by to Wang et al. (2011), with a closed Lagrangian circulation confined to approximately 700 hPa. Only after pre-Jimena escaped the SAL did this closed circulation extend below 850 hPa. This SAL can inhibit the occurrence of deep convection through embedded dry, stable air and strong

easterly wind shear (Dunion and Velden 2004), and thus possibly account for the lack of OTs experienced by pre-Jimena before 30º W.

i. Conclusions

By correlating the number of OTs per day from identification to 30º W and the linearly interpolated vertical component of vorticity at 30º W, the role of identified OTs in the "Vortical" Hot Tower theory for tropical cyclogenesis can be analyzed. Given the correlation coefficient of 0.571 observed in Figure 22, there appears to be at least a moderate to good relationship between OTs with a BT at least or colder than 215 K and the linearly interpolated vertical component of vorticity. This allows for the prediction of genesis based on the OTs to continue under the theory that OTs act to increase a pouch's vertical component of vorticity. In addition, there appears to be a defined threshold at 35 OTs per day between developing and non-developing pouches, with pouches generating more (fewer) OTs undergoing (not undergoing) genesis during the pouch lifetime. However, while this can help predict if a pouch will undergo genesis, 53.4% of the pouches from 2009 and 2010 are missing from this analysis. Thus, a more complete prediction of "if" tropical cyclogenesis will occur is continued in the following section.

2. Predicting if a pouch will develop based on a relationship with OT frequency

The correlation observed in Figure 22 indicates there is a moderate to good correlation between the number of OTs within 200 km of the center of a pouch and that pouch's component of vertical vorticity. Thus, a hypothesis was made that developing pouches would experience more OTs, or VHTs, within 200 km radius of the pouch center than those that did not develop due to this increase in the vertical vorticity component due to the additional convection (Enagonio and Montgomery 2001, Montgomery and Enagonio

1998). Using the data from 2009, a dependent test was conducted to compute the average number of OTs per satellite scan time, which, when reached, would signal if the pouch would undergo tropical cyclogenesis. As there was no consensus model track provided for 2009 data, both the UKMET and the NOGAPS models were individually analyzed. These two NWP models were chosen as they provided the greatest number of 700 hPa pouch forecast locations for analysis, 31. Eight pouches experienced tropical cyclogenesis while 23 pouches were non-genesis cases. It is important to note that this data includes the genesis of TS Henri. However, for both the UKMET and NOGAPS, Henri only had 2 location forecasts 6 days apart, with the second forecast after genesis had occurred. This makes an accurate genesis forecast difficult. Nevertheless, since reasons for the gap in data are unclear, Henri will be included in the statistics to give the lowest potential forecast accuracy.

i. OT BT less than or equal to 215 K

Potential 2-hour average OTs/scan thresholds are compared using the Peirce Skill Score (PSS). Initial analysis of the UKMET and NOGAPS NWP tracks revealed an optimal threshold of 4 OTs/scan (PSS equal to 0.633) and 2 OTs/scan (PSS equal to 0.571) along the respective model tracks, as seen in Table 2a. The optimal model-contingent thresholds were then reversed, with the results observed in Table 2b. The highest average PSS, a value of 0.562, occurs when a threshold of an average of 4 OTs/scan is employed along the forecast tracks for both the UKMET and NOGAPS NWP models. This represents a dependent test, since all of the pouches were utilized in its calculation. Thus, this threshold will thus be utilized for analysis of the PREDICT data in order to provide an independent analysis, allowing for both model comparison and expanded forecast accuracy.

a)	UKMET 4 OTs/scan	NOGAPS 2 OTs/scan
genesis correctly predicted	6	7
genesis incorrect predicted	2	7
Pierce Skill Score	0.659	0.571

b)	UKMET 2 OTs/scan	NOGAPS 4 OTs/scan
genesis correctly predicted	7	4
genesis incorrect predicted	10	1
Pierce Skill Score	0.465	0.457

Table 2: (a) Number of genesis cases correctly and incorrectly predicted for the optimal 2-hour average OTs/scan threshold based of the Pierce Skill Score for an OT BT less then or equal to 215 K. (b) Number of genesis cases correctly and incorrectly predicted and the Pierce Skill Score for the model reversed optimal 2-hour average OTs/scan threshold from (a). The optimal threshold is selected as the highest average Pierce Skill Score.

The 2010 PREDICT field experiment observed 28 pouches. For more information on PREDICT, please see Evans et al. (2011) and Montgomery et al. (2011). Of these pouches, 12 experienced genesis, with 1 pouch not being designated until after tropical cyclogenesis and therefore will not be included in these statistics. This left 11 genesis cases and 16 cases of non-genesis. However, all 4 NWP models were not available every day for each pouch. The UKMET model was absent from analysis for 16 of the 28 pouches, leaving only 12 pouches with the full range of model (5 genesis and 7 non-genesis cases). Yet only 3 of the 16 pouches lacking daily UKMET data lacked consecutive daily forecasts before genesis occurred. These day-old forecasts will be included in the homogeneous analysis, for a dataset of 25 cases, 8 genesis and 17 non-genesis.

The corresponding PSS for each individual model, as well as the consensus model tracks, can be seen in Figure 23a (Figure 23b for the 25 homogeneous pouch dataset). Perhaps surprisingly, the consensus model track does not experience the highest PSS for OTs/scan along the forecasted track. Instead, both the GFS and UKMET have a higher PSS, 0.583 (0.647 for the homogeneous dataset) and 0.556 (0.647), respectfully. Interpretation of these results in Figure 23a can be explained with the help of Figure 24. The OTs along the UKMET model track had the highest POD of any of the model tracks, as one additional pouch was correctly forecasted to undergo genesis, which increases the UKMET PSS. The

OTs along the GFS model track experience the lowest POFD and FAR of all the models, which also acts to increase the PSS.

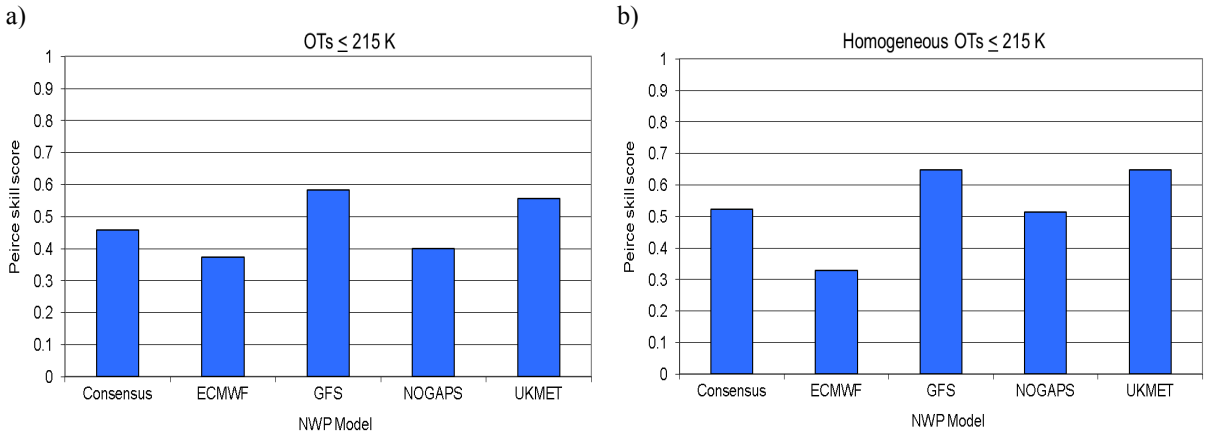

Figure 23: The Peirce skill score for greater than or equal to 4 OTs/scan for a duration of 2 hours for (a) each model used during the PREDICT timeframe and (b) the 25 pouches which were not lacking consecutive daily location forecasts for an OT BT less then or equal to 215 K. A perfect forecast receives a PSS equal to 1.

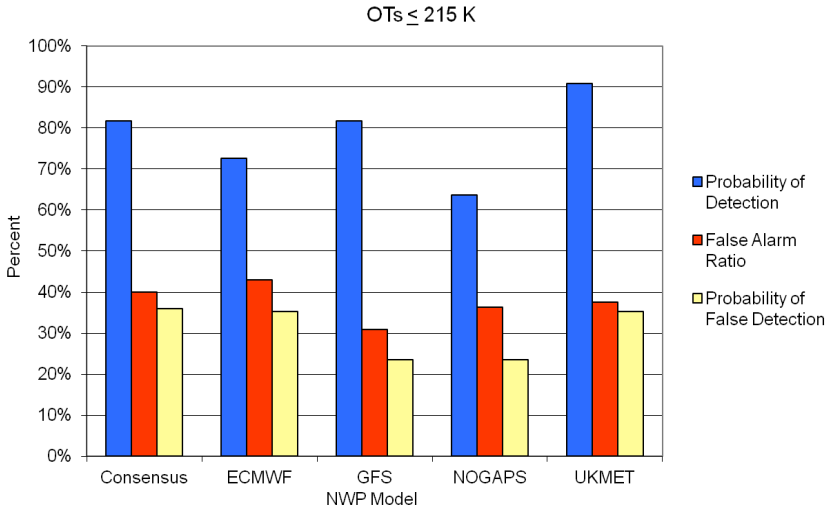

Figure 24: Probability of Detection, False Alarm Ratio, and Probability of False detection for each NWP model during the PREDICT field experiment for an OT BT less then or equal to 215 K.

To account for the occasionally missed UKMET forecasts, the best genesis predicting forecast for the entire PREDICT timeframe, based on the PSS, appears to be the use of the OT detection algorithm along a combination of individual model tracks. While the OTs along the UKMET forecast tracks are only unsuccessful at accurately predicting the genesis of TS Gaston (potentially due to missed forecasts), the OTs along the GFS forecast track

correctly indicated its genesis. In addition, even though the OTs along the GFS forecast tracks do not forecast the genesis of Hurricanes Igor and Lisa, the OTs along the UKMET do. Therefore, by analyzing the OTs along both the GFS and UKMET individual forecast tracks, with genesis forecasted to occur when greater than or equal to 4 OTs/scan is exceeded along either model track, the POD for 2010 PREDICT pouches increases to 100%. In addition, since the number of incorrectly forecasted genesis events does not increase from its maximum observed with the UKMET, as the 4 incorrect genesis forecasts with the GFS model were also incorrectly forecasted with the UKMET model, the resulting FAR decreases by 2.3% when compared to the UKMET (however it does increase by 4.4% when compared to the GFS) to 35.2%. The 6 incorrectly forecasted genesis cases also result in a POFD of 35.2% for a PSS equal to 0.647, the same observed for the homogeneous dataset.

For the 2 year time span, 2009-2010, the individual GFS and UKMET individually-combined forecast experiences a POD of 89.5%. This represents the lowest forecast accuracy, as TS Henri was not forecasted to develop, potentially due to its low temporal data resolution. Removing TS Henri from these statistics increases the POD to 94.4%. Nevertheless, with a FAR of 34.6% and POFD of 23.1%, a POD of 89.5% (94.4%) results in a PSS equal to 0.664 (0.713).

However, this dataset does not represent the entire 2010 Atlantic hurricane season. Before August 15, another 15 pouches were tracked, with 3 undergoing tropical cyclogenesis. However, there are no statistics for this timeframe as pouch location data is unavailable. After September 30, only consensus tracks were available. This dataset includes 14 pouches, 4 of which developed. Thus, overall the consensus track has a POD of

75.0%, FAR of 52.0%, and a POFD of 40.6% for a PSS equal to 0.344, much lower than observed during the PREDICT experiment.

ii. OT BT less than or equal to 205 K

Increasing the maximum BT of the candidate overshooting top pixel from 215 K to 205 K results in a minimum OT height at approximately 14 km based on Jordan (1958). This is also the height of the level of zero net radiative heating (Alcala and Dessler 2002). A dependent analysis of the 2009 pouches is once again calculated for the NOGAPS and UKMET models to reveal the optimal OTs/scan threshold. The best forecasts for if genesis will happen, based on the PSS, occur with a threshold of 3 (2) OTs/scan was applied along the UKMET (NOGAPS) track for a PSS equal to 0.663 (0.614), as seen in Table 3a. When the thresholds are reversed, the optimal genesis predictor at this BT is 2 OTs/scan, observed with the NOGAPS model, as seen in Table 3b. The average PSS for this forecast is equal to 0.593, slightly higher than 2-hour average OTs/scan greater than or equal to 4 when the maximum OT BT is equal to 215 K.

a)	UKMET 3 OTs/scan	NOGAPS 2 OTs/scan	b)	UKMET 2 OTs/scan	NOGAPS 3 OTs/scan
genesis correctly predicted	6	7		7	4
genesis incorrect predicted	2	6		7	2
Pierce Skill Score	0.663	0.614		0.571	0.413

Table 3: (a) Same as Table 3a but for an OT BT less then or equal to 205 K. (b) Number of genesis cases correctly and incorrectly predicted and the Pierce Skill Score for the model reversed optimal 2-hour average OTs/scan threshold from (a). The optimal threshold is selected as the highest average Pierce Skill Score.

The corresponding PSS, as well as POD, FAR, and POFD, for the 4 NWP model tracks and the consensus track can be seen in Figure 25. Compared to 215 K, Figure 23a, the PSS when looking for OTs colder than 205 K in Figure 25a is slightly lower, indicating a less accurate forecast than for the warmer OTs. This is due the fact that, while the POD is higher when observing OTs colder than 205 K (Figure 25b) than at 215 K (Figure 24), the FAR is

also higher. In addition, the individually-combined GFS and UKMET forecast (PSS equal to 0.471) is worse than the individual GFS forecast (PSS equal to 0.505).

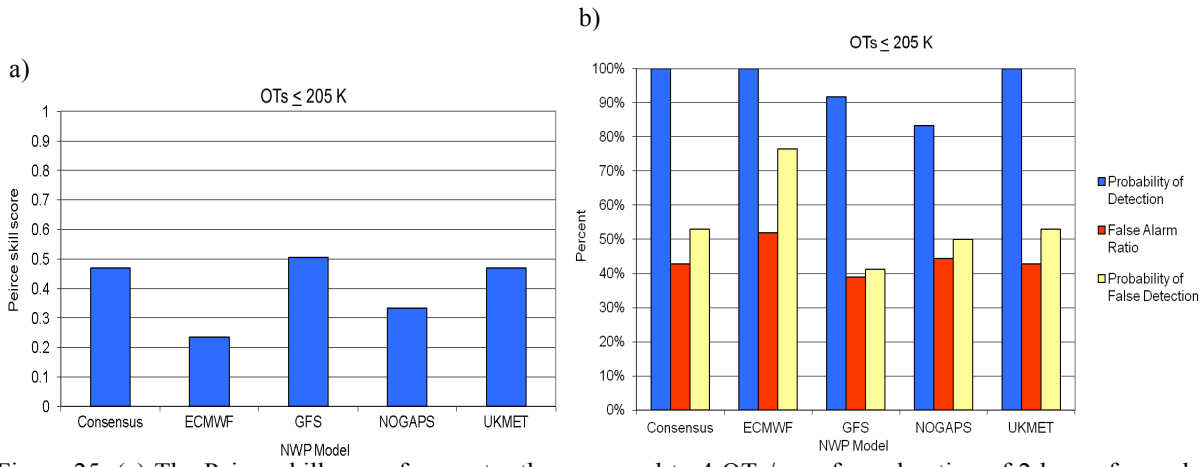

Figure 25: (a) The Peirce skill score for greater than or equal to 4 OTs/scan for a duration of 2 hours for each model used during the PREDICT timeframe for an OT BT less then or equal to 205 K. A perfect forecast receives a PSS equal to 1. (b) Probability of Detection, False Alarm Ratio, and Probability of False detection for each NWP model during the PREDICT field experiment.

iii. OT BT less than or equal to 200 K

Further reducing the OT BT maximum to 200 K results in OTs at an approximate height of 16 km (Jordan 1958). This is the height used by M06 and Simpson et al. (1998) to define the tropical tropopause. As previously done, pouches from 2009 along the UKMET and NOGAPS model were analyzed to find an optimal threshold. At a PSS equal to 0.620, the 2-hour average OTs/scan greater than or equal to 2 along the UKMET model track is the highest, with the highest PSS along the NOGAPS model track (PSS equal to 0.489) occurring when a threshold of 1 OTs/scan for 2 hours was reached, as seen in Table 4a. Switching the thresholds, Table 4b, reveals an optimal threshold of 2 OTs/scan, with an average PSS equal to 0.516. This is slightly lower than the PSS equal to 0.560 (0.593) for a maximum OT BT of 215 K (205 K). However, even though the analysis from OTs with an OT BT maximum of 205 K revealed a higher combined PSS than when OT BT were colder than 215 K, a

forecast using OT BT maximum of 215 K was still more accurate.

a)	UKMET 2 OTs/scan	NOGAPS 1 OTs/scan
genesis correctly predicted	6	6
genesis incorrect predicted	3	6
Pierce Skill Score	0.620	0.489

b)	UKMET 1 OTs/scan	NOGAPS 2 OTs/scan
	7	4
	11	2
	0.351	0.413

Table 4: (a) Same as Table 3a but for an OT BT less then or equal to 200 K. (b) Number of genesis cases correctly and incorrectly predicted and the Pierce Skill Score for the model reversed optimal 2-hour average OTs/scan threshold from (a). The optimal threshold is selected as the highest average Pierce Skill Score.

The corresponding PSS, as well as POD, FAR, and POFD, for the 4 NWP models and the consensus track when decreasing OT BT maximum to 200 K can be seen in Figure 26. The maximum PSS is the highest for the consensus model track, 0.529. Yet it is still slightly lower than with an OT BT maximum of 215 K. This, again, is due the fact that, while the POD is higher when observing OTs colder than 200 K (Figure 26b) than at 215 K (Figure 24), the FAR is also much higher. Almost every model track experiences 100% POD, yet the FAR is no lower than 40%. Thus, more pouches are inaccurately flagged as developers, increasing the POFD and decreasing the PSS.

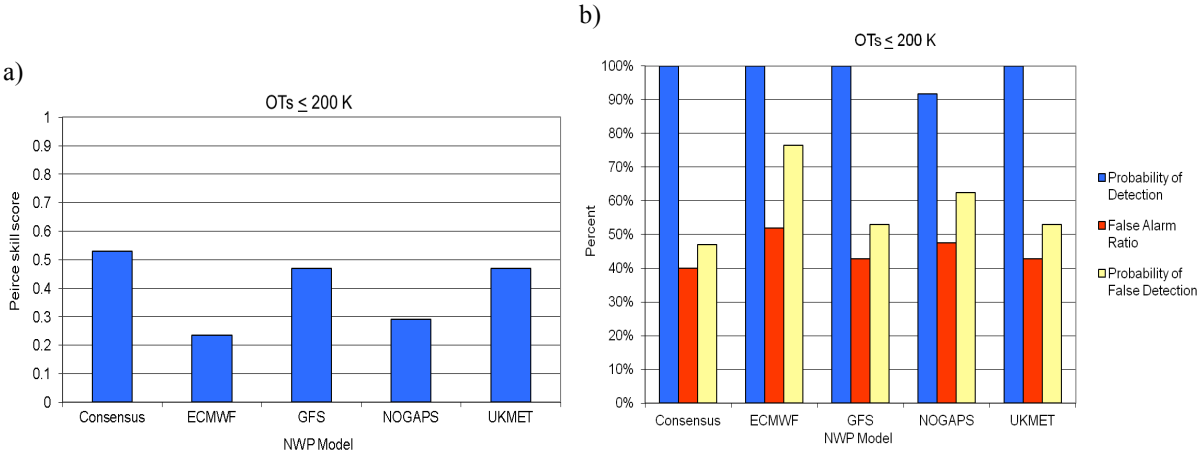

Figure 26: (a) The Peirce skill score for greater than or equal to 4 OTs/scan for a duration of 2 hours for each model used during the PREDICT timeframe for an OT BT less then or equal to 200 K. A perfect forecast receives a PSS equal to 1. (b) Probability of Detection, False Alarm Ratio, and Probability of False detection for each NWP model during the PREDICT field experiment.

iv. OT BT less than or equal to 225 K

Since the optimal forecast peaked when the OT BTs were at least 215 K or colder, the warmest temperature analyzed, the same dataset was recalculated allowing for the maximum BT to be 225 K. These "OTs," as Jordan (1958) indicates 225 K is at a height of 11 km and therefore much lower than the level of zero net radiative heating (Alcala and Dessler 2002), will be referred to as "convective towers" (CTs). CTs were found using the same method as the OTs with BTs less than or equal to 215 K. Pixels flagged a potential CTs had to at least be 225 K. Those at least 9 K colder than the surrounding anvil BT, with a maximum BT of 235 K, were flagged as overshooting. These BTs were chosen as the original algorithm has a 10 K BTD.

The results from a dependent test of the 2009 data can be seen in Table 5. As with analysis of the 215 K OTs, the optimal is again a 2-hour average of 4 CTs/scan as observed when using the UKMET model. This CT threshold was again employed on the 2010

a)	UKMET 4 CTs/scan	NOGAPS 2 CTs/scan	b)	UKMET 2 CTs/scan	NOGAPS 4 CTs/scan
genesis correctly predicted	6	7		7	4
genesis incorrect predicted	2	1		9	1
Pierce Skill Score	0.659	0.602		0.466	0.454

Table 5: (a) Same as Table 3a but for an OT BT less then or equal to 225 K. (b) Number of genesis cases correctly and incorrectly predicted and the Pierce Skill Score for the model reversed optimal 2-hour average OTs/scan threshold from (a). The optimal threshold is selected as the highest average Pierce Skill Score.

PREDICT pouches. The corresponding PSS, as well as POD, FAR, and POFD, for the 4 NWP models and the consensus track when can be seen in Figure 27. The maximum PSS, 0.550, is the highest for OTs along the UKMET model track. Yet, once again it is slightly lower then with an OT BT maximum of 215 K. While the POD is higher when observing CTs colder than 225 K (Figure 27b) than at 215 K (Figure 24), the FAR is also much higher. Almost every model track experiences 100% POD, yet the FAR is no lower than 50%. With

more pouches inaccurately flagged as developers, the POFD increases and thus the PSS decreases.

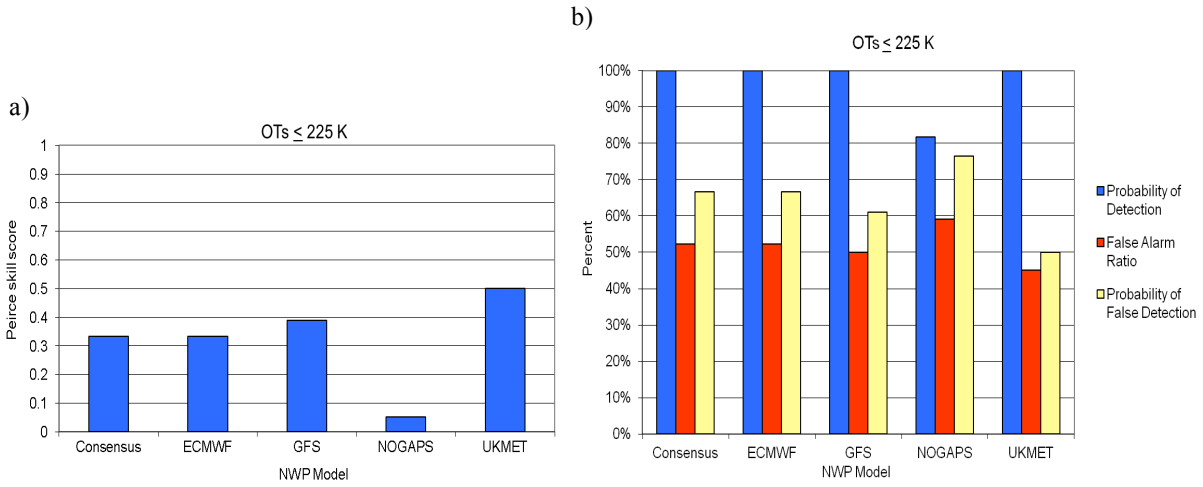

Figure 27: (a) The Peirce skill score for greater than or equal to 4 OTs/scan for a duration of 2 hours for each model used during the PREDICT timeframe for an OT BT less then or equal to 200 K. A perfect forecast receives a PSS equal to 1. (b) Probability of Detection, False Alarm Ratio, and Probability of False detection for each NWP model during the PREDICT field experiment.

v. Comparison to the National Hurricane Center genesis forecasts

As demonstrated above, the most accurate forecast for if an area of potential tropical cyclogenesis will develop occurs when OTs at a BT of 215 K or colder are compared individually along both the GFS and UKMET model tracks with combined results. This will now be known as the "Individual Model Combined Results" (IMCR) forecast. The accuracy of this forecast can be compared to the forecasts issued by the NHC; however the OT forecast looks at any point along the pouch lifetime. Currently, forecasters at the NHC issue a "Chance of Tropical Cyclone Formation" within the next 48 hours for potential areas of tropical cyclogenesis. Probabilities less than 30% are considered low, while a medium probability of development is defined as 30%-50% and a high probability of development greater than 50%. During the 2009 and 2010 Atlantic hurricane seasons, 36 instances of high probability of development were issued for individual time frames (available at

http://www.nhc.noaa.gov/archive/gtwo/gtwo_archive_list.php?basin=atl). Twenty-two of these instances occur when daily pouch forecasts for the either UKMET or GFS model is available.

Of these 22 high probabilities issued by the NHC, 4 (18.2%) of the pouches during 2009 and the 2010 PREDICT experiment did not experience development within 48 hours, with 7 (19.4%) out of the two-year total of 36 not experiencing development. Two of these 4 instances occurred during the potential re-development of pre-existing systems, TD 5 and TS Gaston from 2010. However, no 2-hour OTs/scan were greater than or equal to 4 were detected along the model track of TD 5, therefore indicating no re-development of the pouch. TS Gaston, on the other hand, reached the 4 OTs/scan threshold multiple times while at TD or greater strength. Nevertheless, the last reached threshold occurred 12 hours before TS Gaston was undesignated as a TC in the NHC best track data (Blake 2010). Therefore, again there was no indication of re-development according to the OTs. The other 2 instances with a non-developing NHC high probability are a result of dry air intrusion, resulting from an increase in vertical wind shear or large-scale subsidence (Wang et al. 2010).

These two TCs helped contribute to the under-verification of 60% and 70% chance of formation forecasts issued by the NHC in 2010, as seen in Figure 28. The remnants of TD5 and TS Gaston account for 5 (6) unverified 60% (70%) forecasts. Reducing the chance of formation percentage forecast, due to the lack of an OT signal, would improve the NHC verification percentage to ~55% of a 60% forecast verifying and ~35% of the 70% forecasts verifying. However, the other two instances where the NHC issued a high chance of TC formation, the OTs also indicated development of the pouch. Furthermore, assuming a high probability of development would be issued at some point after an exceeded OT/scan

threshold, this OT forecast includes 8 more instances with an inaccurately issued high chance of TC formation compared to the NHC 2010 forecasts.

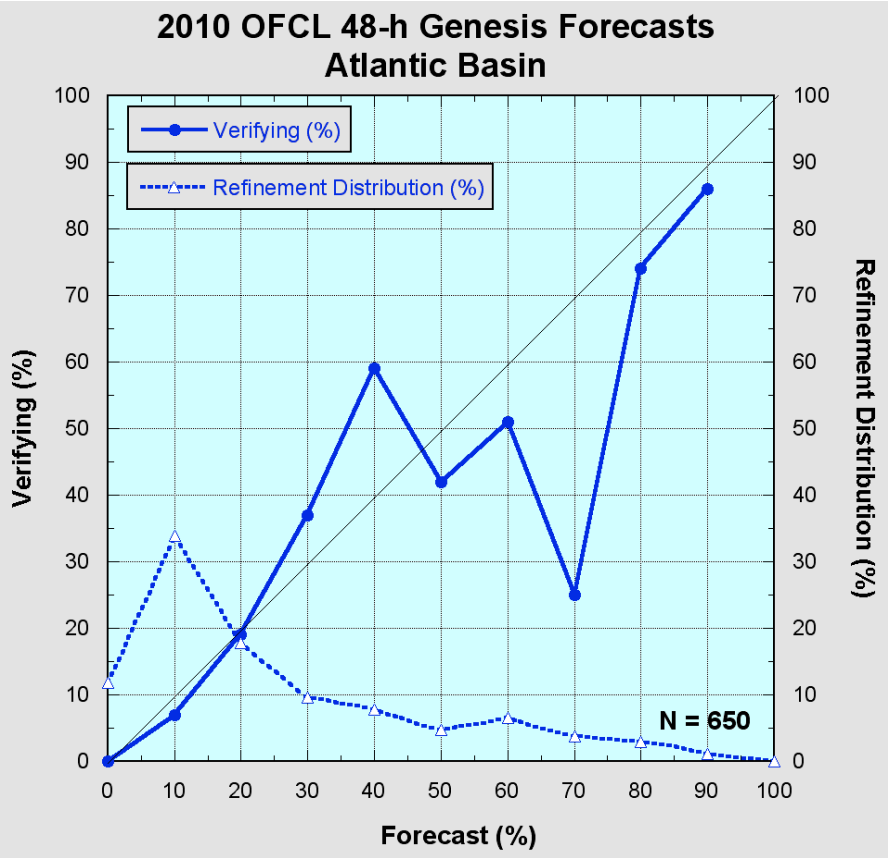

Figure 28: NHC 48-h Atlantic Basin Genesis Forecast verification for 2010 comparing the percent chance of formation (x-axis) and the percent of verifying forecasts for each issued forecast percentage (y-axis). A perfect seasonal forecast verification would follow the grey line. Figure courtesy of Franklin and Cangialosi (2011).

vi. Conclusions

While the IMCR forecast predicts whether an area of potential tropical cyclogenesis will undergo genesis more accurately than the previous comparison to the vertical vorticity component, the timing of that genesis has yet to be addressed. The IMCR forecast of the OTs with a brightness temperature colder than 215 K along the GFS and UKMET model track produced the best result for the entire dataset based on the Peirce Skill Score, with an 89.5% probability of detection for if a pouch would undergo genesis and a false alarm ratio of only 37.0%. When compared to the NHC issued high probabilities of development, 2

inaccurate NHC high chances of formation were not indicated by the OTs. However, an additional 8 pouches were forecasted to develop by the IMCR forecast but did not. In addition, cyclogenesis could occur at any subsequent time after a 2-hour average OTs/scan threshold of 4 was exceeded, not in the following 48 hours as compared to the NHC chance of formation forecasts. The next section looks to use the value of this exceeded threshold in the calculation of a more accurate forecast of when the pouch will develop.

3. Calculation of when a pouch will develop

While the knowledge of "if" a potential area of tropical cyclogenesis will undergo genesis is beneficial, even more advantageous would be the knowledge of "when" the pouch will become a TC. The hypothesis was made that the value of the initial time when 2-hour OTs/scan is greater than or equal to 4, the forecast threshold previously defined for if a pouch would undergo genesis, would provide some insight. The reasoning is the greater the number of OTs generated by the pouch, the stronger the pouch's vertical vorticity component, based on the VHT theory (M06), other numerical models (Enagonio and Montgomery 2001, Montgomery and Enagonio 1998) and the correlation observed in Figure 22. Thus, there is a greater the likelihood the pouch will undergo genesis. The IMCR forecast of the GFS and UKMET, described in section IV.a.2.i, is used, as its Peirce Skill Score indicated it is the most accurate forecast. Thus, the correlation between the first passed threshold value in either the GFS or UKMET, or the greatest number of OTs/scan if the 4 OTs/scan threshold is exceeded at the same time along both model tracks, and the time before genesis, is calculated. However, seen in Figure 29a, the Pearson correlation coefficient is only slightly positive, indicating there is no valuable forecast temporal information to be gained from an analysis using the value of the initial OTs/scan value greater than or equal to 4.

However, most pouches have more than one occurrence of 2 hour period if OTs greater than or equal to 4 OTs/scan threshold between the time of identification/exiting Africa and cyclogenesis. Of the 17 correctly predicted genesis events, 76.5% (13 cases) exceeded this threshold more than once along the track of the model which correctly indicated genesis first. Of those experiencing less than or equal to 4.25 OTs/scan when they initially reached the threshold, only Hurricane Julia did not experience another reached threshold along the same NWP model track before genesis. Therefore, the correlation between the pouches with an average 2-hour OTs/scan rate greater than 4.25, if available, and genesis time could be greater than the 0.19 observed in Figure 29a. Yet, in spite of changing threshold value, the correlation coefficient decreases. Seen in Figure 29b, it is now even closer to zero than when analyzing any 2-hour average OTs/scan greater than or equal to 4, Figure 29a.

Yet, the downward trend, as initially hypothesized, is more defined in Figure 29b when compared to Figure 29a despite its decrease in correlation. The TCs that do not fit into this downward trend include Hurricanes Fred, Julia, and Igor, tropical depression (TD) 8, as well as TS Claudette. These three hurricanes all have one common factor: they reached TD strength or greater east of 25º W. This is of significance, as pouch data from over the African continent is removed from this analysis. Thus, of the 3 hurricanes, the greatest time between the African coast and genesis is 41 hours, which, while possible to predict if OTs/scan greater than 7, is more likely scenario of enhanced OTs over the African continent or other environmental genesis factors. This is further confirmed as Wang et al. (2010) indicates pre-Fred was associated with active convection over West Africa. When removing these 3 TCs from analysis, as well as TD 8, which can be dropped from the record as TDs are

not included in the post-season records such as the Hurricane Database (HURDAT) from the correlation in Figure 29c, the correlation coefficient increases to a more respectable -0.55. This indicates a moderate relationship between the strength of the first OT/scan average greater than 4.25 and the time until the pouch develops.

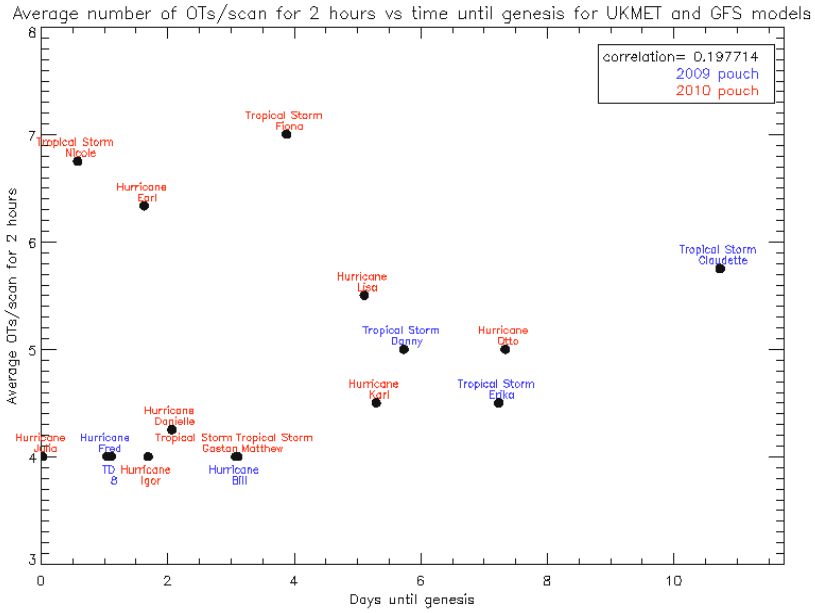

Figure 29a: Value of first 2-hour average OTs/scan greater than or equal to 4 (y-axis) and the time until genesis (x-axis). The correlation of approximately 0.198 indicates little correlation.

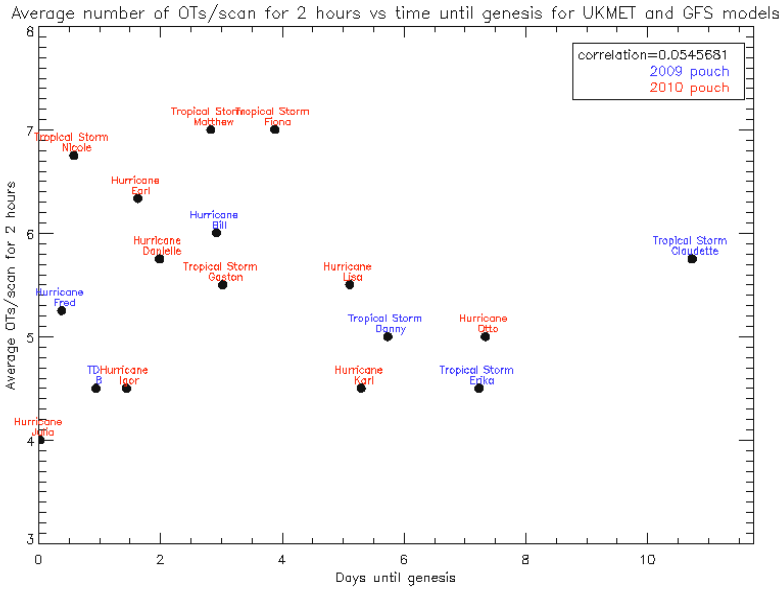

Figure 29b: Value of first 2-hour average OTs/scan greater than 4.25 (y-axis) (if available) and the time until genesis (x-axis). The correlation of approximately 0.05 indicates even less correlation than Figure 29a.

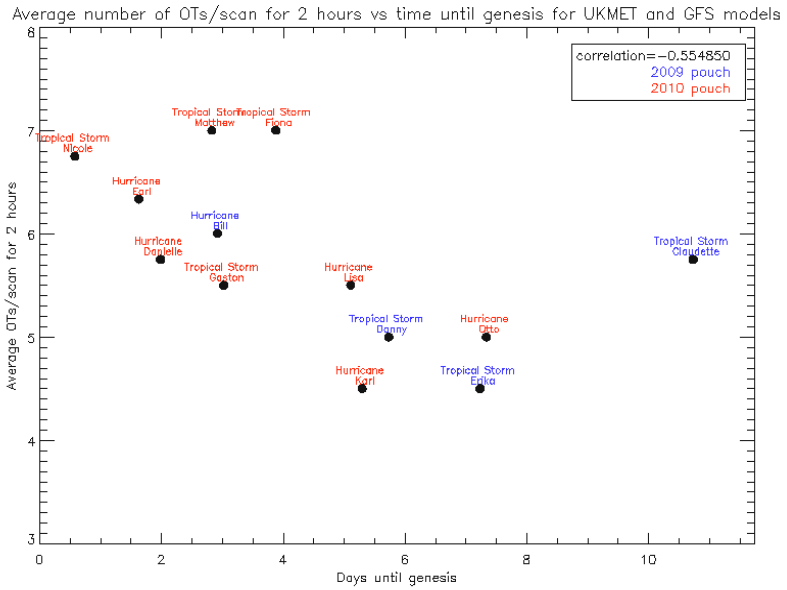

Figure 29c: Value of first 2-hour average OTs/scan greater than 4.25 (y-axis) and the time until genesis (x-axis) when removing the pouches which developed east of 25º W or are not included in the HURDAT season results. The correlation of approximately 0.55 indicates greater correlation than Figures 29a and 29b.

A forecast line can be fitted to the data observed in Figure 29c to provide the most optimal forecast genesis time. After removing TS Claudette from the statistics, which increases the correlation between first OT/scan average greater than 4.25 and the time until the pouch develops to an even stronger -0.75, using the equation for a straight line and solving for the x variable gives a forecast equation based on the initial OT threshold greater than 4.25 OTs/scan, seen in Equation 4:

$$\text{Days until genesis} = \frac{(\text{Number of OTs} > 4.25) - 7.8}{-0.5}. \qquad \text{(Eq. 4)}$$

Given that the correlation between the number of observed OTs/scan and the days until genesis is not a perfect 1, there is error associated with the forecast in Equation 4. Equation 4 is chosen as the most accurate forecast since it gave the most symmetric distribution of forecasted genesis times around the official genesis. While the error associated with the above forecast equation can be as small as 0.140 days (3.36 hours), the maximum error occurs with the genesis of TS Fiona (2010), 2.28 days (54.7 hours) too early and the average error is 1.21 days. The range of forecast error times is 4.39 days, with 3 pouches

experiencing a genesis forecast greater than 1 day prior to genesis and 5 pouches experiencing a genesis forecast greater than 1 day after genesis has occurred.

i. Forecast Modification

Forecast error times can be reduced by accounting for the number of instances where the OTs/scan greater than or equal to 4 threshold is exceeded. Ignoring the first reached threshold and reserving it for indicating whether genesis will occur and the initial forecast genesis time, reached threshold can be categorized into individual instances by identifying where 0.5 days (12 hours) elapses between separately exceeded thresholds. If additional thresholds are reached within 12 hours of the first threshold, these can be counted as an individual instance. If only 1 threshold is reached, the forecast is not modified. Of the 11 pouches used in this sample, as Hurricane Otto (2010) did not have forecasts from pouch development to genesis and thus will not be included in this modification, half (all from 2010) exceeded the 4 OTs/scan threshold on 2 separate occasions greater than 12 hours apart. Of the 5 pouches which did not experience this, 4 have genesis forecasted within 1 day of the actual development.

Comparison of the 5 pouches experiencing a forecast error greater than 1 day later after genesis reveals an average error time of approximately 1.5 days. Of these 5 pouches, 4 (80%) exceeded the 2 hour threshold greater than or equal to 4 OTs/scan at least twice with 12 hours elapsing between. On this occurrence, indicating the pouch is undergoing genesis quicker than forecasted due to the increased vertical vorticity component from the additional convection, the initial forecast genesis time can be decreased by 1.5 days, or 1.5 days earlier than previously predicted. For pouches which do not experience 2 individual instances of exceeded thresholds before the forecasted genesis time, but do experience more than 1

exceeded threshold, the forecasted time of genesis for these pouches can be moved back 1.5 days.

The results of the modified forecast, not including TS Claudette, can be seen in Figure 30. Positive (negative) values indicate where the forecasted time of genesis preceded (succeeded) official genesis. Of the 11 pouches, 5 experienced less forecast error when compared to the initial forecast. Two, however, experienced a worse forecast. These inaccurate changes occurred either when 2 individual instances of exceeded thresholds were reached or only 1 exceeded threshold is experienced before forecasted genesis. Overall, the absolute value of the mean forecast time error reduces by almost a half, from 1.21 days to 0.75 days. The forecast error spread also decreases from 4.39 days to 3.413 days. Yet, exceeding the greater than or equal to 4 OTs/scan threshold twice does not itself indicate the

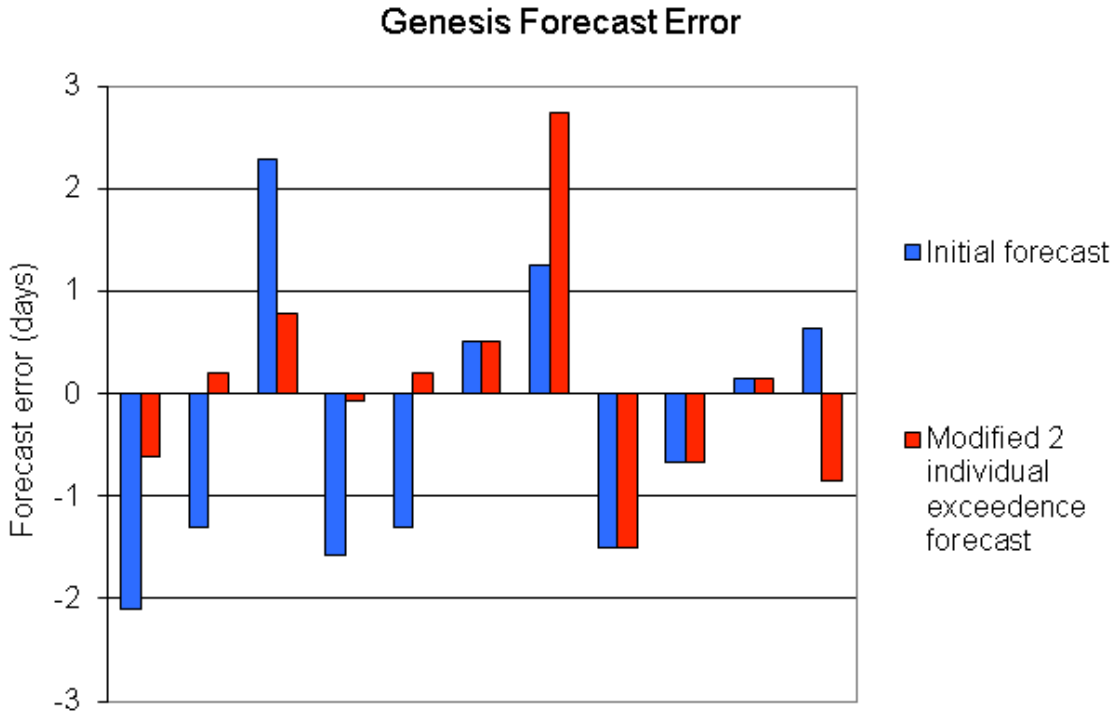

Figure 30: Difference between the actual and predicted forecasts based on initial value of exceeded threshold (blue) and modified initial genesis forecast based on occurrences of 2-hour OTs/scan greater than or equal to 4 greater than 12 hours apart (red). Positive (negative) values indicate where the forecasted time of genesis preceded (succeeded) official genesis.

time of genesis, as genesis occurred within 0.15 to 2.375 days after the second reached threshold. In addition, pouches such as TS Erika (2009) experienced 10 instances were the 4 OTs/scan threshold is exceeded, however greater than 12 hours did not elapse between scans. If Erika's forecast is altered, it now is a TC undergoing genesis earlier than predicted. Then the average error increases to 0.87 days with the forecast error spread increasing to 4.913 days. Instead, the time of genesis for TS Erika is pushed back in this analysis

ii. Comparison to the National Hurricane Center genesis forecasts

The above forecast is a dependent analysis of 11 of the 12 TCs observed in Figure 29c. TS Claudette was not used in this analysis, as its "prospects for becoming a tropical cyclone were never stated to be good" (Pasch 2010), with the OTs further confirming that while TS Claudette had a 63% chance of development, its timing for development did not fit the rest of the TCs seen in Figure 29c. These 11 TCs also do not include those which developed east of 25º W, as well as systems whose maximum wind speed did not exceed 34 knots (only achieved tropical depression strength). This forecast is developed to minimize the error between OT-indicated genesis and actual genesis, symmetric around a forecast with no error (average error equal to -0.057 and median error equal to 0.14). Thus, it is not a probabilistic forecast, unlike the forecasts issued by the NHC.

Attempts at a probability forecast can be made; however in a different manner than those made by forecaster at NHC. As seen in Figure 30, 9 TCs out of the 11 (81.8 %) experienced a forecast error of ± 1 day. Combined with the 17 correctly predicted instances of genesis identified by the IMCR forecast in the previous section and the 10 incorrectly predicted instances of genesis, 33% (9 out of 27) of the pouches predicted to undergo genesis developed in the 48 hour timeframe surround the OT-indicated time of genesis. However,

unlike the NHC, which issues a 48 hour probability of development forecast based on the current state of the pouch, this probability forecast depends on the existence of OTs at any given time prior to the forecasted development of the storm, with lead time ranging from 6 hours before genesis in the modified forecast of Hurricane Danielle to 5 days before genesis in the forecast of TS Danny. A higher probability of development forecast can be issued based on the existence of 2 separate instances of OTs/scan greater than or equal to 4 as described above. Of the 8 pouches which produce this, 5 develop within ± 24 hours of their forecasted genesis time, while 2 do not develop at all and one develops outside this time frame, a 63% probability of development. In addition, 63% of these TCs underwent genesis within the 48 hours after 2 individual instances of exceeded OT/scan thresholds occurs, however the time before development extends from 6 hours until 48 hours. In addition, this forecast is only valid for 5 out of the 17 pouches. Therefore, this is still different from the NHC probability of development forecast.

iii. Case Study: Genesis of Hurricane Karl

The genesis of Hurricane Karl (2010) proved especially difficult to predict. Forecasters at the NHC began issuing "chance of tropical cyclone formation" for the next 48 hours in their Tropical Weather Outlook for pre-Karl at 18Z on 20100908. This chance of formation continued to increase, peaking at 60% from 12Z on 20100911 to 6Z on 20100912, as seen in Figure 31. However, the chance of formation was reduced, due to the lack of sufficient organized deep convection near its center (Stewart 2011). Karl eventually developed at 18Z on 20100914 under a NHC 40 % chance of tropical cyclone formation, a medium risk as defined by the NHC.

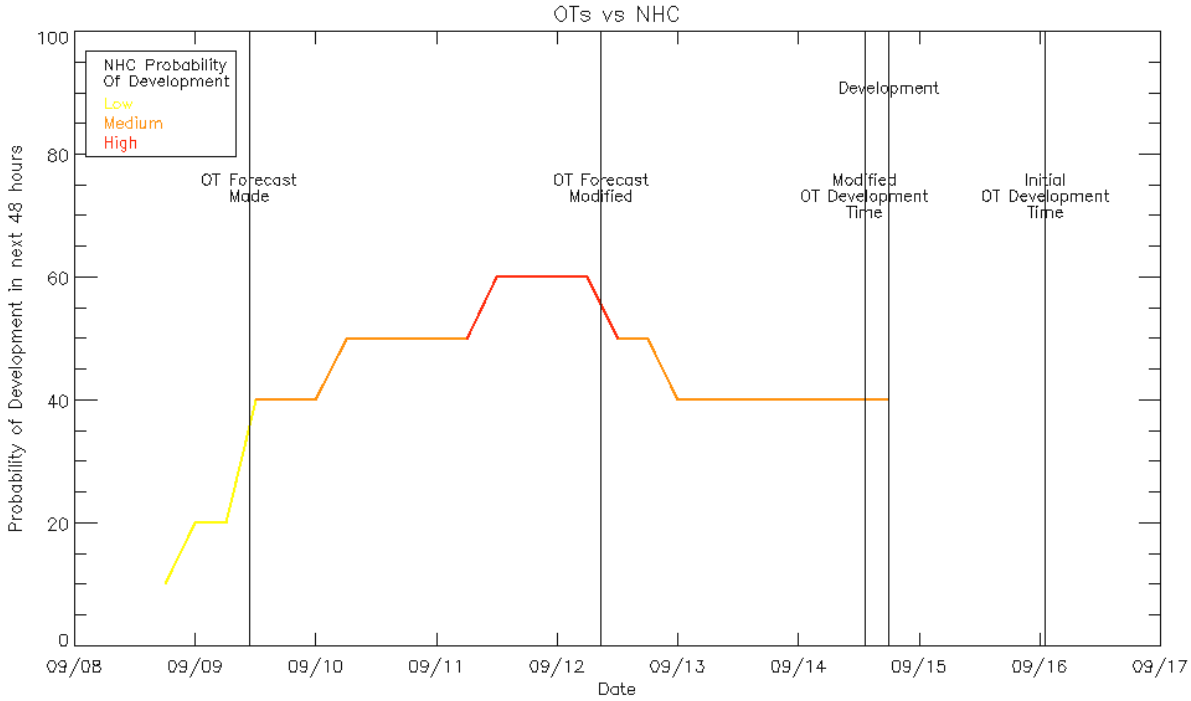

Figure 31: NHC probability of development of Karl within 48 hours (color) versus OT genesis forecast and modified forecast times (lines).

Tracking, and therefore OT monitoring, of the pouch which became Karl began at 00Z on 9 Sept 2010. Retroactively, given the forecast genesis procedure explained above, at 12Z on 9 Sept 2010, Karl would have been forecasted to develop at 00Z on 16 Sept 2010. However, while this forecast provides 6.5 days of lead time, it is inaccurate (Figure 31). At 9Z on 12 Sept 2010, the forecast time of development would be modified, increased by 1.5 days, to 12Z at 14 Sept2010. With a lead time of 2 days and 9 hours, the OT-forecasted genesis of Karl experiences an error of only 6 hours.

iv. Addition of OTs into a Tropical Cyclone Formation Probability product

While the OTs have shown some skill at predicting if, and potentially when, a pouch will undergo TC genesis, there are still a considerable number of false alarms associated with this method. Only 2 of these 10 instances had a high chance of formation issued by the

NHC. Therefore, other factors are hindering the development of these pouches. In an attempt to account for these factors, the OTs are added to the Tropical Cyclone Formation Probability (TCFP) Guidance Product developed by the Regional and Mesoscale Meteorology Branch (RAMMB) at the Cooperative Institute for Research in the Atmosphere (CIRA). This product estimates the probability of genesis within a 5º of latitude by 5º of longitude region based on 10 input parameters (Office of Satellite Data Processing and Distribution 2011). More information about the TCFP can be found in Schumacher et al. (2009).

The OTs are added to the TCFP by Andrea Schumacher (CIRA, Colorado State University). OT averages every 1, 3, 6, 12 and 24 hours prior to the synoptic times within radii of 200, 300, 400 and 500 km in attempts to improve the TCFP forecast skilled compared to climatology. Skill was compared using the Brier Skill Score (BSS), where

$$BSS = 1- (BS_{TCFP}/BS_{ref}) \text{ with } BS=1/n \sum_{k=1,\, n} (y_k - o_k)^2 \qquad \text{(Eq. 5)}$$

and y_k and o_k are the predicted and observed probabilities (Wilks 2006). For this research, the BS_{ref} represents the Brier Score of the climatological formation probability. However, no hour and radius combination produced a higher BSS the TCFP without the OTs, indicating the TCFP without the OTs (BSS equal to 0.0173) has higher skill compared to climatology than the TCFP with OTs (highest BSS equal to 0.0165 for 3-hour average OT/scan within 300 km).

Another gauge of forecast skill is the relative operating characteristic (ROC). ROC diagrams are created by plotting the POD against the POFD using a set of increasing probability thresholds (probability increasing by 0.1%) for a yes-no decision. The area under

the POFD versus POD curve is designated the ROC value, with a value of 1 being a perfect forecast. For verification, ROC values can be converted into a ROC skill score (RSS), where

$$RSS = (ROC_{TCFP} - ROC_{ref})/(1 - ROC_{ref}) \quad \text{(Eq. 6)}$$

(Wilks 2006). As the POFD in the TCPF for a given probability threshold decreases upon the addition of the OTs, reducing the number of regions with an incorrect genesis forecast, so does the POD. Therefore, the RSS increases with the addition of the OTs (0.409) compared to the TCFP without the OTs (0.381). This increase in the RSS and decrease in BSS can be compared with the non-OT TCFP by calculating the percent increase/decrease between the OT and non-OT forecast skills. The BSS experiences a 4.82% decrease, while the RSS experiences a 7.11% increase. While the reduction in predicted probability is observed, illustrated through the decrease of the BSS, this reduction affects both genesis and non-genesis events, allowing for a greater POD for a given POFD when including the OTs in the TCFP, represented by the increase in the RSS. Since the base equations (not shown) for the RSS and BSS are identical, and the percent increase in the RSS is greater than the percent decrease of the BSS, the OTs can positively contribute to a multivariate tropical cyclogenesis prediction scheme depending on the preferred forecast method. This signal could be further solidified by performing an analysis with more storms and over a longer time period, as the TCFP has been developed with 13 years of data and only 2 years of OT data is provided (A. Schumacher 2011, personal communication).

One reason for the lower BSS associated with the addition of the OTs in the length of predictability time for the TCFP. Currently, the TCFP predicts genesis within the next 24 hours (A. Schumacher 2011, personal communication). However, VHTs need time to allow vortex spin-up. While Sipple et al. (2006) indicates the generation and merger of PV few

hours before genesis, potentially due to the radar reflectivity range of 286 miles (Cain and Kirkwood 2011) used in their detection, and Simpson et al. (1958) identifies the results of mergers 12 hours before genesis, potentially due to the lack of convection identification resulting from no satellite data, other sources indicate 1-2 days elapses before TC genesis (Hendricks et al. 2004, Venkatesh and Mathew 2004, M06). Therefore, TC genesis via VHTs may have greater predictability at greater lengths, such as 48 hours. In addition, double the number of maximum OTs/scan are observed within 48 hours of genesis than 24 hours.

v. Conclusions

A forecast for the genesis of a pouch is presented. By using the equation for a straight line, the initial average 2-hour OTs/scan value greater than 4.25 can be equated into a time of genesis. However, if 4 OTs/scan value is reached on two separate occasions prior to development, this forecast is increased by 1.5 days due to the increase in the vertical vorticity component. Likewise, if this does not occur by the forecasted genesis time, the forecast time is pushed back 1.5 days. Overall, this forecast resulted in 9 out of 11, or 81.8%, of the TCs developing within a day of the forecasted genesis time, or 33% when accounting for the 17 developing pouches and 10 pouches incorrectly forecasted to undergo genesis. In addition, 63% of the pouches which generate 2 individual thresholds with 12 hours elapsing between undergo genesis within 48 hours. Yet, this cannot be compared to the NHC "chance of tropical cyclone formation" forecasts, as it is not valid for the succeeding 48 hours. This forecast has proven to be accurate in cases where development was difficult to forecast. The development Hurricane Karl (2010), which developed under a 40% chance of formation issued by the NHC, would have been forecasted 2.375 days in advance by the OTs, with an

error of only 6 hours. Furthermore, OTs can positively contribute to a multivariate tropical cyclogenesis prediction scheme, as seen with their addition into the Tropical Cyclone Probability Forecast. However, more data is needed to help to solidify this trend.

b. Applications to Rapid Intensification

A number of the RI indicators used by RII can be potentially be represented by an increases in the number of OTs within a disk of the TC center. Thus, a hypothesis was made that TCs about to undergo RI would have a marked increase in the number of OTs than those which do not. Initial analysis of the OTs indicates this marked different. Table 6a, b, and c expresses the average number of OTs/scan for 1, 3, and 6 hour time periods before each synoptic time within a disk of a certain distance from the center of the TC for 25, 30, and 35 knot RI, respectfully. This data only looks at synoptic times when data used the RII is available. These times are courtesy of Dr. Christopher Rozoff (CIMSS). No synoptic times are removed if various scans are missing during the averaged timeframe.

Predictors utilized by the RK11 RI forecast models need to exhibit a mean difference between RI and non-RI TCs significant at the 95% confidence interval accorded in the two-sided Student's T-test. Based on this test, with unequal size and unequal variance, the average number of OTs/scan over the 1, 3, and 6 hour time period before the synoptic times for RI within 24 hours and non-RI cases are significantly different at the 99% confidence level (based on infinite degrees of freedom) for each radius from the center of the TC for all RI thresholds. The only exception is for a radius of 50 km, which is significantly different at the 95% confidence level at all RI thresholds. Therefore, OTs could be an optimal predictor or RI.

25 kts in 24 hours RI N=977/143	r=50 km	r=100 km	r=150 km	r=200 km	r=300 km	r=500 km
OTs (1 hr)	0.10/0.19	0.34/0.57	0.65/1.03	1.08/1.66	2.17/3.10	3.94/5.45
OTs (3 hr)	0.10/0.16	0.33/0.48	0.64/0.91	1.04/1.47	2.04/3.00	3.69/5.34
OTs (6 hr)	0.12/0.15	0.33/0.47	0.64/0.91	1.04/1.50	2.07/2.99	3.77/5.30

Table 6a: Average OTs/scan in the 1, 3, and 6 hours before synoptic time for 25 knot RI for non-RI and RI TCs within 24 hours. Values are significantly different at the 99% confidence level except at a radius of 50 km, where the difference is significant at the 95% confidence level.

30 kts in 24 hours RI N=1017/103	r=50 km	r=100 km	r=150 km	r=200 km	r=300 km	r=500 km
OTs (1 hr)	0.11/0.15	0.34/0.58	0.65/1.16	1.08/1.84	2.15/3.58	3.89/6.60
OTs (3 hr)	0.11/0.15	0.33/0.51	0.63/1.02	1.04/1.66	2.03/3.37	3.66/6.31
OTs (6 hr)	0.11/0.15	0.33/0.50	0.64/1.00	1.04/1.67	2.06/3.47	3.73/6.30

Table 6b: Average OTs/scan in the 1, 3, and 6 hours before synoptic time for 30 knot RI for non-RI and RI TCs within 24 hours. Values are significantly different at the 99% confidence level except at a radius of 50 km, where the difference is significant at the 95% confidence level.

35 kts in 24 hours RI N=1032/88	r=50 km	r=100 km	r=150 km	r=200 km	r=300 km	r=500 km
OTs (1 hr)	0.11/0.19	0.34/0.70	0.63/1.40	1.06/2.25	2.11/4.34	3.81/7.90
OTs (3 hr)	0.11/0.17	0.32/0.59	0.63/1.18	1.02/1.97	2.01/4.01	3.59/7.51
OTs (6 hr)	0.12/0.18	0.33/0.56	0.63/1.15	1.02/1.97	2.03/4.04	3.67/7.42

Table 6c: Average OTs/scan in the 1, 3, and 6 hours before synoptic time for 35 knot RI for non-RI and RI TCs within 24 hours. Values are significantly different at the 99% confidence level except at a radius of 50 km, where the difference is significant at the 95% confidence level.

1. 25 knot RI

The statistics of the resulting optimal forecasts when analyzing all 125 Atlantic TCs for RI at 25 knots can be seen in Figure 32. Based on the PSS, this forecast is a threshold 3 OTs/scan with a BT less than or equal to 215 K within a 200 km disk of the TC center over a 3 hour running average. With a PSS equal to 0.356, this forecast, which ignores all OTs after a threshold is reached, has a POD of 59.6% with a FAR of 70.4% and POFD of 24.0%. As finally 36 of the 57 TCs correctly predicted by the respective forecasts, while the FAR remains consistently around 72%. Yet, 21 TCs are not forecasted to undergo RI even when

an updated forecast is issued at each satellite scan. Some of these could be attributed to the temporal resolution of the satellite scan, as 28.6% (6 out of 21) of these TCs underwent RI when only having 30 minute temporal resolution as opposed to the optimal 15 minutes for full OT detection.

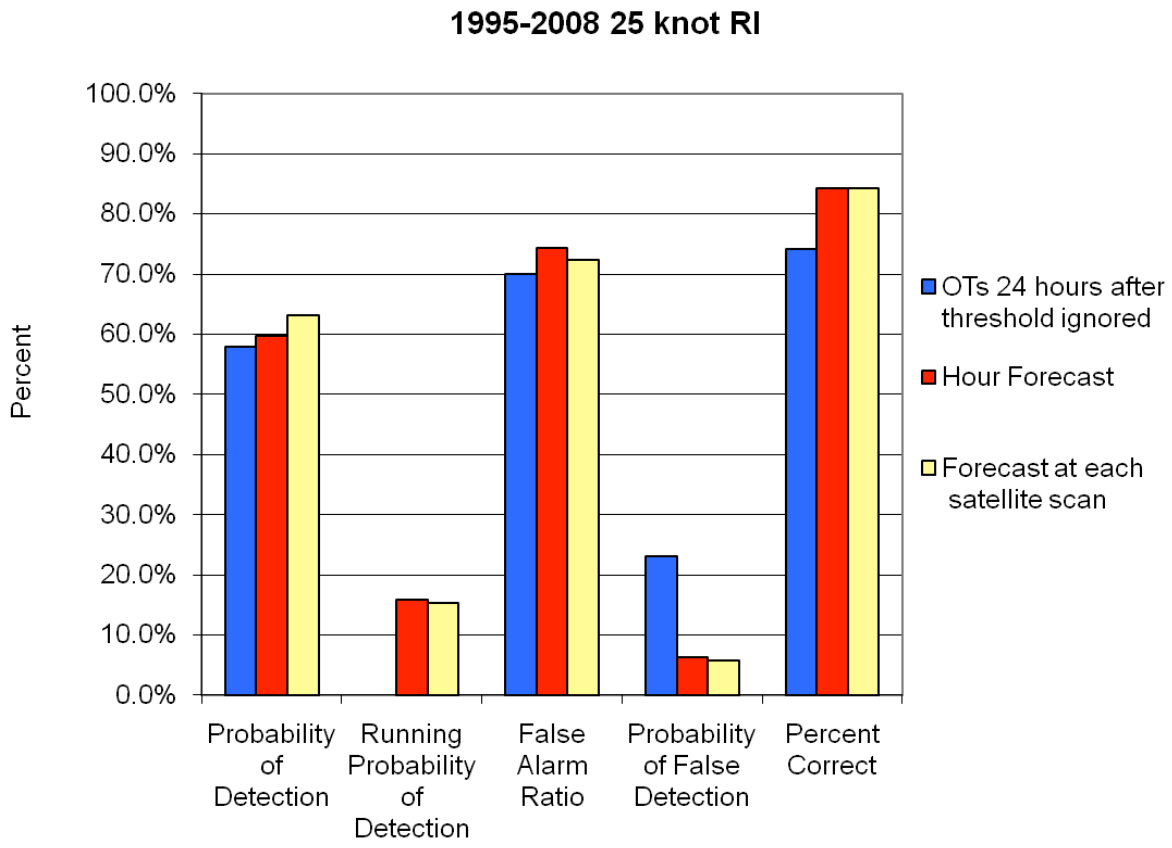

Figure 32: Probability of Detection, Running Probability of Detection, False Alarm Ratio, Probability of False Detection, and Percent Correct for the 3 25 knot RI forecast of 3 OTs/scan average for 3 hours with a BT of 215 K or colder within 200 km of the TC center for 1995-2008.

However, it is important to note that the OTs do not encompass the array of optimal predictors currently used by operational RI forecast models. One of these predictors includes OHC, which is a potential contributor to the RI of Hurricane Floyd (1999) (Pasch et al. 1999). Other TCs, such as Hurricane Erin (2001), underwent RI after departing synoptic scale features which would inhibit OTs, such as the SAL (Dunion and Velden 2004).

This forecast can be applied to just TCs from 2006-2007 to provide a correct comparison to operational RI forecasts as well as the forecast method described by KDK10. Results from the 2006-2007 OT RI Index can be seen in Figure 33. The POD ranges from 57.1% to 71.4% for the 7 TCs underwent open-water RI during this time frame. This is higher than any of the other intensity guidance options during this time period, with their POD is comparable to the RPOD from this forecast, and is comparable to the RII POD of 59%. As with the full dataset, the FAR for this time period is approximately 72% (70.4% to 74.2%). While the FAR associated with these forecasts are high, they are within the envelope of the operational forecasts used during the 2006 and 2007 Atlantic Hurricane Season and compared to the RII FAR of 71% (KDK10). Despite the high FAR, all 3 forecasts are skillful, indicated by positive values of the PSS.

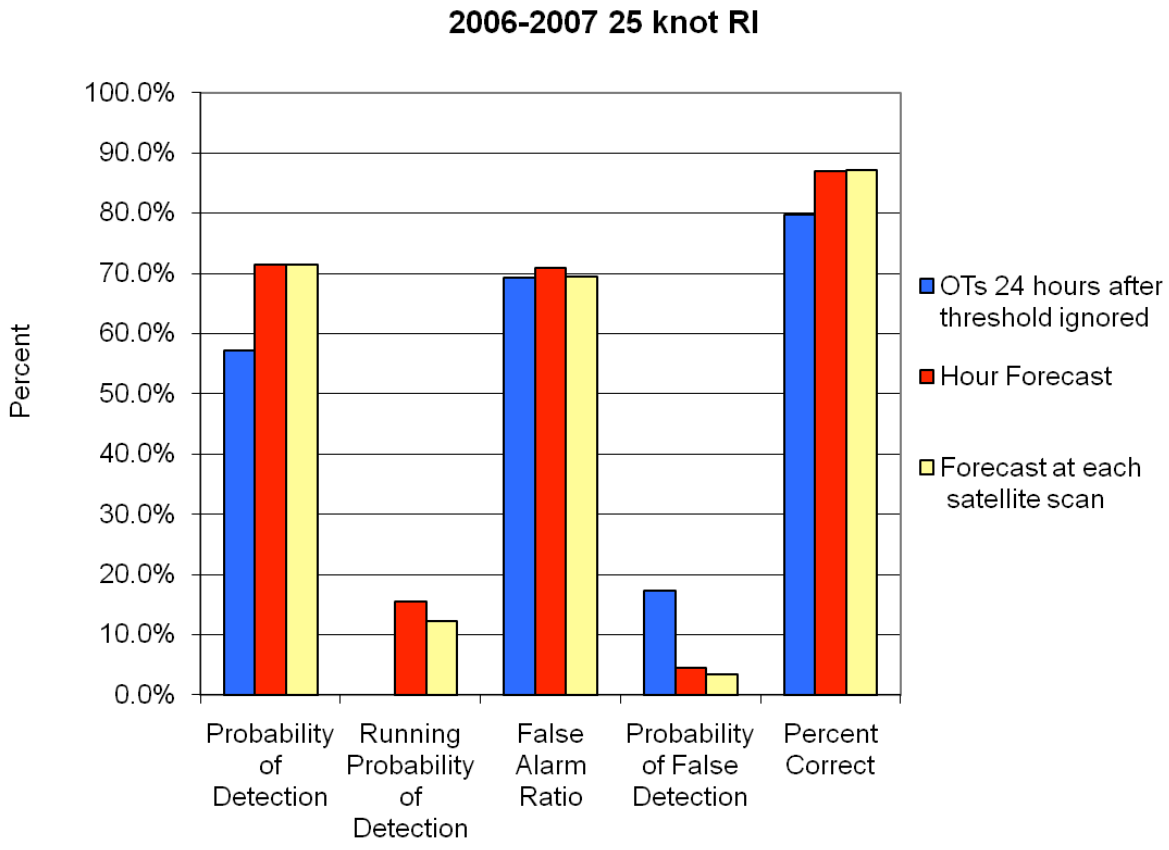

Figure 33: Same as Figure 32 but for all 2006-2007 TCs.

2. 30 knot RI

Even though Steranka (1986) indicated there was a relationship between convective bursts within 200 km of a TC and intensification, 4 different radii where analyzed to find the optimal forecast for RI. Analysis of these radii for 30 knot RI indicates the most optimal forecast occurs when averaging OTs within a 300 km disk of the TC center, not 200 km as in 25 knot RI. Thus, the same spectral analysis was re-run on OTs within 300 km to verify this distance does not experience a diurnal or semidiurnal signal. With 9.9% (23.1%) of the TCs indicating the presence of a diurnal (semidiurnal) signal, it was decided no modifications were needed to account for theses signals.

The results for the 3 distinct forecasts can be seen in Figure 34. This optimal forecast is a 3-hours average of 4.5 OTs/scan at a BT equal to or colder than 215 K within 300 km of the TC center. With a PSS equal to 0.379, ignoring all OTs 24 hours after a threshold is reached has a POD of 69.0% with a FAR of 80.0% and POFD of 31.1%. Again, the POD increases when accounting for more OTs/scan averages. Here, the highest POD corresponds to a forecast issued every hour; however this is due to the fact that this forecast does not require a full 3 hours of OT data before making an average like the other 2 forecasts. When requiring a full 3 hours of OTs to average, 30 of the 42 TCs are indicated to undergo RI when issuing a forecast for each new satellite scan. Of the 12 misses, 5 of these TCs only had a temporal scan resolution of 30 minutes, while 2 others did not have a full 24 hours between the end of one RI cycle and the beginning of another.

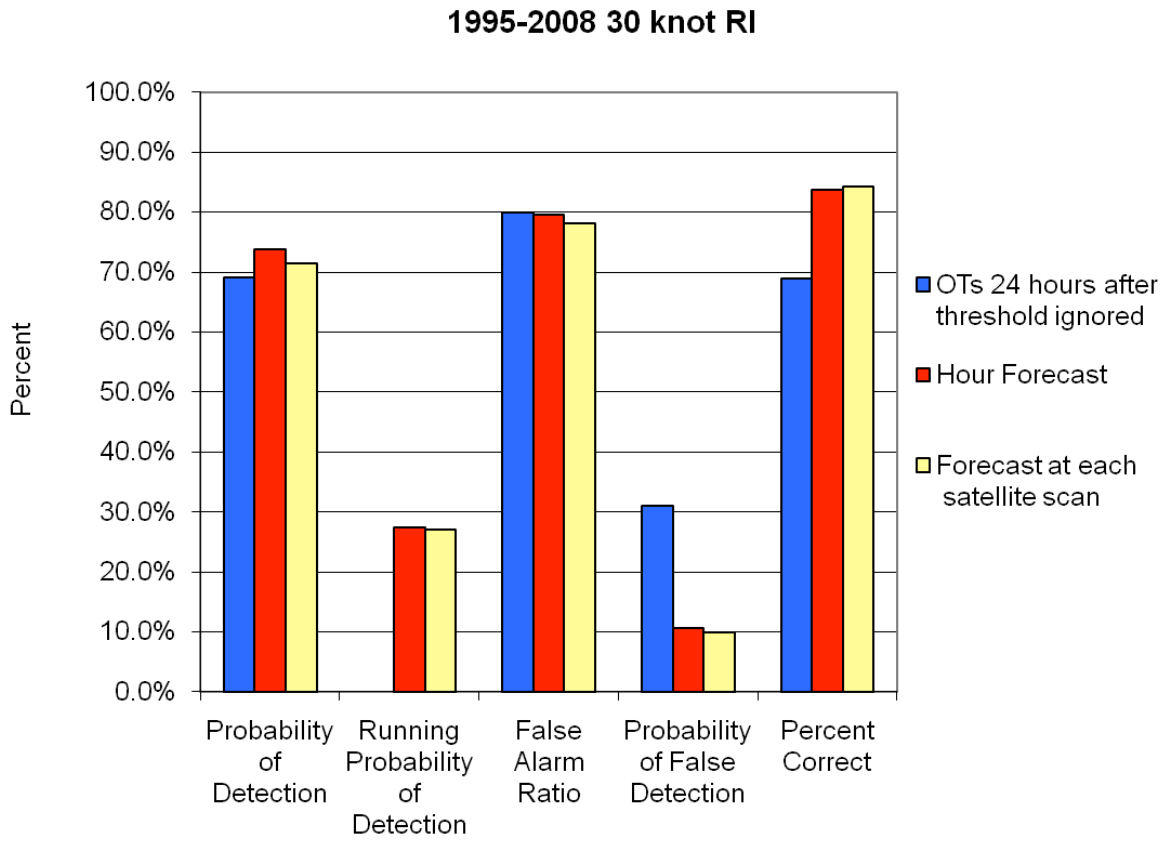

Figure 34: Probability of Detection, Running Probability of Detection, False Alarm Ratio, Probability of False Detection, and Percent Correct for the 30 knot RI forecast of 4.5 OTs/scan average for 3 hours with a BT of 215 K or colder within 300 km of the TC center for 1995-2008.

Potentially due to the increased in analyzed radius, the 30 knot RI forecast can make up for shortfalls in the 25 knot RI forecast. Of the 21 TCs missed by the 25 knot RI forecast, 13 of them underwent intensity changes greater than 30 knots. Four of these storms, are correctly predicted to undergo RI by this forecast. However, the Hurricane Floyd (1999) RI potentially contributed to by OHC is still missed by this forecast. Another RI event missed by both the 25 knot and 30 knot RI forecast is the RI of Hurricane Danny (1997) before landfall along the Gulf Coast. This RI has been contributed to moderate vertical shear (Molinari et al. 2004), as Hurricane Danny formed from non-tropical origins (Pasch 1997). However, it is widely accepted that vertical shear hinders TC intensification, with RI TCs experiencing less vertical wind shear than non-RI TCs (KDK10, RK11). Accounting for

wind shear by ignoring OT/scan averages with an ASD of 36º or lower improves the overall OT RI index PSS by reducing the number of incorrectly forecasted RI events, and will therefore be continued.

Again, this forecast can be applied to just TCs from 2006-2007 to provide direct comparison to the RII from KDK10. The statistics associated with these forecasts can be seen in Figure 35. With a POD of 60.0%, these forecasts have a higher detection rate of the 5 open-water RI events than the intensity guidance options during this time period and the RII. However, FAR around 85% (84.1% to 86.8%) is higher than both the NHC official forecast and the RII; however it is still lower than the Geophysical Fluid Dynamic Laboratory model (GFDL). Finally, in terms of optimality, the PSS for the RII is greater than the OT RI Index

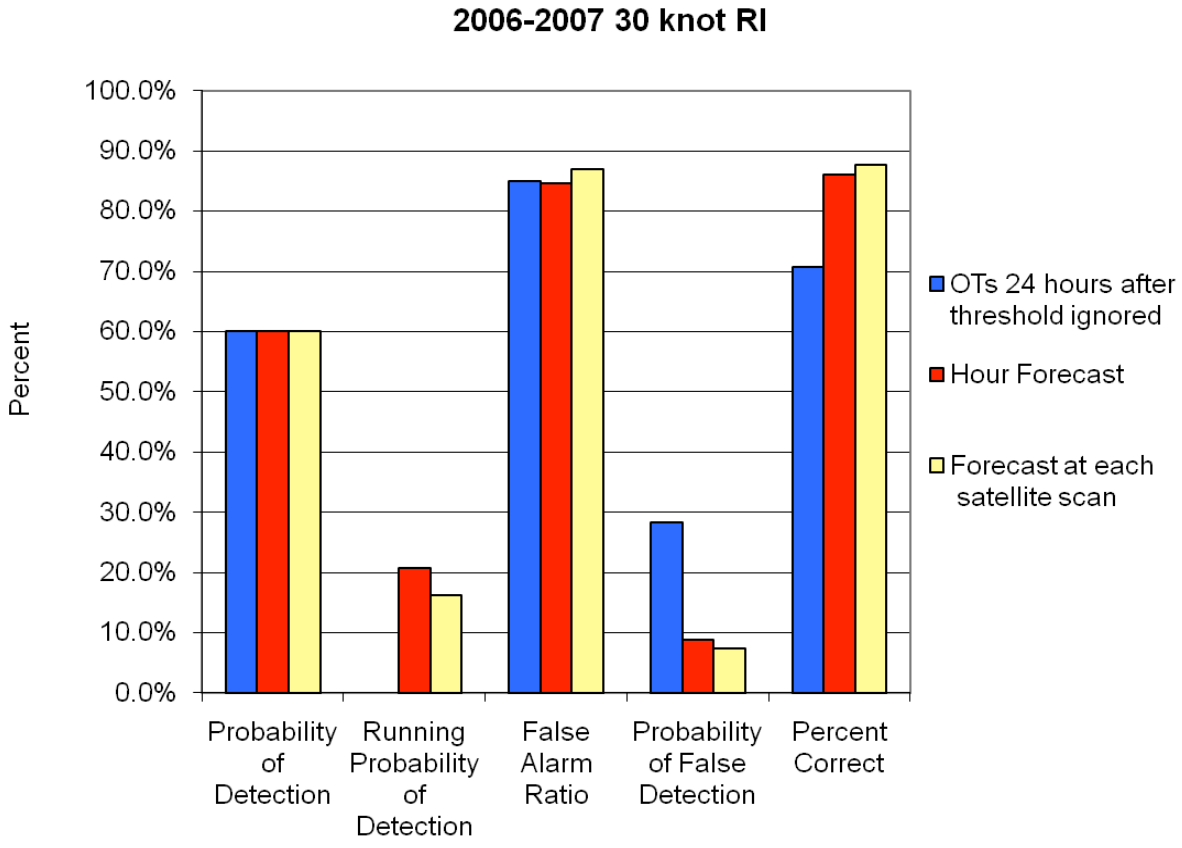

Figure 35: Same as Figure 34 but for all 2006-2007 TCs.

when ignoring OTs 24 hours after a threshold is reached (now shown), however the RII PSS is less than both the hourly forecast and the forecast at each satellite scan.

3. 35 knot RI

As with 25 knot RI, the optimal forecast for 35 knot RI, according to the PSS, occurs when averaging OTs within 200 km of the TC center. This forecast is a 3-hour average of 4 OTs/scan with a BT at least 215 K or colder, more than for 25 knot RI. When ignoring all OTs 24 hours after an exceeded threshold, this forecast has a POD of 57.6% with a FAR of 78.9% and POFD of 18.8% for a PSS equal to 0.388, as seen in Figure 36. The POD increases to its maximum of 60.6% (20 out of 33 TCs) when issuing a forecast with each new satellite scan. Thus, 13 TCs are not correctly forecasted to undergo RI by this forecast. Five

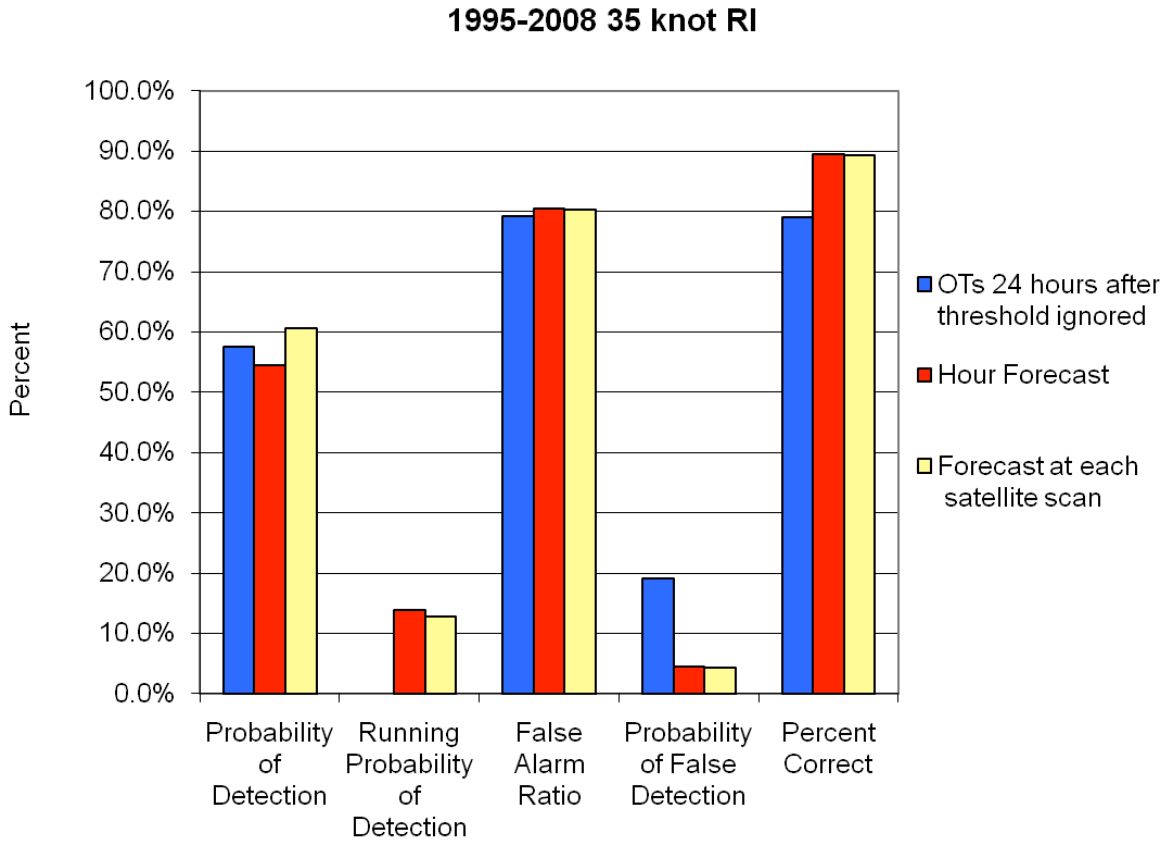

Figure 36: Probability of Detection, Running Probability of Detection, False Alarm Ratio, Probability of False Detection, and Percent Correct for the 35 knot RI forecast of 4 OTs/scan average for 3 hours with a BT of 215 K or colder within 200 km of the TC center for 1995-2008.

of these (38.5 %) only have a satellite scan temporal resolution of 30 minutes. Six of these (46.2 %) were correctly forecasted to undergo 30 knot RI, which is forecasted by OTs within a 300 km radius, but not 35 knot RI. While the initial thought was this is due to the different TC sizes, analysis of the RMW from the Automated Tropical Cyclone forecast (ATCF) revealed no significant different between these 6 storms and those correctly forecasted to undergo 35 knot RI. The final missed RIs belong to Hurricane Floyd (1999), which has been attributed to high OHC (Paush 1997), and Hurricane Alex (2004). The RI of Hurricane Alex was aided by warm Gulf waters and light shear (Franklin 2004) and continues to exemplify the shortcomings of the OT RI index, as no RI was forecast at 25, 30, or 35 knots for this TC.

When comparing OT RI forecasts from 2006-2007 to the RII, while the OT RI index was on par with the RII at 25 and 30 knots, the OT RI does drastically worse than the RII at 35 knots. Of the 4 OTs which underwent 35 knot RI during this time period, the OT RI index did not forecast any of them with any of the 3 forecast types. This results in FAR of 100%, as seen in Figure 37. With a negative PSS (not shown), this forecast has no skill at 35 knots, compared to RII with a PSS equal to 0.1 (KDK10). One of these TCs missed by the 35 knot forecast was missed by every RI forecast, Hurricane Dean (2007). This RI has been attributed to an increase in upper-level outflow (Franklin 2008), again illustrating the weakness of using the single predictor OT RI index.

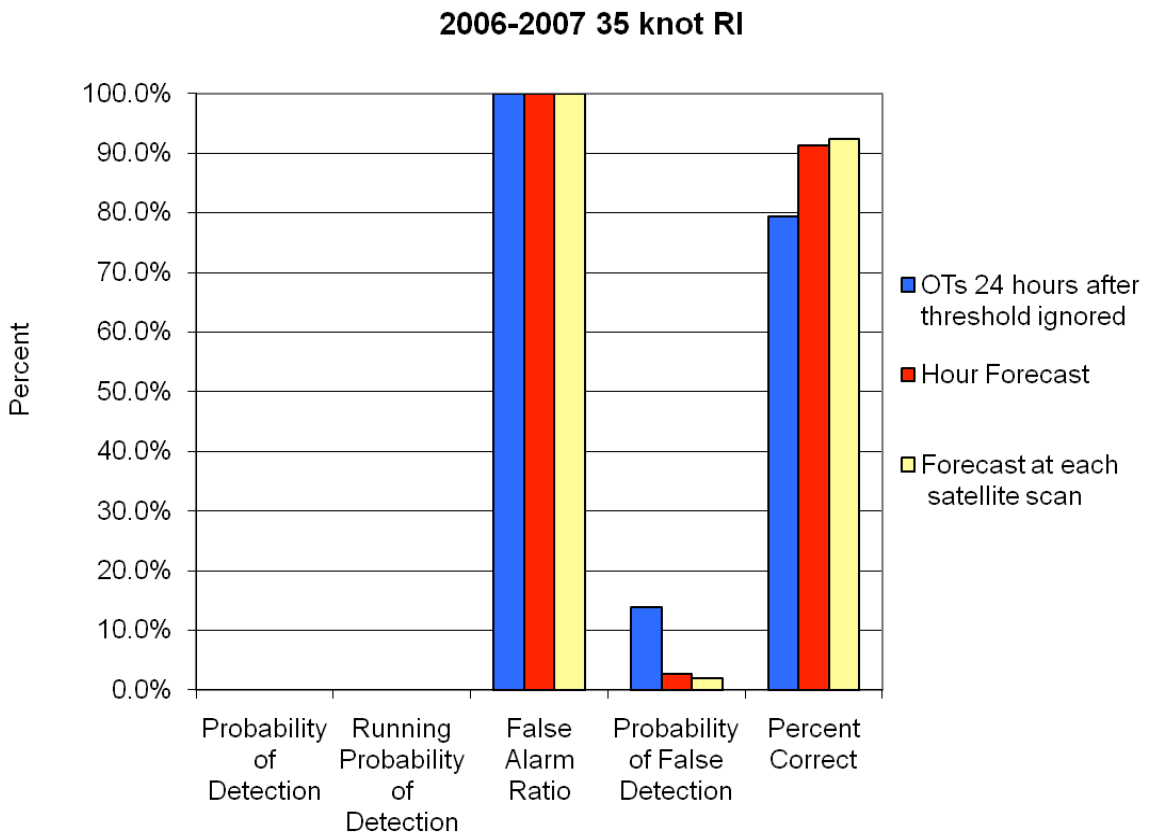

Figure 37: Same as Figure 36 but for all 2006-2007 TCs.

4. Logistic regression model

Several cases of RI missed by the OT RI index can be attributed to other RI factors, such as OHC. Since the mean average OTs prior to synoptic times between RI and non-RI cases is different at the 95% confidence level, OTs can be added as an indicator to the logistic regression scheme employed by RK11 to observe their impact on forecast skill. Analysis reveals the optimal OT predictors are 3 hour average OTs within 50 km of the TC center as well as 6 hour average OTs within 200 km of the TC center. These time frames are at least 3 hours in duration, which is the length of time investigated by the spectral analysis in section III.b.1, so no modifications for a semidiurnal signal are necessary.

These 2 OT predictors are added to the 7 predictors defined by Table 1 in RK11 for

forecast skill verification. Addition of the OT predictors reduces the size of the RK11 dataset from N= 2572 to N=1308, as only the TCs from 1995-2008 meeting the criteria from section III.c.1 are analyzed by the OTs. The addition of the OTs on the logistical regression RI forecast skill can be assessed by the BSS, as is done in RK11. Here, the BSS is with respect to the training data's baseline climatological probability of RI, and can be seen in Figure 38 for the logistic regression scheme. As expected, the BSS decrease with increasing RI thresholds, as RI becomes even more of a rare event (RK11).

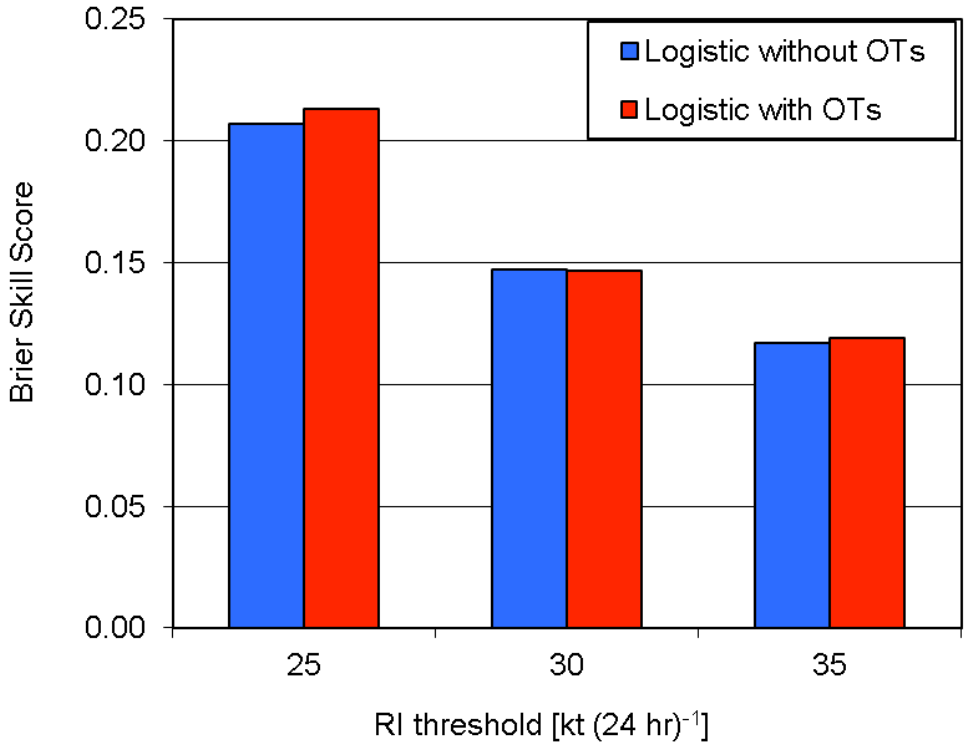

Figure 38: Brier Skill Score for the logistic regression model presented by RK11 for the 125 TCs analyzed by the OTs. Increase (constancy) in the BSS represents improved (constant) forecast skill with the OT additions.

Addition of the OTs to the logistic regression scheme has an overall improvement on the forecast skill. The BSS for the 25 and 35 kt RI forecast increases when adding the two OT predictors, indicating increased forecast skill through a leave-one-season-out cross validation. While the BSS for 30 kt RI does not increase, it does not decrease, indicating no

forecast improvement or deterioration with the addition of the OTs. Therefore, the addition of the OTs to the predictors already deemed optimal by RK11 further increases skill of the logistical regression scheme at predicting RI when compared to climatology.

Optimal RI predictors for the logistic regression scheme are found using a stepwise algorithm. Based on this algorithm, the 9 predictors (7 from RK11 and 2 OT) analyzed in Figure 38 are not deemed optimal when including the OT predictors in finding the set of optimal OT and SHIPS predictors. These chosen predictors produced a lower BSS than the logistic regression scheme without OTs in Figure 38. However, they do produce a higher PSS at 35 knots. Therefore, the stepwise procedure used in this analysis is not the best when optimizing the BSS (C. Rozoff 2011, personal communication).

5. Conclusions

An OT RI index is developed for the Atlantic basin which utilized average OT/scan within a disk of specific radii from the center of the TC to predict RI within the subsequent 24 hours. Separate OT/scan and radii thresholds are developed for 25, 30, and 35 knot RI thresholds. While a direct response by the OTs is not obtainable for all the indicators used to predict RI (KDK10, RK11), hourly averages based on Statistical Hurricane Intensity Prediction Scheme (SHIPS) data availability indicated the potential for OTs as an indicator, as the mean difference between RI and non-RI TCs significant at the 95% confidence interval accorded in the two-sided Student's T-test.

A dependent test was conducted based on 125 landfalling Atlantic TCs between 1995 and 2008 and TCs from 2004-2008 whose tracks remained east of 55º W based on HURDAT. The OT/scan thresholds were then applied to a subset of all the TCs from 2006-2007 regardless of location to provide comparison between the OT RI index and the RII.

Based on this data, the OT RI index proved to be skillful at 25 and 30 knots; however no TCs were forecasted to undergo 35 knot RI during this time frame. The POD ranges from 0.0% to 60.0% while the FAR ranges from 70.4% to 100.0% when ignoring OTs within 24 hours of an exceeded OT/scan threshold. The POD and FAR continue to increase when issuing more frequent forecasts every hour or with every new satellite scan. While the OTs are only one indicator, their modest POD and high FAR are consistent with other intensity guidance options. Addition of the OTs to the logistic regression scheme from RK11 indicated increased or constant BSS, indicating increased forecast skill for the 125 TCs used in this analysis when adding the OTs.

VI. Conclusions

This research applies an objective overshooting top (OT) detection algorithm for detection of intense convection in the tropics associated with the formation and intensification of TCs. While no measure for evaluating the ambient height of the tropical tropopause has been included in the final modification from Bedka et al. (2010) algorithm, the modified algorithm captures potential OTs in tropical pouches as well as weak TCs. OT detection does extend to strong TCs; however some of their characteristics, such as the CDO, reduce detection. OTs are averaged within varying radii from the center of the pre- or post-genesis TC for varying lengths of time to find optimal thresholds to forecast genesis and rapid intensification (RI) of TCs.

The role of convection has been hypothesized and modeled to be associated with the development of TCs. The “Vortical” Hot Tower theory can be investigated by the OT detection algorithm, as a VHT in Supertyphoon Jangmi (2008), while at TS strength. Pre-

genesis TCs are tracked using the marsupial pouch paradigm (Wang et al. 2009, Dunkerton et al. 2009) for 2009-2010, a necessary condition for this forecast. It was found that:

1. Moderate to good correlation (0.576) exists between the OTs and the vertical vorticity component at 30º W, allowing for genesis prediction under the VHT theory.
2. When dividing the track of pre-genesis pouches into 2 hour periods, 63.0% of the 2009 and 2010 PREDICT pouches exceeding a threshold of 4 OTs/scan along either the UKMET or GFS track underwent tropical cyclogenesis. This 63.0% developing is this is still below the NHC 83.3% of pouches developing when a high chance of formation is issued. However, the OTs could further increase the NHC percent of pouches developing from 83.3% as 2 of the 4 non-developing high probabilities were not indicated by the OTs.
3. Predicting when genesis will occur, a correlation of -0.75 exists between the first 2-hour OT/scan average exceeding 4.25 and the days until genesis for 12 TCs: TCs developing east of 25º W or not exceeding TD strength, as well as TS Claudette (2009) are not included in this correlation.
    a. The time of forecasted genesis relies on the linear decrease in the number of days until genesis from the exceeded OT/scan time as the value of the OT/scan increases. This forecast has a mean error of 1.25 days (30 hours).
    b. Forecast modification occurs if 4 OTs/scan is exceeded twice with 12 hours elapsing between them. The average forecast error is reduced to 0.75 days (18 hours), with 81.8% of correctly predicted TCs developing within ± 24 hours of their forecasted time. This corresponds to 32.1% of all predicted genesis events.

   c. While the genesis of Hurricane Karl (2010) was difficult to predict, OTs would have been predicted genesis within 6 hours of actual development.

4. OTs could add to a TC formation probability product, however better results should be observed for genesis within 48 hours as 1-2 elapses between VHT detection and TC genesis.

While RI has been shown to be a result of multiple environmental and oceanic influences, OTs can be an optimal predictor, as the average OTs prior to synoptic times between RI and non-RI cases differs at the 95% confidence level. For the OT RI index:

1. In an independent test of 2006-2007 RI cases, the POD ranged from 0.0% to 60.0% with a FAR of 70.4% to 100.0% when ignoring OTs within 24 hours of an exceeded OT/scan threshold. Each RI threshold has a defined radius and OT/scan threshold; however OTs consistently missed the RI of Hurricane Dean (2007), which has been attributed to an increase in upper-level outflow, indicating the weakness of the OTs as a single predictor.
2. When adding the OTs to the logistical regression model for RI prediction from RK11, the BSS either increased (25-kt and 35 kt RI) or remained constant (30-kt RI), indicating an increased or constant forecast skill. This increase in forecast skill in addition to the increase in the Brier Skill Score (BSS) associated with current operational RI forecasts (RK11).

The most significant finding of this research is with respect to the RI of TCs. As indicated in RK11, the logistic regression scheme of RI prediction has greater forecast skill, represented by the BSS, than the current operational model, the RII. The addition of the OTs into a subset of the logistic regression model has been shown to even further improve the

BSS, and it can be assumed that the logistic regression model BSS in RK11 would further improve with OT additions, increasing forecast skill in an area which has been deemed a top priority of the NHC (RK11). In addition, exceeding a threshold of 4 OT/scan along the UKMET or GFS marsupial pouch track is almost necessary, however not sufficient, for TC genesis in the Atlantic Basin, with 63% of instances developing into TCs. If this threshold is exceeded twice with 12 hour elapsing in between, there is also a 63% chance of formation within 24 hours.

VII. Future Work

The current TC probability forecast from RAMMB at CIRA predicting the probability of TC genesis for the next 24 hours. While the OTs did not perform well at 24 hours, there is the potential for better performance with a 48 hour forecast as twice as many maximum OTs/scan are observed within 48 hours of genesis than 24 hours. Once the TCFP is extended to 48 hours, the OTs may again be included as an additional genesis predictor. Furthermore, data will continually be gathered, assuming pouch forecasts are available for 2011 and subsequent years, to continue to modify the OT/scan thresholds defined in section IV.a.2.

Given the potential for improvement of operational RI forecasts models with the addition of the OTs, the OTs will be a part of the 2011 National Hurricane Center Proving Ground (PG). As one of the few selected GOES satellite products to be demonstrated during the hurricane season, forecasters at NHC will be able to assess the potential usefulness of this product. In addition, feedback on performance and potential improvements will also be provided by NHC.

While the use of the OTs can provide almost consistent 15 minute data, satellite

eclipses due occur. These eclipses usually occur in a 48 day period symmetric around the Vernal and Autumnal Equinoxes and can last from 0 to 3 hours (Pinkine and Motta 1999). Lightning could potentially act as a proxy for the missed satellite data, as Bedka et al. (2010) indicated there is a 70% frequency of a cloud-to-ground lightning strike within 5 km of an OT. Using the World Wide Lightning Location Network (WWLLN), lightning has been compared to intensity changes in TCs (Solorzano et al. 2011). Collaboration will be done with Drs. Solorzano and Thomas at the Digipen Institute of Technology to compare detected lightning strikes and OTs.

VIII. Acknowledgments

I would like to thank the multitude of people who helped make this work possible. To my advisor Wayne Feltz, thanks for offering me the chance to continue my education and work on this research and Kristopher Bedka for allowing me to modify the original OT detection algorithm. Also, thanks to Lee Cronce, Justin Seiglaff, and Jason Brunner for their assistance with GeoCAT and the OT algorithm. Thanks to Chris Velden for his willingness to help me as I began working in the tropical world and Kyle Griffin and John Sears for answering all the seemingly easy questions about TCs that I did not know due to my initial lack of tropical cyclone knowledge. To Drs. James Kossin, Chris Rozoff, and Mark Boothe, thanks for all the data you provided to help make this thesis possible.

Special thanks to Greg Tripoli, Larissa Back, and Steve Ackerman for providing insight on this manuscript. Finally, thanks to my family and friends for their support through this entire experience.

This research is funded by the NOAA GOES-R Proving Ground Program: Contract No.:NA06NES4400002 Fund:144PH46.

IX. References

Adler, R. F., M. J. Markus, D. D. Fen, G. Szejwach, and W. E. Shenk, 1983: Thunderstorm top structure observed by aircraft overflights with an infrared radiometer. *J. Appl. Meteor. And Climatol.*, **22**, 579-593.

_____ and E. B. Rodgers, 1997: Satellite-Observed Latent Heat Release in a Tropical Cyclone. *Mon. Wea. Rev.*, **105**, 956-963

Alcala, C. M., and A. E. Dessler, 2002: Observations of deep convection in the tropics using the Tropical Rainfall Measuring Mission (TRMM) precipitation radar, *J. Geophys. Res.*, **107**, doi:10.1029/2002JD002457.

Barton, J., J. Bass and M. Milnes, 2004: MTSAT Image Data Acquisition and Control System. *American Institute of Aeronautics and Astronautics*. [Available online at http://www.aiaa.org/spaceops2004archive/downloads/papers/SPACE2004sp-template00309F.pdf]

Bedka, K. M., J. Brunner, R. Dworak, W. Feltz, J. Otkin and T. Greenwald, 2010: Objective Satellite-Based Overshooting Top Detection Using Infrared Window Channel Brightness Temperature Gradients. *J. Appl. Meteor. And Climatol.*, **49**, 181-202.

_____, R. Dworak, J. Brunner, and W. Feltz, 2011a: Validation of Satellite-Based Objective Overshooting Cloud Top Detection Methods Using CloudSat Cloud Profiling Radar Observations. *Submitted to J. Appl. Meteor. and Climatol.*

_____, J. Brunner, W. Feltz, R. Dworak, cited 2011: Overshooting Top and Enhanced-V Detections. Convection Working Group [Available online at http://www.convection-wg.org/doc_bedka.php]

Bender, M. A., I. Ginis, and Y. Kurihara, 1993: Numerical simulations of tropical cyclone–ocean interaction with a high-resolution coupled model. *J. Geophys. Res.,* **98,** 23 245–23 263.

Bister, M., and K. A. Emanuel, 1997: The Genesis of Hurricane Guillermo: TEXMEX Analyses and Modeling Study. *Mon. Wea. Rev.*, **125**, 2662-2682.

Blake, E. S., 2010: Tropical Cyclone Report, Tropical Storm Gaston. *National Hurricane Center*. Available at http://www.nhc.noaa.gov/pdf/TCR-AL092010_Gaston.pdf

Bosart, L. F., W. E. Bracken, J. Molinari, C. S. Velden, and P. G. Black, 2000: Environmental Influences on the Rapid Intensification of Hurricane Opal (1995) over the Gulf of Mexico. *Mon. Wea. Rev.*, **128**, 322–352.

Brunner, J. C., S. A. Ackerman, A. S. Bachmeier, and R. M. Rabin, 2007: A quantitative analysis of the enhanced-V feature in relation to severe weather. *Wea. Forecasting*, 22, 853–872.

Cain, D. R. and P. Kirkwood, cited 2011: WSR-88D Radar FAQ's. [Available online at http://weather.noaa.gov/radar/radinfo/radinfo.html]

Charney, J. G., and A. Eliassen, 1964: On the Growth of the Hurricane Depression. *J. Atmos. Sci.*, **21**, 68-75.

Corbosiero, K. L., and J. Molinari, 2002: The Effects of Vertical Wind Shear on the Distribution of Convection in Tropical Cyclones. *Mon. Wea. Rev.*, **130**, 2110–2123.

Culverwell, I. D., and S. F. Milton, 2000: An Evaluation of The Met. Office Global NWP Model by Comparison with ARM Data in the Tropical Western Pacific. *Proc. Tenth ARM Science Team Meeting,* San Antonio, Texas, American Radiation Measurement. [Available online at http://www.arm.gov/publications/proceedings/conf10/extended_abs/culverwell_id.pdf].

DeMaria, M., and J. Kaplan, 1994a: A Statistical Hurricane Intensity Prediction Scheme (SHIPS) for the Atlantic Basin. *Wea. Forecasting*, 9, 209-220.

_____, 1996: The effect of Vertical Shear of Tropical Cyclone Intensity Changes. *J. Atmos. Sci.*, **53**, 2717-2745.

_____, and J. Kaplan, 1999: An Updated Statistical Hurricane Intensity Prediction Scheme (SHIPS) for the Atlantic and Eastern North Pacific Basins. *Wea. Forecasting*, 14, 326–337.

_____, M. Mainelli, L. K. Shay, J. A. Knaff, and J. Kaplan, 2005: Further Improvements to the Statistical Hurricane Intensity Prediction Scheme (SHIPS). *Wea. Forecasting*, 20, 531–543.

Dunkerton, T. J., M. T. Montgomery, and Z. Wang, 2009: Tropical cyclogenesis in a tropical wave critical layer: easterly waves, *Atmos. Chem. Phys*., **9**, 5587-5646.

Dunion, J. P., and C. S. Velden, 2004: The impact of the Saharan air layer on Atlantic tropical cyclone activity. *Bull. Amer. Meteor. Soc.*, **85**, 353–365.

_____ and C. S. Marron, 2008: A Reexamination of the Jordan Mean Tropical Sounding Based on Awareness of the Saharan Air Layer: Results from 2002. *J. Climate*, **21**, 5242–5253.

Elsberry, R. L., T. D. B. Lambert, and M. A. Boothe, 2007: Accuracy of Atlantic and Eastern North Pacific Tropical Cyclone Intensity Forecast Guidance. *Wea. Forecasting*, **22**, 747–762.

Emanuel, K. A., 1986: An Air-Sea Interaction Theory for Tropical Cyclones. Part I: Steady-State Maintenance. *J Atmos. Sci.*, **43**, 585-605.

_____, 1989: The Finite-Amplitude Nature of Tropical Cyclogenesis. *J. Atmos Sci.*, **46**, 3431-3455.

_____, 1999: Thermodynamic control of hurricane intensity. *Nature,* **401**,665–69.

Enagonio, J., and M. T. Montgomery, 2001: Tropical Cyclogenesis via Convectively Forced Vortex Rossby Waves in a Shallow Water Primitive Equation Model. *J. Atmos. Sci.*, **58**, 685–706.

Evans, C., H. Archambault, J. Cordeira, C. Fritz, T. Galarneau, Jr., S. Gjorgjievska, K. Griffin, A. Johnson, W. Komaromi, S. Monette, P. Muradyan, B. Murphy, M. Riemer, J. Sears, D. Stern, B. Tang, and S. Thompson, 2011: The PRE-Depression Investigation of Cloud-systems in the Tropics (PREDICT) Field Campaign: Perspectives of Early Career Scientists. *In Review, Bull. Amer. Meteor. Soc.*

Frank, N. L., 1970: Atlantic tropical systems of 1969, *Mon. Wea. Rev*., **98**, 307–314.

Franklin, J. L., 2004: Tropical Cyclone Report, Hurricane Alex. *National Hurricane Center*. [Available online at http://www.nhc.noaa.gov/pdf/TCR-AL012004_Alex.pdf].

_____, 2008: Tropical Cyclone Report, Hurricane Dean. *National Hurricane Center*. [Available online at http://www.nhc.noaa.gov/pdf/TCR-AL042007_Dean.pdf].

_____ and J. Cangialosi, 2011: National Hurricane Center 2010 Forecast Verification. *2011 Interdepartmental Hurricane Conference*. Miami, FL. [Available online at http://www.ofcm.gov/ihc11/linking_file_ihc11.htm]

Gettelman, A., M. L. Salby, and F. Sassi, 2002: Distribution and influence of convection in the tropical tropopause region, *J. Geophys. Res.*, **110,** 4080, doi:10.1029/2001JD001048.

Glickman, T., Ed., 2000: *Glossary of Meteorology*. 2nd ed. Amer. Meteor. Soc., 855 pp.

Gray, W. M., 1968: Global View of the Origin of Tropical Disturbances and Storms. *Mon. Wea. Rev.*, **96**, 669-699.

Guimond, S. R., G. M. Heymsfield, and F. J. Turk, 2010: Multiscale Observations of Hurricane Dennis (2005): The Effects of Hot Towers on Rapid Intensification. *J. Atmos. Sci.*, **67**, 633–654.

Hendon, H. H. and K. Woodberry, 1993: The Diurnal Cycle of Tropical Convection. *J. Geophys. Res.*, **98,** 16,623–16,637, doi:10.1029/93JD00525.

Hendricks, E. A., M. T. Montgomery, and C. A. Davis, 2004: The Role of "Vortical" Hot Towers in the Formation of Tropical Cyclone Diana (1984). *J. Atmos. Sci.*, **61**, 1209-1232.

_____, M. S. Peng, B. Fu, and T. Li, 2010: Quantifying Environmental Control on Tropical Cyclone Intensity Change. *Mon. Wea. Rev.*, **138**, 3243–3271.

Heidinger, A., 2008: GEOCAT, The Geostationary Cloud Algorithm Test-Bed. Satellite Algorithm Test Bed Workshop, Suitland, MD, National Satellite Operations Facility. [Available online at http://www.star.nesdis.noaa.gov/star/documents/corp/SATB/SATBgeocat.pdf.]

Hennon, 2002: Exploring the connections of extreme convective events and upper-ocean heat content in the tropical cyclone. *25th conference on Hurricanes and Tropical Meteorology*, *San Diego, CA, April 29-May 3*.

Heymsfield, G. M., J. B. Halverson, J. Simpson, L. Tian, and T. P. Bui, 2001: ER-2 Doppler Radar Investigations of the Eyewall of Hurricane Bonnie during the Convection and Moisture Experiment-3. *J. Appl. Meteor.*, **40**, 1310–1330.

Hong, X., S. W. Chang, S. Raman, L. K. Shay, and R. Hodur, 2000: The Interaction between Hurricane Opal (1995) and a Warm Core Ring in the Gulf of Mexico. *Mon. Wea. Rev.*, **128**, 1347–1365.

Hurricane Research Division, cited 2011: Frequently Asked Questions: What is a tropical disturbance, a tropical depression, or a tropical storm? [Available online at http://www.aoml.noaa.gov/hrd/tcfaq/A5.html]

Jarvinen, B. R., and C. J. Neumann, 1979: Statistical forecasts of the tropical cyclone intensity for the North Atlantic Basin. NOAA Tech. Memo. NWS NHC-10, 22 pp.

_____, _____, and M. A. S. Davis, 1984: A tropical cyclone data tape for the North Atlantic basin, 1886—1983: Contents, limitations, and uses. NOAA Tech. Memo. NWS NHC 22, Miami, FL, 21 pp.

Jascourt, S. D., 1997: Convective Organizing and Upscale Development Processes Explored through Idealized Numerical Experiments. Ph.D. Dissertation, University of Wisconsin-Madison, 267 pp.

Jordan, C. L., 1958: MEAN SOUNDINGS FOR THE WEST INDIES AREA. *J. Meteor*., **15**, 91-97.

Kaplan, J. and M. DeMaria, 2003: Large-Scale Characteristics of Rapidly Intensifying Tropical Cyclones in the North Atlantic Basin. *Wea. Forecasting*, 18, 1093–1108.

_____, _____, and J. A. Knaff, 2010: A Revised Tropical Cyclone Rapid Intensification Index for the Atlantic and Eastern North Pacific Basins. *Wea. Forecasting*, 25, 220–241.

Kossin, J. P., 2002: Daily Hurricane Variability Inferred from GOES Infrared Imagery*, Mon. Wea. Rev.*, **130**, 2260-2270

_____, and M. Sitkowski, 2009: An Objective Model for Identifying Secondary Eyewall Formation in Hurricanes. *Mon. Wea. Rev.*, **137**, 876–892.

Kuo, H. L., 1965: On Formation and Intensification of Tropical Cyclones through Latent Heat Release by Cumulus Convection. *J. Atmos. Sci*., **22**, 40-63.

Lau, K.-M., H.-T. Wu, and S. Bony, 1997: The Role of Large-Scale Atmospheric Circulation in the Relationship between Tropical Convection and Sea Surface Temperature. *J. Climate*, **10**, 381–392.

Liu, C., and E. J. Zipser, 2005: Global distribution of convection penetrating the tropical tropopause. *J. Geophys. Res.*, **110**, D23104, doi:10.1029/2005JD006063.

_____, _____, and S. W. Nesbitt, 2007: Global Distribution of Tropical Deep Convection: Different Perspectives from TRMM Infrared and Radar Data. *J. of Climate,* **20**, 489-503.

Moller, D. J., and M. T. Montgomery, 2000: Tropical cyclone evolution via potential vorticity anomalies in a three-dimensional balance model. *J. Atmos. Sci.,* **57,** 3366–3387.

Molinari, J., D. Vollaro, and K. L. Corbosiero, 2004: Tropical Cyclone Formation in a Sheared Environment: A Case Study. *J. Atmos. Sci*., **61**, 2493-2509.

Montgomery, M. T., and B. F. Farrell, 1993: Tropical Cyclone Formation. *J. Atmos. Sci.*, **50**, 285-310.

_____, and R. J. Kallenbach, 1997: A theory for vortex Rossby waves and its application to spiral bands and intensity changes in hurricanes. *Quart. J. Roy. Meteor. Soc.,* **123,** 435–465.

_____ and J. Enagonio, 1998: Tropical Cyclogenesis via Convectively Forced Rossby Waves in a Three-Dimensional Quasigeostrophic Model. *J. Atmos. Sci*., **55**, 3176-3207.

_____, M. E. Nicholls, T. A. Cram, and A. B. Saunders, 2006: A Vortical Hot Tower Route to Tropical Cyclogenesis. *J. Atmos. Sci.*, **63**, 355-384.

_____, N. Van Sang, R. K. Smith, and J. Persing, 2009: Do tropical cyclones intensity by WISHE? *Q. J. R. Meteorol. Soc.*, **153**: 1697-1714.

_____ and R. K. Smith, 2010: Paradigms for tropical-cyclone intensification. *Q. J. R. Meteorol. Soc.*, **136**: 1-34.

_____, C. Davis, T. Dunkerton, Z. Wang, C. Velden, R. Torn, S. Majumdar, F. Zhang, R. K. Smith, L. Bosart, M. M. Bell, J. S. Haase, A. Heymsfield, and M. A. Boothe, 2011: The Pre-Depression Investigation of Cloud Systems in the Tropics (PREDICT) Experiment: Scientific Basis, New Analysis Tools, and Some First Results, *Bull. Amer. Meteor. Soc.*, *In Review.*

Naval Research Laboratory, 2002: Tropical Cyclone SSMI – 85 GHz PCT Tutorial. [Available online at http://www.nrlmry.navy.mil/sat_training/tropical_cyclones/ssmi/pct/index.html]

Nolan, D.S. and L. D. Grasso, 2003: Nonhydrostatic, Three-Dimensional Perturbations to Balanced, Hurricane-Like Vortices. Part II: Symmetric Response and Nonlinear Simulations. *J Atmos. Sci.*, **60**, 2076-2087.

_____, M. Yumin, and D. P. Stern, 2007: Tropical Cyclone Intensification from Asymmetric Convection: Energetics and Efficiency. *J. Atmos. Sci.*, **64**, 3377–3405.

Office of Satellite Data Processing and Distribution, cited 2011: Tropical Cyclone Formation Probability Product Description. [Available online at http://www.ssd.noaa.gov/PS/TROP/TCFP/description.html]

Pasch, R. J., 1997: Preliminary Report, Hurricane Danny. *National Hurricane Center*. [Available online at http://www.nhc.noaa.gov/1997danny.html]

_____, T. B. Kimberlain, and S. R. Stewart, 1999: Preliminary Report, Hurricane Floyd. *National Hurricane Center*. [Available online at http://www.nhc.noaa.gov/1999floyd.html]

_____, 2010: Tropical Cyclone Report, Tropical Storm Claudette. *National Hurricane Center*. [Available online at http://www.nhc.noaa.gov/pdf/TCR-L042009_Claudette.pdf]

Petty, G. W., 2006: A First Course in Atmospheric Radiation. 2nd ed. Sundog Publishing, 458 pp.

Pinkine, N. and B. Motta, cited 2011: NWS Southern Region GOES Satellite FAQs: What is a satellite eclipse period. [Available online at http://www.srh.noaa.gov/ssd/html/goesfaqs.htm]

Rodgers, R., 2010: Convective-Scale Structure and Evolution during a High-Resolution Simulation of Tropical Cyclone Rapid Intensification. *J. Atmos. Sci.*, **67**, 44-70.

Romps, D. M., and Z. Kuang, 2009: Overshooting convection in tropical cyclones, *Geophys Res. Lett.*, **36**, L0984, doi:10.1029/2009GL037396.

Rozoff, C. M., and J. P. Kossin, 2011: New probabilistic forecast models for the prediction of tropical cyclone rapid intensification. *Wea. Forecasting*, *In press*.

Schubert, W. H., and J. J. Hack, 1982: Inertial Stability and Tropical Cyclone Development. *J. Atmos. Sci.*, **39**, 1687-1697.

Schumacher, A. B., M. DeMaria, and J. A. Knaff, 2009: Objective Estimation of the 24-h Probability of Tropical Cyclone Formation. *Wea. Forecasting*, **24**, 456–471.

Sherwood, S. C., J.-H. Chae, P. Minnis, and M. McGill, 2004: Underestimation of deep convective cloud tops by thermal imagery. *J. Geophys. Res.*, **31,** L11102, doi:10.1029/2004GL019699

Simpson, J., E. Ritchie, G. J. Holland, J. Halverson, and S. Stewart, 1997: Mesoscale Interactions in Tropical Cyclone Genesis. *Mon. Wea. Rev*., **125**, 2643-2661.

_____, J. B. Halverson, B. A. Ferrier, W. A. Peterson, R. H. Simpson, R. Blackeslee, and S. L. Durden, 1998: On the Role of "Hot Towers" in Tropical Cyclone Formation, *Meteorol. Atmos. Phys.*, **67**, 15-35.

Sippel, J. A., J. W. Nielsen-Gammon, and S. E. Allen, 2006: The Multiple-Vortex Nature of Tropical Cyclogenesis. *Mon. Wea. Rev.*, **134**, 1796–1814.

Smith III, J. O., cited 2011: Spectral Audio Signal Processing: Generalized Hamming Window Family. [Available online at https://ccrma.stanford.edu/~jos/sasp/Generalized_Hamming _Window_Family.html#eq:ghwf]

Space Science and Engineering Center, cited 2011: SSEC Data Center Archive. [Available online at http://www.ssec.wisc.edu/datacenter/archive.html]

Solorzano, N. N., J. N. Thomas, and R. H. Holzworth, 2011: Lightning flashed in 2005-2010 tropical cyclones: implications for intensity change and comparisons with convective and environmental parameters. *Extended Abstracts Fifth Conference on the Meteorological Applications of Lightning Data*. Seattle, WA, Amer. Meteor. Soc. [Available online at http://ams.confex.com/ams/91Annual/webprogram/Paper185752.html]

Steranka, J., E. B. Rodgers, and R. C. Gentry, 1986: The Relationship between Satellite Measured Convective Bursts and Tropical Cyclone Intensification *Mon. Wea. Rev.*, **114**, 1539-1546.

Stewart, S. R., 2010: Tropical Cyclone Report, Hurricane Karl. *National Hurricane Center*. [Available online at http://www.nhc.noaa.gov/pdf/TCR-AL132010_Karl.pdf]

Tang, B. and K. Emanuel, 2010: Midlevel ventilation's constraint on tropical cyclone intensity. *J. Atmos. Sci.*, **67**, 1817-1830.

Thorncroft, C. and K. Hodges, 2001: African Easterly Wave Variability and Its Relationship to Atlantic Tropical Cyclone Activity. *J. of Climate*, **14**, 1166-1179.

Venkatesh, T. N. and J. Mathew, 2004: Prediction of tropical cyclone genesis using a vortex Merger. *Geophys. Res. Lett*., **31**, L04105, doi:10.1029/2003GL019005, 2004.

Wang, Y., J. D. Kepert, and G. J. Holland, 2001: The Effect of Sea Spray Evaporation on Tropical Cyclone Boundary Layer Structure and Intensity*. *Mon. Wea. Rev.*, **129**, 2481–2500.

Wang, Z., M. T. Montgomery, and T. J. Dunkerton, 2009: A dynamically-based method for forecasting tropical cyclogenesis location in the Atlantic sector using global model products, *Geophys. Res. Lett*., **36**, L03801, doi:10.1029/2008GL035586.

_____, _____, and C. Fritz, 2010: A first look at the structure of the wave pouch during the 2009 PREDICT-GRIP "dry run" over the Atlantic, *Mon. Wea. Rev.*, *In Review*.

Wilks, D. S., 2006: Statistical Methods in the Atmospheric Sciences. 2nd ed. Academic Press, 627 pp.

Yang, G.-Y., and J. Slingo, 2001: The Diurnal Cycle in the Tropics. *Mon. Wea. Rev.*, **129**, 784–801.

Zipser, E. J., 2003: Some views on "hot towers" after 50 years of tropical field programs and two years of *TRMM* data. *Cloud Systems, Hurricanes, and the Tropical Rainfall Measuring Mission (TRMM), Meteor. Monogr.,* No. 51, Amer. Meteor. Soc., 49–58.